INFORMATION TO USERS

This manuscript has been reproduced from the microfilm master. UMI films the text directly from the original or copy submitted. Thus, some thesis and dissertation copies are in typewriter face, while others may be from any type of computer printer.

The quality of this reproduction is dependent upon the quality of the copy submitted. Broken or indistinct print, colored or poor quality illustrations and photographs, print bleedthrough, substandard margins, and improper alignment can adversely affect reproduction.

In the unlikely event that the author did not send UMI a complete manuscript and there are missing pages, these will be noted. Also, if unauthorized copyright material had to be removed, a note will indicate the deletion.

Oversize materials (e.g., maps, drawings, charts) are reproduced by sectioning the original, beginning at the upper left-hand corner and continuing from left to right in equal sections with small overlaps.

Photographs included in the original manuscript have been reproduced xerographically in this copy. Higher quality 6" x 9" black and white photographic prints are available for any photographs or illustrations appearing in this copy for an additional charge. Contact UMI directly to order.

UMI®

SINGLE AND MULTIPLE ELECTROMAGNETIC SCATTERING BY SIZE-SHAPE DISTRIBUTIONS OF SMALL NONSPHERICAL PARTICLES

A

THESIS

Presented to the Faculty

of the University of Alaska Fairbanks

in Partial Fulfillment of the Requirements

for the Degree of

DOCTOR OF PHILOSOPHY

By

Frank Michael Schulz

Diplom-Physiker

Fairbanks, Alaska

August 1998

UMI Number: 9991027

UMI®
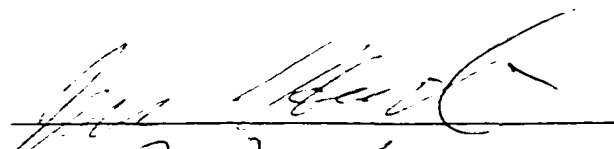
SINGLE AND MULTIPLE ELECTROMAGNETIC SCATTERING BY SIZE-SHAPE DISTRIBUTIONS OF SMALL NONSPHERICAL PARTICLES

By
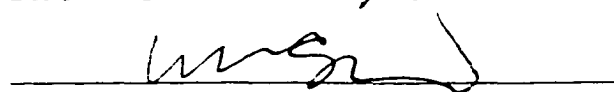
Frank Michael Schulz

RECOMMENDED:

_____

_____

_____

_____
Advisory Committee Chair

_____
Department Head

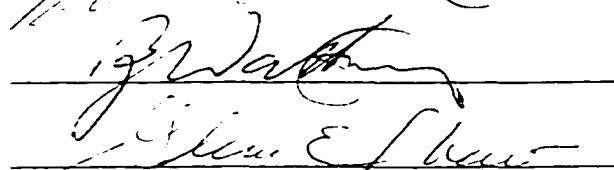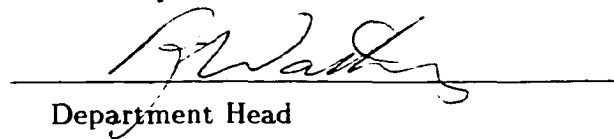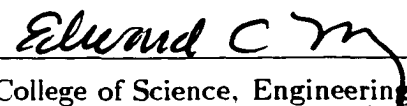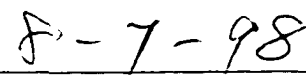APPROVED:

_____
Dean, College of Science, Engineering and Mathematics

_____
Dean of the Graduate School

_____
Date

Abstract

A comprehensive model for light scattering by size-shape distributions of randomly oriented nonspherical particles is developed. The model uses spheroids as model particles. The vector Helmholtz equation is solved with a new separation of variables (SVM) approach that allows one to calculate the ensemble-averaged single scattering optical properties of ensembles of randomly oriented particles analytically. Since the use of the SVM in spheroidal coordinates properly accounts for the geometry of the particles, the method is applicable to a large range of shapes ranging from elongated prolate needles via spheres to flat oblate disks.

The relation between geometric symmetries of particles and symmetry relations of the electromagnetic scattering solution is investigated systematically in the general framework of the theory of point groups. The results are exploited in the model for increasing the computational efficiency.

A comprehensive vector radiative transfer model is in part developed in this work. This radiative transfer model takes the output of the single scattering model as input and computes the Stokes vector components in a vertically inhomogeneous, plane parallel medium as a function of polar and azimuth angle and as a function of optical depth.

The single scattering model is applied to investigate the impact of particle shape on the optical properties of size-shape distributions of randomly oriented particles, such as aerosol layers or ice clouds in the atmosphere. The optical properties are found to be much more sensitive to a variation in the effective aspect ratio than to a variation in the effective variance of a shape-distribution. The results of this study are used as input to the vector radiative transfer model in order to study the shape-sensitivity of the radiation field in a macroscopic medium containing a size-shape distribution of randomly oriented particles. It is found that both the radiance, and the degree of linear polarization, and the degree of circular polarization are strongly shape-sensitive in most viewing directions.

3

Contents

4

List of Figures

List of Tables

Acknowledgements

10

Chapter 1

Introduction

Many particles encountered in nature have irregular nonspherical shapes. Examples are ice crystals and aerosols in the atmosphere, organic and inorganic hydrosols in the ocean, and air bubbles and brine pockets in sea ice. Several theoretical and laboratory studies have clearly shown that the scattering and absorption characteristics of nonspherical particles are fundamentally different from those of spherical particles [1, 2, 3, 4]. It has been demonstrated that spherical particle models are inadequate for modeling the optical properties of ice clouds and aerosol layers [1, 5]. Thus, in order to adequately account for particle shape in climate models and remote sensing retrieval algorithms, the development of suitable nonspherical particle models has become an important field of atmospheric research. The development of shape parameterization schemes for cirrus clouds [6] or aerosols can also greatly benefit from the development of accurate models that are based on first principles.

The main scientific question is: To what extent does the shape of particles in the atmosphere influence their optical properties and the radiation transmitted through, absorbed by and backscattered from the earth-atmosphere system? The heating/cooling rates of ice clouds are determined by their optical properties. Therefore, this question is of high relevance for climate studies. Another related question is: How does particle shape influence our ability to retrieve accurate information about ice clouds and aerosols

11

by remote sensing techniques? Precise knowledge with regard to this question is essential for the development of robust and accurate remote-sensing retrieval algorithms.

The answer to these questions requires an extensive study due to the multitude of different particle shapes encountered in nature. In spite of the considerable progress that has been made in recent years in the field of nonspherical particle scattering, the quest for a thorough understanding of the subject has just begun. Existing models only provide us with insights for narrow ranges of shapes, sizes and refractive indices, and although overlapping ranges between existing models could be established, many important ranges still remain unexplored.

The geometrical optics approximation, e.g., has been used to study the optical properties of hexagonal ice crystals, including hexagonal plates, columns, and hollow columns, as well as bullet rosettes and snowflakes [7, 8, 9, 10, 11, 12]. However, the geometric optics approximation is limited to large particles that are at least 40 times larger than the wavelength of light.

Another technique which is widely used is the Extended Boundary Condition Method (EBCM), which rigorously solves the electromagnetic scattering problem [13, 14, 15, 16, 17]. This method produces accurate results for particles ranging from sizes comparable to the wavelength of light to sizes 150 larger than the wavelength, thus providing a strong overlap with the size validity range of the geometric optics approximation [18]. However, the EBCM is limited in the range of particle shapes to which this method can be applied. For particles deviating too far from spherical shape, the EBCM becomes ill-conditioned, which limits the usefulness of this method in studies of the effect of particle shape on optical properties and radiative transfer.

The Separation of Variables method can be applied to certain nonspherical particle geometries, such as bricks, spheroids [2, 19, 20, 21, 22], infinite circular or elliptical cylinders [23, 24, 25, 26], or ellipsoids. In practice, the computational effort of this method is rather high, and the computation of the optical properties of a size-shape distribution of randomly oriented particles becomes impractical.

A strong desire to find adequate models that are based on reasonable and simplifying assumptions arises from the significant complexity of the problem. The objective of the work presented here is to develop and apply a new, comprehensive and innovative approach to scattering by nonspherical particles that can be used to undertake a systematic study of scattering by atmospheric nonspherical particles for ranges of particle size, refractive index, and (most importantly) shape in which existing models fail to provide accurate results. The approach is to model size-shape distributions of randomly oriented nonspherical particles by dielectric spheroids. This approach is based on the following perception:

- Averaging over size, orientation, and, most importantly, shape in a size-shape distribution of small randomly oriented particles produces smooth, featureless phase functions in which any conspicuous shape-related features are averaged out [27].

- Thus, the essential improvement required in comparison to a spherical particle model is an additional parameter that accounts for shape, such as a spheroid's aspect ratio. The essential difference between a spherical and a nonspherical particle model is the averaging of the optical properties over orientation and shape in addition to the integration over the size distribution.

- Since shape-related features disappear in the orientational and shape averaging, one can choose a simple shape, such as spheroids, for modeling size-shape distributions of randomly oriented nonspherical particles.

Chapter 2 introduces the new approach to the single scattering problem and addresses the calculation of ensemble-averaged optical properties in a size-shape distribution of randomly oriented nonspherical particles. In contrast to other models, the approach developed here allows one both to perform the ensemble-average analytically and thus very efficiently, and to cover a large range of particle shapes including highly elongated (prolate) particles, spheres, as well as flat (oblate) particles.

In Chapter 3, a group theoretical approach is developed for systematically accounting

for geometrical symmetries of scattering particles in the single scattering theory developed here. The symmetry relations for the electromagnetic scattering solution found in this study lead to significant reductions in the necessary numerical computations.

A new vector radiative transfer model (VDISORT) based on the discrete ordinate method is in part developed in this work. A comprehensive model description and model tests are presented in Chapter 4. In contrast to DISORT. which computes only the intensity (and irradiance) of the radiation field in a vertically inhomogeneous. plane-parallel medium. this model also computes the other three Stokes parameters describing the polarization of the radiation field. The model has been generalized in such a way that it can also be applied to nonspherical particles.

Chapter 5 describes an analytical method developed in this work to compute the angular distribution of the Stokes vector from the VDISORT solution. This method is shown to be superior to the common spline interpolation scheme. both in terms of accuracy and in terms of computer time.

As a model application. the sensitivity of the single scattering optical properties of a size-shape distribution of randomly oriented spheroids to shape is investigated in Chapter 6. The large validity range in terms of shape of the model developed in this work allows one to put special emphasis on moderately and highly aspherical particles. The results of this study clearly underscore the significant impact of particle shape on the optical properties. even after averaging over size. shape. and orientation.

In Chapter 7 the results of the sensitivity study for the optical properties are used in the vector radiative transfer code VDISORT to investigate the shape-sensitivity of the radiation field in a macroscopic multiply-scattering medium. The strong shape-sensitivity of the single scattering optical properties results in an equally strong shape-sensitivity of both the intensity. and the degree of linear polarization. and the degree of circular polarization of the radiation field in a medium containing a size-shape distribution of randomly oriented nonspherical particles. This shape-sensitivity is found to be equally strong for moderately and highly aspherical particles. which demonstrates the impor-

tance of having access to a model that can treat highly aspherical shapes.

Chapter 2

A Novel Separation of Variables Approach to the Electromagnetic Single Scattering Problem

The solution to the electromagnetic single scattering problem can be expressed in terms of the so-called T-matrix. The T-matrix can be computed with the Extended Boundary Condition Method (EBCM). which is based on an integral equation approach to the scattering problem. In this chapter. a method other than the EBCM is presented to compute the T-matrix for electromagnetic scattering [28]. The separation of variables method (SVM) is used to solve the electromagnetic scattering problem for a spheroidal particle and to derive its $\mathcal{T}$-matrix in spheroidal coordinates (denoted by caligraphic font). The computation of the $\mathcal{T}$-matrix in the particle's natural coordinates entirely circumvents the notorious ill-conditioning that has plagued the EBCM for highly aspherical particles. which is based on the use of spherical coordinates. A transformation is developed for transforming the $\mathcal{T}$-matrix in spheroidal coordinates into the corresponding T-matrix in spherical coordinates (denoted by Roman font). The T-matrix so obtained can be used to compute optical properties of ensembles of randomly oriented particles by employing

16

an existing well-established and efficient analytical method to average over orientational angles. The T-matrices and optical properties computed with the SVM and the EBCM. respectively. are compared for five different test cases. The comparisons show that for mildly aspherical particles the two methods give indistinguishable results. Differences appear when the departure from spherical shape becomes significant. Comparisons for large departures from spherical shape are not possible. because the EBCM becomes ill-conditioned. Contrary to the EBCM. the new approach can be used to compute optical properties for arbitrary values of the aspect ratio. The SVM relies heavily on the use of spheroidal functions. To test the accuracy of the expansion coefficients of these functions for complex arguments and arbitrary shapes. a new testing method based on the completeness relation of the spheroidal functions is presented.

2.1   Introduction

In previous studies of scattering by nonspherical particles. some researchers have focused on regular crystal shapes. such as hexagonal ice crystals. columns. hollow columns and bullet rosettes. and even more sophisticated but still highly regular snowflake shapes [7. 8. 9. 10. 11. 12]. Very often. however. observations show that regularly shaped crystals are the exception rather than the rule in natural cirrus clouds. Thus. highly irregular and widely ranging shapes are by far the most commonly observed in natural ensembles of ice crystals [29]. The computed scattering properties of perfectly symmetric crystals are useful for comparisons with laboratory experiments conducted under controlled conditions. However. comparisons of measured scattering properties of natural cirrus clouds with laboratory-measured phase functions show significant differences [30]. More and more evidence indicates that ice crystals of a definite regular shape. such as hexagons. are of limited use for modeling the radiative transfer through ice clouds in nature [31].

Because highly irregular and widely ranging shapes are common-place in nature. attempts to account for the shape of each individual particle become impractical. if not impossible. A spherical particle model is definitely too crude for many applications.

and the assumption of ideal crystal shapes is seldom justified in natural cirrus clouds. Nevertheless. to obtain computational expedience a practical nonspherical particle model must be based on simplifying assumptions. This requirement also reflects the recognition that often one does not have the information required to specify all the exact shapes actually present.

It is well-known that by averaging over size and orientation for a distribution of randomly oriented particles of identical shape. one is left with features in the phase function characteristic of the assumed shape. However. observations typically show no shape-related features. This is precisely the reason why the assumption of an ensemble of ice crystals of a definite ideal shape gives unsatisfactory results when compared to observations of scattering by natural cirrus clouds. A recent study on scattering by small particles has shown that by averaging both over shape and size for a distribution of randomly oriented particles. one obtains a smooth featureless phase function as typically encountered in a system of natural scatterers [27]. Thus. to improve a spherical particle model for scattering by an ensemble of small crystals or aerosol particles of irregular and widely varying shapes. it is important to introduce. in addition to the size parameter. a second parameter that accounts for the variation in shape of the particle. The additional averaging over shape is the crucial difference between a spherical and a nonspherical particle model. Since the averaging over shape tends to smear out any conspicuous features produced by individual shapes of small particles. one might just as well choose a simple particle shape. For this reason. several investigators have focused on scattering by spheroidal particles [2. 3. 19. 20. 21. 22. 32]. Spheroids have a simple axially-symmetric shape. but can be used to span shapes ranging from flat oblate disks via spheres to elongated prolate needles by varying just one parameter. namely the particle's aspect ratio. Mishchenko [27] has pointed out that the phase function of a size-shape distribution of randomly oriented spheroids closely resembles that of an ensemble of bricks (West et al. [33]). even though spheroids have a perfectly smooth surface. while bricks have sharp rectangular edges. Thus. the simple spheroidal shape is a convenient and natural choice

for modeling the optical properties including the Stokes scattering matrix of a size-shape distribution of randomly oriented nonspherical particles.

The scattering problem can be divided in two parts. The first part involves scattering of light by a single particle. while the second part involves scattering by an ensemble of particles of a variety of sizes. shapes. and orientations. The separation of variables method (SVM) and the extended boundary condition method (EBCM. which computes the T-matrix) are two widely used rigorous methods to solve the scattering problem for a single particle. Unfortunately. when applied to axisymmetric particles. the EBCM becomes ill-conditioned if the particle shape departs significantly from sphericity. This shortcoming limits the usefulness of the EBCM to mildly aspherical particles. When using the SVM for calculating scattering by spheroidal particles. on the other hand. one accounts for the geometry of the particle by expanding each of the incident. internal and scattered fields in the proper basis of spheroidal wave functions. Consequently. this method is not limited to a certain range of the aspect ratio. This independence of the aspect ratio has been demonstrated for two-dimensional scattering by elliptical cylinders. where the SVM has been successfully applied also to the extreme shape in which the cylinder degenerates into a strip [23. 24. 25. 26].

For an ensemble of randomly oriented particles. the computation of the light scattering properties of the ensemble involves an integration over particle orientation. For spheroidal particles. this integration has been done numerically when using the SVM [2]. In applications of the EBCM to nonspherical axisymmetric particles. which (as currently practised) relies on the use of spherical coordinates. the T-matrix that describes scattering by a single particle can also be employed to calculate the scattering properties of an ensemble of randomly oriented particles. Since the integration over orientational angles can be done *analytically* [32]. the T-matrix method becomes very efficient within its range of validity for nonspherical particles. The integration over orientational angles yields the absorption and extinction cross section as well as the expansion coefficients of the Stokes scattering matrix in terms of the T-matrix elements. This is another im-

portant advantage of the T-matrix method, since some of the most versatile radiative transfer codes require these expansion coefficients of the Stokes scattering matrix as input [34, 35, 36].

On this background the work presented in this chapter is based on the following premise:

- Just like a particle's mass determines its inertia *independent of any forces*, the light scattering properties of a dielectric particle can be expressed in terms of a T-matrix which depends only on the particle size parameter, shape and complex refractive index and is *independent of the incident electromagnetic field*.

A single scattering method should therefore (if possible) be aimed at computing the T-matrix, rather than the fields. Since the SVM, as commonly used, has focused on computing the fields, it will be modified in this study in order to derive and compute the T-matrix, using a new transformation from the $\mathcal{T}$-matrix in spheroidal coordinates to the corresponding T-matrix in spherical coordinates. Then the resulting T-matrix will be used to compute optical properties. As mentioned above, this SVM approach entirely circumvents the problems encountered in applications of the EBCM to highly aspherical particles while it retains the analytical-averaging advantage of the T-matrix method for computing the single scattering properties of an ensemble of randomly oriented particles.

2.2 Theory

2.2.1 Spheroidal coordinates and wave functions

A spheroid can be constructed by rotating an ellipse with a certain interfocal distance d about one of its axes. By performing a rotation about the major or minor axis, one obtains a prolate or oblate spheroid, respectively. An advantage of modeling nonspherical particles by spheroids is that the scalar Helmholtz equation is separable in spheroidal coordinates. Thus, the general solution of the scalar Helmholtz equation can be written

as a linear combination of spheroidal wave functions $\psi_{n,m}^{(j)}(\mathbf{r})$. which can be written as the product of a radial function $R_{n,m}^{(j)}(c;\xi)$. $j = 1.\ldots.4$. an angular function $S_{n,m}(c;\eta)$. and an azimuthal function $\Phi_m(o)$. Here. $c = kd/2$. where the wave number k is real for non-absorbing particles and complex for absorbing particles. A time dependence $\exp(-i\omega t)$ is assumed and suppressed throughout this and the following chapters. The spheroidal coordinates $(\eta.\xi.o)$ are related to Cartesian coordinates in the following way [37]

$$x = \frac{d}{2}\sqrt{(1-\eta^2)(\xi^2 \pm 1)} \cos o \qquad (2.1)$$

$$y = \frac{d}{2}\sqrt{(1-\eta^2)(\xi^2 \pm 1)} \sin o \qquad (2.2)$$

$$z = \frac{d}{2}\eta\xi \qquad (2.3)$$

where the upper and lower signs pertain to oblate and prolate spheroidal coordinates. respectively. In the former case. $0 \le \xi < \infty$. and in the latter case. $1 \le \xi < \infty$. In either case. $-1 \le \eta \le 1$. and $0 \le o < 2\pi$. The coordinate hypersurfaces characterized by $\eta = $ constant. $\xi = $ constant. and $o = $ constant. are hyperboloids. spheroids. and planes containing the rotation axis of the ellipse. respectively. For each finite d. the spheroidal hypersurfaces approach spherical shape as $\xi \to \infty$. and

$$c\xi \to kr \qquad (2.4)$$

$$\eta \to \cos\theta \qquad (2.5)$$

where $(r.\theta.o)$ are spherical coordinates. The unit vectors show the following asymptotic behavior as $\xi \to \infty$

$$\hat{\xi} \to \hat{r} \qquad (2.6)$$

$$\hat{\eta} \to -\hat{\theta} \qquad (2.7)$$

where the sign in (2.7) comes from the fact that the cosine is monotonically decreasing in the interval $0 \le \theta \le \pi$. With $\hat{r} \times \hat{\theta} = \hat{o}$. it follows that $(\hat{\eta}.\hat{\xi}.\hat{o})$ is a right-handed coordinate system. i.e. $\hat{\eta} \times \hat{\xi} = \hat{o}$.

By substituting the separation of variables ansatz into the scalar Helmholtz equation

$$(\nabla^2 + k^2)\varphi = 0 \tag{2.8}$$

and expressing the Laplacian differential operator ∇^2 in prolate or oblate spheroidal coordinates. one finds the differential equation for each of the functions $R_{n,m}^{(j)}(c\colon \xi)$. $S_{n,m}(c\colon \eta)$. and $\Phi_m(\varphi)$. The solution for the azimuthal function is simply

$$\Phi_m(\varphi) = e^{im\varphi} \tag{2.9}$$

or alternatively. with even and odd functions.

$$\Phi_{e,m}(\varphi) = \cos m\varphi \tag{2.10}$$

$$\Phi_{o,m}(\varphi) = \sin m\varphi. \tag{2.11}$$

The solutions of the other two differential equations [37] are the angular spheroidal functions $S_{n,m}(c\colon \eta)$ and the radial spheroidal functions $R_{n,m}^{(j)}(c\colon \xi)$ of the jth kind. where $j = 1,\ldots, 4$. and $R_{n,m}^{(3)} = R_{n,m}^{(1)} + i\, R_{n,m}^{(2)}$ and $R_{n,m}^{(4)} = R_{n,m}^{(1)} - i\, R_{n,m}^{(2)}$. In the electromagnetic scattering problem. the functions of the first kind are appropriate for expanding the incident wave. while functions of the third kind must be used for the scattered wave. In the prolate case. the general solution to the scalar scattering problem can be written as a linear combination of prolate spheroidal wave functions

$$\varphi_{n,m}^{(j)}(c\colon \eta.\xi.\varphi) = S_{n,m}(c\colon \eta)\, R_{n,m}^{(j)}(c\colon \xi)\, e^{im\varphi} \tag{2.12}$$

or of analogously defined even and odd functions $\varphi_{\sigma.n.m}^{(j)}$. where $\sigma = e.o$. The oblate functions can be obtained from these by making the substitution

$$\xi \rightarrow i\xi \tag{2.13}$$

$$c \rightarrow -ic. \tag{2.14}$$

If an exponential φ-dependence is chosen. then $n = 0.1\ldots$ and $m = -n. -n+1.\ldots.n$: if even and odd functions are chosen. then $m = 0.1\ldots$ and $n = m. m+1.\ldots.$

The angular functions can be expanded in associated Legendre functions $P_n^{(m)}$ [37]

$$S_{n,m}(c;\eta) = \sum_{r=0,1}^{\infty}{}' d_r^{(m,n)}(c) P_{|m|+r}^{(m)}(\eta) \tag{2.15}$$

where the primed sum extends over even (odd) indices r if $(n-m)$ is even (odd). and where $|m| \le n$. The expansion coefficients $d_r^{(m,n)}$ can be computed by Bouwkamp's method [38]. They satisfy the relation

$$d_r^{(m,n)}(0) = \text{const}\,\delta_{|m|+r,n} \tag{2.16}$$

where $\delta_{p,q}$ is the Kronecker-delta. and where the constant can be set equal to unity such that

$$S_{n,m}(0.\eta) = P_n^{(m)}(\eta). \tag{2.17}$$

The angular functions are orthogonal in the first index [37]:

$$\int_{-1}^{1} d\eta S_{n,m}^*(c;\eta) S_{n',m}(c;\eta) = N_{m,n}\,\delta_{n,n'} \tag{2.18}$$

where

$$N_{m,n} = \sum_{r=0,1}^{\infty}{}' \frac{(|m|+m+r)!}{(|m|-m+r)!} \frac{2}{2(|m|+r)+1} d_r^{(m,n)*}(c)\, d_r^{(m,n)}(c). \tag{2.19}$$

Here the asterisk denotes complex conjugation. $N_{m,n}$ has been defined here such that it is always real. even if c is complex. which deviates from other authors [19. 37].

Two useful relations for the spheroidal expansion coefficients

Defining

$$f_r^{(m,n)}(c) = \begin{cases} \sqrt{\dfrac{1}{N_{m,n}} \dfrac{2}{2(|m|+r)+1} \dfrac{(|m|+m+r)!}{(|m|-m+r)!}}\, d_r^{(m,n)}(c) & : \text{ if } r \text{ and } (n-m) \\ & \quad \text{ have same parity} \\ & \quad \text{ and } |m| \le n \\ 0 & : \text{ otherwise} \end{cases} \tag{2.20}$$

and substituting (2.15) into (2.18). one obtains

$$\sum_{r=0.1}^{\infty}{}' f_r^{(m.n)*}(c)\, f_r^{(m.n')}(c) \;=\; \delta_{n.n'} \tag{2.21}$$

where the orthogonality property of the associated Legendre functions has been used.

For convenience. one now defines normalized angular spheroidal functions

$$Z_{n.m}(c;\eta.\circ) \;=\; \frac{1}{\sqrt{2\pi.N_{m.n}}}\, S_{n.m}(c;\eta)\, e^{im\circ}. \tag{2.22}$$

These functions can be expanded in the basis of spherical harmonics

$$|j.m\rangle = Y_{j.m}(\theta.\circ) \;=\; \sqrt{\frac{2j+1}{4\pi}\,\frac{(j-m)!}{(j+m)!}}\, P_j^{(m)}(\cos\theta)\, e^{im\circ} \tag{2.23}$$

by using (2.15) and (2.20):

$$|Z_{n.m}\rangle \;=\; \sum_{r=0.1}^{\infty}{}' f_r^{(m.n)}(c)\, ||m|+r.m\rangle. \tag{2.24}$$

Since the spherical harmonics are complete. every arbitrary function $|v\rangle$ can be expanded in this basis. i.e.

$$|v\rangle \;=\; \sum_{n.m'} \alpha_{n.m'} |n.m'\rangle. \tag{2.25}$$

To show the completeness of the $|Z_{n.m}\rangle$. one can start with the ansatz

$$|v\rangle \;=\; \sum_{n.m'} \beta_{n.m'} |Z_{n.m'}\rangle \tag{2.26}$$

and construct the coefficients by applying the bra $\langle q+|m|.m|$ to both (2.25) and (2.26). and using (2.24) and (2.21). This yields

$$\sum_{q=0.1}^{\infty}{}' \alpha_{q+|m|.m}\, f_q^{(m.n)*}(c) \;=\; \beta_{n.m}. \tag{2.27}$$

By substituting $\alpha_{q+|m|.m} = \langle q+|m|.m|v\rangle$ in (2.27) and using (2.24) and (2.26). one obtains the completeness relation in the usual form

$$\sum_{n=0}^{\infty}\sum_{m=-n}^{n} |Z_{n.m}\rangle\langle Z_{n.m}| \;=\; i \tag{2.28}$$

where $\hat{1}$ is the identity operator. One can express the completeness relation in terms of the coefficients $f_r^{(m,n)}$ in (2.20) by taking the matrix elements on both sides of (2.28) in the basis of the spherical harmonics. The left hand side is $\langle s+|m|. m|\hat{1}|t+|m|. m\rangle = \delta_{s,t}$. and the right hand side is obtained by substituting (2.24) and using the orthogonality of the spherical harmonics and (2.20). Thus.

$$\sum_{n=|m|.|m|+1}^{\infty}{}' f_s^{(m,n)*}(c)\, f_t^{(m,n)}(c) = \delta_{s,t}. \tag{2.29}$$

The relations (2.21) and (2.29) are useful for deriving the transformation in Eq. (2.129) of the spheroidal $\mathcal{T}$-matrix into the spherical T-matrix (see Section 2.4). Eq. (2.29) can also be used for checking the numerical accuracy of the spheroidal expansion coefficients $d_r^{(m.n)}$.

2.2.2 Solenoidal solutions to the vector Helmholtz equation

In an isotropic. homogeneous. charge-free medium. the general solution to the vector Helmholtz equation in spheroidal coordinates can be written as a linear combination of solenoidal vector spheroidal wave functions $\mathbf{V}_{n.m}^{(j)}$ and $\mathbf{W}_{n.m}^{(j)}$ of the jth kind. These can be constructed in the following way [19. 37]:

$$\mathbf{V}_{n.m}^{(j)} = \nabla \times (\mathbf{a} \cdot \varphi_{n.m}^{(j)}). \tag{2.30}$$

$$\mathbf{W}_{n.m}^{(j)} = k^{-1} \cdot \nabla \times \mathbf{V}_{n.m}^{(j)}. \tag{2.31}$$

where the $\varphi_{n.m}^{(j)}$ are the scalar spheroidal wave functions. The vector $\mathbf{a}$ can be any constant vector or the position vector $\mathbf{a} = \mathbf{r}$. Alternatively. one can define even and odd vector functions

$$\mathbf{V}_{\sigma.n.m}^{(j)} = \nabla \times (\mathbf{a} \cdot \varphi_{\sigma.n.m}^{(j)}) \tag{2.32}$$

$$\mathbf{W}_{\sigma.n.m}^{(j)} = k^{-1} \cdot \nabla \times \mathbf{V}_{\sigma.n.m}^{(j)} \tag{2.33}$$

where $\sigma = \epsilon. o$. Explicit expressions for the latter functions can be found in the literature [37].

Since some authors use vector functions with an exponential o-dependence. while others prefer even and odd functions. the following useful relations are given to transform from one convention to the other:

The relation between the functions (2.30). (2.31) and (2.32). (2.33) is given by

$$\mathbf{V}^{(j)}_{n,m} = (\mathbf{V}^{(j)}_{e,n,m} + i\mathbf{V}^{(j)}_{o,n,m}) \tag{2.34}$$

$$\mathbf{V}^{(j)}_{n,-m} = (-1)^m \frac{(n-m)!}{(n+m)!} (\mathbf{V}^{(j)}_{e,n,m} - i\mathbf{V}^{(j)}_{o,n,m}). \tag{2.35}$$

and similar expressions for $\mathbf{W}^{(j)}_{n,\pm m}$. where $m \geq 0$. For $m = 0$ the odd functions vanish. so that $\mathbf{V}^{(j)}_{n,0} = \mathbf{V}^{(j)}_{e,n,0}$. If one expands an electromagnetic field in either basis of vector wave functions. i.e.

$$\mathbf{E} = \sum_{n,m} [\epsilon^{(1)}_{n,m} \mathbf{V}^{(j)}_{n,m} + \epsilon^{(2)}_{n,m} \mathbf{W}^{(j)}_{n,m}]$$

$$= \sum_{\sigma=e,o} \sum_{n,m} [\eta^{(1)}_{\sigma,n,m} \mathbf{V}^{(j)}_{\sigma,n,m} + \eta^{(2)}_{\sigma,n,m} \mathbf{W}^{(j)}_{\sigma,n,m}]. \tag{2.36}$$

then the relation between the coefficients is given by

$$\epsilon^{(k)}_{n,m} = \frac{\eta^{(k)}_{e,n,m} - i\eta^{(k)}_{o,n,m}}{2} \tag{2.37}$$

$$\epsilon^{(k)}_{n,-m} = (-1)^m \frac{(n+m)!}{(n-m)!} \frac{\eta^{(k)}_{e,n,m} + i\eta^{(k)}_{o,n,m}}{2}. \tag{2.38}$$

where $m > 0$. and

$$\epsilon^{(k)}_{n,0} = \eta^{(k)}_{e,n,0} \tag{2.39}$$

for $m = 0$. These relations will be used in Section 2.3.2.

2.2.3   The Separation of Variables Method

To expand the field incident to and scattered by a spheroidal particle. Asano and Ya-mamoto [19] chose even and odd vector spheroidal wave functions $\mathbf{V}^{(j)}_{\sigma,n,m}$ and $\mathbf{W}^{(j)}_{\sigma,n,m}$ with the choice $\mathbf{a} = \mathbf{r}$ in the definitions (2.30) and (2.31) of these functions. Farafonov [20] and Voshchinnikov [21, 22] used a mixed set of vector functions with $\mathbf{a} = \mathbf{r}$ and

$\mathbf{a} = \hat{z}$, where $\hat{z}$ is the unit vector in the z-direction. In this study, Asano and Yamamoto's method will be used, since, due to their choice of the expansion functions, it is conceptually easier to develop a connection to the T-matrix method.

Asano and Yamamoto considered a spheroidal particle in a coordinate system with the z-axis coinciding with the particle's symmetry axis, and a polarized plane wave incident in the x-z- plane at an angle ζ with the z-axis. The electric field vector is either in the incident plane (TM mode) or perpendicular to it (TE mode). The electric field of the incident plane wave in the TE mode is given by

$$\mathbf{E}^i = \sum_{m=0}^{\infty} \sum_{n=m}^{\infty} i^n [f_{n,m}^{(2)}(\zeta)\, \mathbf{V}_{e,n,m}^{(1)}(k_2\mathbf{r}) + i f_{n,m}^{(1)}(\zeta)\, \mathbf{W}_{o,n,m}^{(1)}(k_2\mathbf{r})]. \tag{2.40}$$

and the corresponding field in the TM mode is

$$\mathbf{E}^i = \sum_{m=0}^{\infty} \sum_{n=m}^{\infty} i^n [f_{n,m}^{(1)}(\zeta)\, \mathbf{V}_{o,n,m}^{(1)}(k_2\mathbf{r}) - i f_{n,m}^{(2)}(\zeta)\, \mathbf{W}_{e,n,m}^{(1)}(k_2\mathbf{r})]. \tag{2.41}$$

The plane wave expansion coefficients are [19, 37]:

$$f_{n,m}^{(1)}(\zeta) = \frac{4m}{N_{m,n}} \sum_{r=0,1}^{\infty}{}' \frac{d_r^{(m,n)}}{(r+m)(r+m+1)} \frac{P_{m+r}^{(m)}(\cos\zeta)}{\sin\zeta} \tag{2.42}$$

$$f_{n,m}^{(2)}(\zeta) = \frac{2(2-\delta_{0,m})}{N_{m,n}} \sum_{r=0,1}^{\infty}{}' \frac{d_r^{(m,n)}}{(r+m)(r+m+1)} \frac{dP_{m+r}^{(m)}(\cos\zeta)}{d\zeta} \tag{2.43}$$

The scattered and internal field in the TE mode are given by

$$\mathbf{E}^s = \sum_{m=0}^{\infty} \sum_{n=m}^{\infty} i^n [\pi_{1,n,m}^{(2)}\, \mathbf{V}_{e,n,m}^{(3)}(k_2\mathbf{r}) + i\pi_{1,n,m}^{(1)}\, \mathbf{W}_{o,n,m}^{(3)}(k_2\mathbf{r})]. \qquad \xi > \xi_0. \tag{2.44}$$

$$\mathbf{E}^{int} = \sum_{m=0}^{\infty} \sum_{n=m}^{\infty} i^n [\lambda_{1,n,m}^{(2)}\, \mathbf{V}_{e,n,m}^{(1)}(k_1\mathbf{r}) + i\lambda_{1,n,m}^{(1)}\, \mathbf{W}_{o,n,m}^{(1)}(k_1\mathbf{r})]. \qquad \xi < \xi_0. \tag{2.45}$$

and in the TM mode by

$$\mathbf{E}^s = \sum_{m=0}^{\infty} \sum_{n=m}^{\infty} i^n [\pi_{2,n,m}^{(1)}\, \mathbf{V}_{o,n,m}^{(3)}(k_2\mathbf{r}) - i\pi_{2,n,m}^{(2)}\, \mathbf{W}_{e,n,m}^{(3)}(k_2\mathbf{r})]. \qquad \xi > \xi_0. \tag{2.46}$$

$$\mathbf{E}^{int} = \sum_{m=0}^{\infty} \sum_{n=m}^{\infty} i^n [\lambda_{2,n,m}^{(1)}\, \mathbf{V}_{o,n,m}^{(1)}(k_1\mathbf{r}) - i\lambda_{2,n,m}^{(2)}\, \mathbf{W}_{e,n,m}^{(1)}(k_1\mathbf{r})]. \qquad \xi < \xi_0. \tag{2.47}$$

where $k_j = k_0 n_j$ $(j = 1, 2)$ with k_0 being the wave number in vacuum and n_1 and n_2 being the complex refractive indices inside and outside the particle, respectively. $\xi = \xi_0$ is the coordinate hypersurface coinciding with the surface of the spheroidal particle. Similar relations can be written for the magnetic field [19].

The problem is to compute the unknown constants of integration in the expansions (2.44) – (2.47) by using the boundary conditions for the electric field

$$E_\eta^i + E_\eta^s = E_\eta^{int} \qquad \text{at } \xi = \xi_0. \tag{2.48}$$

$$E_o^i + E_o^s = E_o^{int} \qquad \text{at } \xi = \xi_0. \tag{2.49}$$

and analogous conditions for the magnetic field [19]. The boundary conditions have to be expressed explicitly in terms of the spheroidal wave functions. This yields a system of linear equations for each value of the index m of the form

$$\mathbf{A}_k(m) \cdot \mathbf{x}_k(m) = \mathbf{b}_k(m). \qquad k = 1, 2 \tag{2.50}$$

and

$$\mathbf{x}_k(m) = [\pi_{k,m,m}^{(1)}, \pi_{k,m+1,m}^{(1)} \cdots \cdots \pi_{k,m,m}^{(2)}, \pi_{k,m+1,m}^{(2)} \cdots \cdots$$
$$\lambda_{k,m,m}^{(1)}, \lambda_{k,m+1,m}^{(1)} \cdots \cdots \lambda_{k,m,m}^{(2)}, \lambda_{k,m+1,m}^{(2)} \cdots \cdots]^T \tag{2.51}$$

is the vector of the unknown coefficients for the TE $(k = 1)$ and the TM mode $(k = 2)$, and where both the coefficient matrix $\mathbf{A}_k(m)$ and the inhomogeneity $\mathbf{b}_k(m)$ depend on the coefficients $d_r^{(m,n)}(c)$ and the radial spheroidal wave functions of the first and third kind at $\xi = \xi_0$, $R_{n,m}^{(j)}(c; \xi_0)$, and their derivative $dR_{n,m}^{(j)}(c; \xi)/d\xi|_{\xi=\xi_0}$. The solution of the electromagnetic scattering problem is obtained by solving (2.50) for each value of m and for both modes. Equation (2.50) can be found in explicit form in the paper by Asano and Yamamoto [19], which also includes a discussion of the numerical implementation of this system of linear equations and ways to avoid numerical ill-conditioning.

2.2.4 The Extended Boundary Condition Method

The T-matrix method as commonly used relies on expanding each of the incident, scattered, and internal electric fields in vector *spherical* functions $\mathbf{M}_{n,m}^{(j)}$ and $\mathbf{N}_{n,m}^{(j)}$ according to

$$\mathbf{E}^i = \sum_{n=1}^{\infty} \sum_{m=-n}^{n} [a_{n,m}^{(1)} \mathbf{M}_{n,m}^{(1)}(k_2\mathbf{r}) + a_{n,m}^{(2)} \mathbf{N}_{n,m}^{(1)}(k_2\mathbf{r})] \tag{2.52}$$

$$\mathbf{E}^s = \sum_{n=1}^{\infty} \sum_{m=-n}^{n} [p_{n,m}^{(1)} \mathbf{M}_{n,m}^{(3)}(k_2\mathbf{r}) + p_{n,m}^{(2)} \mathbf{N}_{n,m}^{(3)}(k_2\mathbf{r})] \tag{2.53}$$

$$\mathbf{E}^{int} = \sum_{n=1}^{\infty} \sum_{m=-n}^{n} [b_{n,m}^{(1)} \mathbf{M}_{n,m}^{(1)}(k_1\mathbf{r}) + b_{n,m}^{(2)} \mathbf{N}_{n,m}^{(1)}(k_1\mathbf{r})]. \tag{2.54}$$

The vector spherical functions are defined in complete analogy to the vector spheroidal wave functions. To obtain the vector spherical functions, one has to replace the scalar spheroidal wave functions $\varphi_{n,m}$ in Eqs. (2.30) and (2.31) by the scalar spherical wave functions $v_{n,m}$ given by

$$v_{n,m}^{(j)} = P_n^{(m)}(\cos\theta) z_n^{(j)}(kr) e^{im\phi}, \qquad j = 1, \ldots, 4 \tag{2.55}$$

where the $z_n^{(1)}$ and $z_n^{(2)}$ denote spherical Bessel and Neumann functions, respectively, while $z_n^{(3)}$ and $z_n^{(4)}$ denote n^{th} order spherical Hankel functions of the first and second kind, respectively.

Since Maxwell's equations and the boundary conditions are linear, there must be a linear relation between the expansion coefficients in (2.52), (2.53), and (2.54), i.e.

$$p_{n,m}^{(k)} = \sum_{n'=1}^{\infty} \sum_{m'=-n'}^{n'} \sum_{k'=1}^{2} T_{n,m,n',m'}^{(k,k')} a_{n',m'}^{(k')} \tag{2.56}$$

or in matrix-vector form

$$\mathbf{p} = \mathbf{T} \cdot \mathbf{a} \tag{2.57}$$

where **T** is called the T-matrix. Similarly, the other relations between coefficients can be written as

$$\mathbf{a} = \mathbf{Q_1} \cdot \mathbf{b} \tag{2.58}$$

$$\mathbf{p} = \mathbf{Q_2} \cdot \mathbf{b} = \mathbf{Q_2} \cdot (\mathbf{Q_1})^{-1} \cdot \mathbf{a} \tag{2.59}$$

Thus. one obtains

$$T = Q_2 \cdot (Q_1)^{-1}. \tag{2.60}$$

In the extended boundary condition method (EBCM) [13. 14. 15. 16. 17]. expressions for the matrices Q_1 and Q_2 are derived from an integral-equation approach. The resulting expressions involve various integrals over the particle's surface of cross products of the vector spherical functions. These surface integrals are usually evaluated numerically. The EBCM method has been applied to nonspherical particles of different shapes. such as spheroids [3. 32. 39]. finite circular cylinders [4. 40]. and Chebyshev particles [32]. As a consequence of the inversion of the matrix Q_1 that has to be carried out in (2.60). numerical problems have been associated with the EBCM. In particular. the calculation of the inverse matrix $(Q_1)^{-1}$ is ill-conditioned for nonspherical particles much larger than a wavelength or with large real or imaginary parts of the refractive index [41]. as well as for non-absorbing or weekly absorbing particles [18]. and for highly aspherical particles. Recent progress in numerical procedures. however. has made it possible to extend the applicability of the EBCM to size parameters larger than 150 for both non-absorbing and weakly absorbing particles [18].

Since the EBCM relies on the use of vector *spherical* functions. its application to particles with shapes departing too much from sphericity remains an inherent ill-conditioning problem. The so-called iterative extended boundary condition method (IEBCM) is based on dividing an elongated prolate spheroid in several sub-domains centered along the symmetry axis. and using spherical function expansions in each sub-domain [42. 43]. Using this iterative technique. Iskander and Lakhtakia were able to extend the EBCM for non-absorbing small prolate spheroids from aspect ratios of 4 to aspect ratios of 7 [43]. However. the price of reducing the ill-conditioning of the EBCM in this iterative manner is a substantial increase in computation time and computer code complexity [41].

The origin of the ill-conditioning problem is that the chosen expansion basis of spherical functions in the EBCM does not suit the geometry of spheroidal particles. A successful formulation of the EBCM in spheroidal coordinates has not yet been established

for electromagnetic scattering. The derivation of the Q- and the T-matrix using the EBCM relies on knowledge of the free space dyadic Green's function [15], which is well known in spherical coordinates [44, 45]. A recent report on the derivation of the dyadic Green's function in prolate spheroidal coordinates [46] was based on the assumption that the vector spheroidal wave functions are orthogonal in both indices. i.e. that the integration over the scalar product of two such vector functions will give two Kronecker-deltas, one for the order and one for the degree of the vector functions. This is, however, not the case. Therefore, the EBCM can, at present, not be reformulated in spheroidal coordinates. A T-matrix in spheroidal coordinates has previously been reported only for acoustical and elastic-wave scattering [47, 48]. For spheroidal particles, the SVM is therefore the method with the widest range of applicability in terms of extreme particle shapes.

In absence of ill-conditioning problems, the T-matrix method has a significant advantage over other methods when it comes to calculating the scattering properties of an ensemble of randomly oriented particles. Tsang et al. [49] derived the scattering matrix for randomly oriented nonspherical particles in terms of their single scattering properties. i.e. in terms of the T-matrix, and performed the averaging over orientation numerically. Mishchenko developed a method to do the integration over orientational angles analytically [32]. taking advantage of the Clebsch-Gordan formalism. By this method, the optical properties including the expansion coefficients of the Stokes scattering matrix of randomly oriented particles, which are required as input to radiative transfer codes [34, 35, 36], can be calculated analytically in terms of the T-matrix of the scattering particles. This analytical averaging makes the T-matrix method very efficient for practical applications.

The T-matrix of a particle depends on its complex refractive index, shape, and size parameter and characterizes its light scattering properties independent of the incident field, just like a particle's mass characterizes its inertia independent of any forces. It is therefore not surprising that Mishchenko was able to express the light scattering

properties of ensembles of particles in terms of the T-matrix. The calculation of the T-matrix was initially developed by Waterman in order to obtain the scattered fields [13]. But since the final goal here is to compute optical properties of ensembles of particles. the calculation of the T-matrix will be considered the primary objective of the single scattering effort. The T-matrix depends also on the orientation of the particle with respect to the laboratory frame and on the choice of vector expansion functions. Since the EBCM has so far been confined to the use of spherical vector functions. as pointed out above. the goal of this work is to overcome the resulting limitations of the EBCM in terms of the aspect ratio of spheroidal particles by calculating the $\mathcal{T}$-matrix in spheroidal coordinates (denoted by a caligraphic $\mathcal{T}$) using the SVM.

2.3 The $\mathcal{T}$-matrix in spheroidal coordinates

2.3.1 Vector spheroidal functions with an azimuthal dependency of definite parity

Asano and Yamamoto chose vector spherical functions of definite azimuthal parity. i.e. with the o-dependence contained in sine and cosine functions rather than in complex exponentials. The $\mathcal{T}$-matrix in the basis of vector spheroidal functions with a definite o-parity will now be defined as a preparation for deriving the $\mathcal{T}$-matrix in this basis.

One expands the incident and scattered fields in the form

$$\mathbf{E}^i = \sum_{\sigma=e,o} \sum_{n=1}^{\infty} \sum_{m=-n}^{n} [a^{(1)}_{\sigma,n,m} \mathbf{V}^{(1)}_{\sigma,n,m} + a^{(2)}_{\sigma,n,m} \mathbf{W}^{(1)}_{\sigma,n,m}] \tag{2.61}$$

$$\mathbf{E}^s = \sum_{\sigma=e,o} \sum_{n=1}^{\infty} \sum_{m=-n}^{n} [\kappa^{(1)}_{\sigma,n,m} \mathbf{V}^{(3)}_{\sigma,n,m} + \kappa^{(2)}_{\sigma,n,m} \mathbf{W}^{(3)}_{\sigma,n,m}] \tag{2.62}$$

where $\mathbf{V}^{(j)}_{\sigma n m}$ and $\mathbf{W}^{(j)}_{\sigma n m}$. $j = 1.3$ are the vector spheroidal wave functions defined in Section 2.2.1. By the same argument as used when defining the T-matrix in spherical coordinates. there must be a linear relation between the incident and scattered field

coefficients. the so-called $\mathcal{T}$-matrix relation

$$\kappa^{(k)}_{\sigma.n.m} \;=\; \sum_{\sigma'=e.o}\sum_{k'=1}^{2}\sum_{n'=1}^{\infty}\sum_{m'=-n}^{n} \mathcal{T}^{(k,k')}_{\sigma.n.m.\sigma'.n'.m'}\, a^{(k')}_{\sigma'.n'.m'}. \tag{2.63}$$

This relation defines the $\mathcal{T}$-matrix in spheroidal coordinates. The $\mathcal{T}$-matrix represents a linear transformation in the space of the coefficient vectors which transforms the coefficient vector of the incident field into that of the scattered field. The crucial idea underlying this section is that any linear transformation can be *unambiguously* characterized by specifying how it acts on a set of chosen basis vectors. i.e. for a given choice of basis vectors one can find an unambiguous explicit matrix representation of a linear transformation. Thus. in order to find the desired matrix representation of electromagnetic scattering in spheroidal coordinates. one needs to specify a set of basis vectors in the space of the coefficient vectors. for instance the canonical basis. with the jth canonical basis vector having components

$$(a^{(k)}_{\sigma.n.m})_j \;=\; \delta_{\sigma.\sigma_j}\,\delta_{n.n_j}\,\delta_{m.m_j}\,\delta_{k.k_j}. \tag{2.64}$$

$$\sigma_j \;=\; \epsilon.o$$

$$k_j \;=\; 1.2$$

$$m_j \;=\; 0.1....$$

$$n_j \;=\; m_j.m_j+1....$$

where $\delta_{p.q}$ is the Kronecker-delta. Then from (2.63)

$$\mathcal{T}^{(k,k_j)}_{\sigma.n.m.\sigma_j.n_j.m_j} \;=\; (\kappa^{(k)}_{\sigma.n.m})_j. \tag{2.65}$$

In other words. the $\mathcal{T}$-matrix is just a matrix representation of a linear transformation in the explicit canonical basis given in (2.64). The practical implication of the choice of basis vectors can be seen by substituting (2.64) into (2.61) to obtain

$$\mathbf{E}^i_j \;=\; \begin{cases} \mathbf{V}^{(1)}_{\sigma_j n_j m_j} & : \;\; \text{if } k_j = 1 \\ \mathbf{W}^{(1)}_{\sigma_j n_j m_j} & : \;\; \text{if } k_j = 2. \end{cases} \tag{2.66}$$

So instead of using plane waves as incident fields. as was done by Asano and Yamamoto [19]. the basis functions $\mathbf{V}_{\sigma nm}^{(1)}$ and $\mathbf{W}_{\sigma nm}^{(1)}$ of various orders. degrees. and of both parities are used here as incident fields. The electromagnetic scattering problem can. using the SVM together with these basis functions. be reduced to solving a system of linear equations (see Eq. (2.50) in Section 2.2.3). which directly yields the $\mathcal{T}$-matrix in the basis of spheroidal functions with definite σ-parity.

Although it may be less appealing to intuition to use the vector spheroidal wave functions as incident waves instead of plane waves. this approach is more pragmatic. One argument in favor of using plane waves is that any arbitrary wave can be expressed as a superposition of plane waves propagating in different directions. When using the SVM. each plane wave must. however. be expanded in terms of the vector spheroidal functions with appropriate expansion coefficients (given in Section 2.2.3 by Eqs. (2.42) and (2.43)). It is therefore a more direct approach to use these vector functions instead of plane waves as basis functions. Besides. when using the incident plane wave coefficients in (2.42) and (2.43). the whole SVM computation of the solution to the scattering problem has to be repeated for each new angle of incidence. In the approach presented here. the $\mathcal{T}$-matrix is computed once and for all. Thus. for any arbitrary wave incident at any angle and specified in terms of its coefficients $a_{\sigma,n,m}^{(k)}$. the scattered field can immediately be computed from (2.63) and (2.62) without having to repeat the SVM procedure. Also. the particular choice of basis in (2.64) in place of the plane wave expansion coefficients in (2.42) and (2.43) simplifies (on account of the Kronecker-delta in n) the system of linear equations in (2.50) that results from using Asano and Yamamoto's implementation of the SVM.

Equations (2.63)-(2.66) lay out the basic idea of the method developed here. In order to make use of Asano and Yamamoto's work. and in particular their computer implementation. one has to translate the basic idea outlined above into the conventions chosen by these authors by comparing Eqs. (2.61) and (2.62) to Asano and Yamamoto's only slightly differently defined incident and scattered fields in the TE and TM mode.

Eqs. (2.40). (2.41). (2.44). and (2.46). For the incident field. Eqs. (2.40). (2.41). one has to replace the plane wave expansion coefficients Eqs. (2.42) and (2.43) by

(a) TE – mode. $f_{n,m}^{(1)} = 0.$ $f_{n,m}^{(2)} = i^{-n_0} \delta_{n,n_0} \delta_{m,m_0}$ (2.67)

(corresponds to $\mathbf{E}^i = \mathbf{V}_{e,n_0,m_0}^{(1)}$)

(b) TM – mode. $f_{n,m}^{(1)} = i^{-n_0} \delta_{n,n_0} \delta_{m,m_0}.$ $f_{n,m}^{(2)} = 0$ (2.68)

(corresponds to $\mathbf{E}^i = \mathbf{V}_{c,n_0,m_0}^{(1)}$)

(c) TM – mode. $f_{n,m}^{(1)} = 0.$ $f_{n,m}^{(2)} = -i^{-(n_0+1)} \delta_{n,n_0} \delta_{m,m_0}$ (2.69)

(corresponds to $\mathbf{E}^i = \mathbf{W}_{e,n_0,m_0}^{(1)}$)

(d) TE – mode. $f_{n,m}^{(1)} = i^{-(n_0+1)} \delta_{n,n_0} \delta_{m,m_0}.$ $f_{n,m}^{(2)} = 0$ (2.70)

(corresponds to $\mathbf{E}^i = \mathbf{W}_{o,n_0,m_0}^{(1)}$).

The system of linear equations (2.50) is then solved for several degrees m_0 and for several orders n_0. Comparing the considerations in (2.61)–(2.65) to the formulation (2.44) and (2.46) in Asano and Yamamoto's method. one obtains the following correspondence between the elements of the solution vector $\mathbf{x}_k(m_0)$ in (2.50) and the $\mathcal{T}$-matrix elements in the four cases (2.67)–(2.70):

(a) $i^n \pi_{1,n,m_0}^{(2)}$ $= \mathcal{T}_{e,n,m_0,e,n_0,m_0}^{(1,1)}$ (2.71)

$i^{n+1} \pi_{1,n,m_0}^{(1)}$ $= \mathcal{T}_{o,n,m_0,e,n_0,m_0}^{(2,1)}$ (2.72)

(b) $i^n \pi_{2,n,m_0}^{(1)}$ $= \mathcal{T}_{o,n,m_0,o,n_0,m_0}^{(1,1)}$ (2.73)

$-i^{n+1} \pi_{2,n,m_0}^{(2)}$ $= \mathcal{T}_{e,n,m_0,o,n_0,m_0}^{(2,1)}$ (2.74)

(c) $i^n \pi_{2,n,m_0}^{(1)}$ $= \mathcal{T}_{o,n,m_0,e,n_0,m_0}^{(1,2)}$ (2.75)

$-i^{n+1} \pi_{2,n,m_0}^{(2)}$ $= \mathcal{T}_{e,n,m_0,e,n_0,m_0}^{(2,2)}$ (2.76)

(d) $i^n \pi_{1,n,m_0}^{(2)}$ $= \mathcal{T}_{e,n,m_0,o,n_0,m_0}^{(1,2)}$ (2.77)

$i^{n+1} \pi_{1,n,m_0}^{(1)}$ $= \mathcal{T}_{o,n,m_0,o,n_0,m_0}^{(2,2)}.$ (2.78)

These are all the $\mathcal{T}$-matrix elements. Thus. one can see that the $\mathcal{T}$-matrix in spheroidal

coordinates is diagonal in m. just like in spherical coordinates [32]. i.e.

$$T^{(k,k')}_{\sigma,n,m,\sigma',n',m'} = \delta_{m,m'} \, T^{(k,k')}_{\sigma,n,m,\sigma',n',m}. \tag{2.79}$$

Also.

$$T^{(1,1)}_{e,n,m,o,n',m} = T^{(1,1)}_{o,n,m,e,n',m} = T^{(2,2)}_{e,n,m,o,n',m} = T^{(2,2)}_{o,n,m,e,n',m}$$

$$= T^{(1,2)}_{enmen'm} = T^{(1,2)}_{onmon'm} = T^{(2,1)}_{enmen'm} = T^{(2,1)}_{onmon'm} = 0 \tag{2.80}$$

$$\forall \quad n, m, n'.$$

The solution of each system of linear equations to given n_0 and m_0 yields the T-matrix elements (2.71)–(2.78). Thus. if the T-matrix is to be determined for $m = 0. \ldots. M$ and $n = m. \ldots. N$. one needs to solve $\sum_{m=0}^{M}(N - m + 1)$ systems of linear equations.

2.3.2 Vector spheroidal wave functions with an exponential o-dependency

Instead of the vector functions (2.32). (2.33). one may choose an exponential o-dependency according to Eqs. (2.30) and (2.31). Eventually. the plan is to apply Mishchenko's procedure for analytically averaging over orientational angles in the computation of optical properties. The formulation of this method is more concise when using an exponential o-dependence. If the fields are expanded in this exponential basis. i.e.

$$\mathbf{E}^i = \sum_{n=0}^{\infty} \sum_{m=-n}^{n} [\mathcal{J}^{(1)}_{n,m} \mathbf{V}^{(1)}_{n,m} + \mathcal{J}^{(2)}_{n,m} \mathbf{W}^{(1)}_{n,m}] \tag{2.81}$$

$$\mathbf{E}^s = \sum_{n=0}^{\infty} \sum_{m=-n}^{n} [\rho^{(1)}_{n,m} \mathbf{V}^{(3)}_{n,m} + \rho^{(2)}_{n,m} \mathbf{W}^{(3)}_{n,m}] \tag{2.82}$$

then the corresponding T-matrix is defined by the relation

$$\rho^{(k)}_{n,m} = \sum_{k'=1}^{2} \sum_{n'=0}^{\infty} \sum_{m'=-n'}^{n'} T^{(k,k')}_{n,m,n',m'} \mathcal{J}^{(k')}_{n',m'}. \tag{2.83}$$

The transformation of the coefficients from the basis with definite o-parity into the one with an exponential o-dependence is given by (2.37)–(2.39). From this. the transforma-

tion of the $\mathcal{T}$-matrix can be inferred:

$$\mathcal{T}^{(k,k')}_{n,m,n',m'} = \frac{1}{2}[\mathcal{T}^{(k,k')}_{e,n,m,e,n',m'} + i\mathcal{T}^{(k,k')}_{e,n,m,o,n',m'}$$
$$- i\mathcal{T}^{(k,k')}_{o,n,m,e,n',m'} + \mathcal{T}^{(k,k')}_{o,n,m,o,n',m'}] \tag{2.84}$$

$$\mathcal{T}^{(k,k')}_{n,-m,n',m'} = \frac{(-1)^m}{2}[\mathcal{T}^{(k,k')}_{e,n,m,e,n',m'} + i\mathcal{T}^{(k,k')}_{e,n,m,o,n',m'}$$
$$+ i\mathcal{T}^{(k,k')}_{o,n,m,e,n',m'} - \mathcal{T}^{(k,k')}_{o,n,m,o,n',m'}] \tag{2.85}$$

$$\mathcal{T}^{(k,k')}_{n,m,n',-m'} = \frac{(-1)^{m'}}{2}[\mathcal{T}^{(k,k')}_{e,n,m,e,n',m'} - i\mathcal{T}^{(k,k')}_{e,n,m,o,n',m'}$$
$$- i\mathcal{T}^{(k,k')}_{o,n,m,e,n',m'} - \mathcal{T}^{(k,k')}_{o,n,m,o,n',m'}] \tag{2.86}$$

$$\mathcal{T}^{(k,k')}_{n,-m,n',-m'} = \frac{(-1)^{m+m'}}{2}[\mathcal{T}^{(k,k')}_{e,n,m,e,n',m'} - i\mathcal{T}^{(k,k')}_{e,n,m,o,n',m'}$$
$$+ i\mathcal{T}^{(k,k')}_{o,n,m,e,n',m'} + \mathcal{T}^{(k,k')}_{o,n,m,o,n',m'}] \tag{2.87}$$

for $m > 0$. For $m = m' = 0$, one simply has

$$\mathcal{T}^{(k,k')}_{n,0,n',0} = \mathcal{T}^{(k,k')}_{e,n,0,e,n',0}. \tag{2.88}$$

For spheroidal particles, Eqs. (2.84)–(2.87) can be simplified with (2.79) by replacing m' by m. One can then see from these equations, using (2.80), that

$$\mathcal{T}^{(k,k')}_{n,-m,n',-m} = (-1)^{k+k'} \mathcal{T}^{(k,k')}_{nmn'm}. \tag{2.89}$$

An analogous relation has been reported for the T-matrix of axially symmetric particles in spherical coordinates [32]. One also obtains from (2.79)

$$\mathcal{T}^{(k,k')}_{n,m,n',m'} = \delta_{m,m'} \mathcal{T}^{(k,k')}_{n,m,n',m}. \tag{2.90}$$

2.4 Transformation of the spheroidal $\mathcal{T}$-matrix into the spherical T-matrix

The work presented here is the first derivation and computation of the $\mathcal{T}$-matrix for electromagnetic scattering in spheroidal coordinates. Therefore, the obtained numerical results can be directly compared only to those of the EBCM. For this purpose, the

$\mathcal{T}$-matrix in spheroidal coordinates has to be transformed into the one in spherical coordinates. Furthermore, as explained in Section 2.5, the rotation of the T-matrix, which is vital for efficient handling of particles of random orientation, is more conveniently carried out in spherical coordinates.

To begin this derivation, one compares the vector spherical to the vector spheroidal wave functions. One can, without loss of generality, restrict the comparison to the far field. The radial component of the vector spherical and vector spheroidal functions vanishes in the far field. The θ- and o-components of the functions $\mathbf{V}_{n,m}^{(3)}$ and $\mathbf{M}_{n,m}^{(3)}$, for instance, show the following asymptotic behavior:

$$V_{n,m:\eta}^{(3)} \longrightarrow -(-i)^{n+1} \frac{imS_{n,m}(c;\theta)}{\sin\theta} \frac{e^{ikr}}{kr} e^{imo} \tag{2.91}$$

$$V_{n,m:o}^{(3)} \longrightarrow -(-i)^{n+1} \frac{dS_{n,m}(c;\theta)}{d\theta} \frac{e^{ikr}}{kr} e^{imo} \tag{2.92}$$

and

$$M_{n,m:\theta}^{(3)} \longrightarrow (-i)^{n+1} \gamma_{n,m} \frac{imP_n^{(m)}(\theta)}{\sin\theta} \frac{e^{ikr}}{kr} e^{imo} \tag{2.93}$$

$$M_{n,m:o}^{(3)} \longrightarrow -(-i)^{n+1} \gamma_{n,m} \frac{dP_n^{(m)}(\theta)}{d\theta} \frac{e^{ikr}}{kr}. e^{imo} \tag{2.94}$$

where an extra factor $\gamma_{n,m}$ has been added in the vector spherical functions, for which many authors use the convention

$$\gamma_{n,m} = \sqrt{\frac{2n+1}{4\pi n(n+1)} \frac{(n-m)!}{(n+m)!}}. \tag{2.95}$$

From (2.7), it follows that $V_{n,m:\eta}^{(3)} = -V_{n,m:\theta}^{(3)}$. Thus, substitution of (2.15) into (2.91) and use of (2.93) yields

$$-V_{n,m:\eta}^{(3)} = V_{n,m:\theta}^{(3)} = (-i)^n \sum_{r=0,1}^{\infty}{}' \frac{i^{|m|+r}}{\gamma_{|m|+r,m}} d_r^{(m,n)}(c) M_{|m|+r,m:\theta}^{(3)}. \tag{2.96}$$

As before, the primed sum goes over even (odd) values of r if $(n-m)$ is even (odd). Analogous relations can be obtained for the o component of $\mathbf{V}_{n,m}^{(3)}$ and $\mathbf{M}_{n,m}^{(3)}$, as well as for the θ- and o-components of $\mathbf{W}_{n,m}^{(3)}$ and $\mathbf{N}_{n,m}^{(3)}$, and for all the corresponding functions

of the first kind. Comparison of the far field expansion of the incident field in the two sets of vector functions

$$
\begin{pmatrix} E_\xi^i \\ E_\eta^i \\ E_\phi^i \end{pmatrix} = \sum_{n,m} \left[a_{n,m}^{(1)} \begin{pmatrix} 0 \\ V_{n,m:\eta}^{(1)} \\ V_{n,m:\phi}^{(1)} \end{pmatrix} + a_{n,m}^{(2)} \begin{pmatrix} 0 \\ W_{n,m:\eta}^{(1)} \\ W_{n,m:\phi}^{(1)} \end{pmatrix} \right] = \begin{pmatrix} E_r^i \\ -E_\theta^i \\ E_\phi^i \end{pmatrix}
$$

$$(2.97)$$

and

$$
\begin{pmatrix} E_r^i \\ E_\theta^i \\ E_\phi^i \end{pmatrix} = \sum_{n,m} \left[a_{n,m}^{(1)} \begin{pmatrix} 0 \\ M_{n,m:\theta}^{(1)} \\ M_{n,m:\phi}^{(1)} \end{pmatrix} + a_{n,m}^{(2)} \begin{pmatrix} 0 \\ N_{n,m:\theta}^{(1)} \\ N_{n,m:\phi}^{(1)} \end{pmatrix} \right]
$$

$$(2.98)$$

yields with the relation analogous to (2.96) between the components of the vector functions

$$
\sum_{n=1}^{\infty} \sum_{m=-n}^{n} [a_{n,m}^{(1)} \mathbf{M}_{n,m}^{(1)} + a_{n,m}^{(2)} \mathbf{N}_{n,m}^{(1)}]
$$
$$
= \sum_{n=0}^{\infty} \sum_{m=-n}^{n} \sum_{q=|m|,|m|+1}^{\infty}{}' \frac{i^{q-n}}{\gamma_{q,m}} d_{q-|m|}^{(m,n)}(c) [a_{n,m}^{(1)} \mathbf{M}_{q,m}^{(1)} + a_{n,m}^{(2)} \mathbf{N}_{q,m}^{(1)}].
$$

$$(2.99)$$

After reordering of summation. renaming of indices. and comparing equal orders and degrees. one obtains

$$
a_{n,m}^{(k)} = \sum_{s=|m|,|m|+1}^{\infty}{}' \frac{i^{n-s}}{\gamma_{n,m}} d_{n-|m|}^{ms}(c) \, a_{s,m}^{(k)}.
$$

$$(2.100)$$

or with (2.95) and (2.20)

$$
a_{n,m}^{(k)} = \sum_{s=|m|}^{\infty} i^{n-s} \sqrt{2\pi n(n+1) N_{m,s}} \, f_{n-|m|}^{m,s} \, a_{s,m}^{(k)}.
$$

$$(2.101)$$

where $n \geq 1$. For the sake of a more compact notation. this relation may be brought into matrix-vector notation by defining for each fixed index m the coefficient vectors

$$
\mathbf{a}^{(k)}(m) = (a_{n,m}^{(k)}) = [a_{M(m),m}^{(k)}, a_{M(m)+1,m}^{(k)} \cdots]^T
$$

$$(2.102)$$

$$
a^{(k)}(m) = (a_{n,m}^{(k)}) = [a_{|m|,m}^{(k)}, a_{|m|+1,m}^{(k)} \cdots]^T
$$

$$(2.103)$$

and transformation matrices

$$
\mathbf{G}_0(m) \;=\; \begin{pmatrix} g_{M(m),|m|}(m) & g_{M(m),|m|+1}(m) & \cdots \\ g_{M(m)+1,|m|}(m) & g_{M(m)+1,|m|+1}(m) & \cdots \\ \vdots & \vdots & \end{pmatrix}
\tag{2.104}
$$

where

$$
g_{n,s}(m) \;=\; i^{n-s}\sqrt{2\pi n(n+1)N_{m,s}}\, f_{n-|m|}^{m,s}
\tag{2.105}
$$

$$
M(m) \;=\; \max\{1,|m|\}.
\tag{2.106}
$$

Then

$$
\mathbf{a}^{(k)}(m) \;=\; \mathbf{G}_0(m)\cdot \mathbf{a}^{(k)}(m).
\tag{2.107}
$$

This can be brought into an even more compact form by summarizing the vectors of different indices m and superscripts k into coefficient super-vectors

$$
\mathbf{a} \;=\; [(a_{n,0}^{(1)}),(a_{n,1}^{(1)}),\ldots,(a_{n,0}^{(2)}),(a_{n,1}^{(2)}),\ldots]^T. \quad n=M(m),M(m)+1,\ldots
\tag{2.108}
$$

$$
\mathbf{a} \;=\; [(a_{n,0}^{(1)}),(a_{n,1}^{(1)}),\ldots,(a_{n,0}^{(2)}),(a_{n,1}^{(2)}),\ldots]^T. \quad n=|m|,|m|+1,\ldots
\tag{2.109}
$$

and analogously. one defines a block diagonal super-matrix

$$
\mathbf{G} \;=\; diag(\mathbf{G}_0(0),\mathbf{G}_0(1),\ldots,\mathbf{G}_0(0),\mathbf{G}_0(1),\ldots)
\tag{2.110}
$$

Then

$$
\mathbf{a} \;=\; \mathbf{G}\cdot \mathbf{a}
\tag{2.111}
$$

Likewise. the scattered field can be expanded in vector spherical or spheroidal wave functions with expansion coefficients $p_{n,m}^{(k)}$ and $\kappa_{n,m}^{(k)}$. respectively. and the relation between the corresponding coefficient super-vectors is

$$
\mathbf{p} \;=\; \mathbf{G}\cdot \boldsymbol{\kappa}.
\tag{2.112}
$$

One can further define a matrix $\mathbf{H}_0(m)$ with elements

$$h_{n,s}(m) = \frac{i^{n-s}}{\sqrt{2\pi s(s+1)N_{m,n}}} f_{s-|m|}^{(m,n)*}$$ (2.113)

$$n = .|m|.|m|+1....$$

$$s = M(m).M(m)+1....$$

and a corresponding block diagonal super-matrix

$$\mathbf{H} = diag(\mathbf{H}_0(0).\mathbf{H}_0(1).....\mathbf{H}_0(0).\mathbf{H}_0(1)....)$$ (2.114)

It is then straight forward to show with (2.29) that

$$\mathbf{G} \cdot \mathbf{H} = 1$$ (2.115)

where 1 is the identity matrix. The commuted product is not in all cases equal to the identity matrix. From (2.105) and (2.113), it follows that

$$\sum_{s=M(m).M(m)+1}^{\infty}{}' h_{n,s}(m)g_{s,l}(m) = \delta_{n,l}$$ (2.116)

unless $m = 0$ and n and l are both even. In this case, using (2.20) and (2.21).

$$\sum_{s=M(0).M(0)+1}^{\infty}{}' h_{n,s}(0)g_{s,l}(0)$$

$$= i^{n-l}\sqrt{\frac{N_{0,l}}{N_{0,n}}}\sum_{s=1}^{\infty}{}' f_s^{(0,n)*}(c) f_s^{(0,l)}(c)$$

$$= i^{n-l}\sqrt{\frac{N_{0,l}}{N_{0,n}}}\left\{\sum_{s=0}^{\infty}{}' f_s^{(0,n)*}(c) f_s^{(0,l)}(c) - f_0^{(0,n)*}(c) f_0^{(0,l)}(c)\right\}$$

$$= \delta_{n,l} - F_{n,l}(c;0)$$ (2.117)

where

$$F_{n,l}(c;m) = \begin{cases} i^{n-l}\sqrt{\frac{N_{0,l}}{N_{0,n}}} f_0^{(0,n)*}(c) f_0^{(0,l)}(c) & : \quad n,l \text{ even and } m = 0 \\ 0 & : \quad \text{otherwise} \end{cases}$$ (2.118)

and $M(m)$ is defined in (2.106). From the matrix $\mathbf{F}_0(m)$ with elements $F_{n,l}(c;m)$ one can again construct a super-matrix $\mathbf{F}$ analogous to (2.110) and (2.114). Equation (2.117) can then be brought into the compact form

$$\mathbf{H} \cdot \mathbf{G} \;=\; 1 - \mathbf{F}. \tag{2.119}$$

From the definition (2.118), it follows that $\mathbf{F}$ is idempotent, i.e.

$$\mathbf{F} \cdot \mathbf{F} \;=\; \mathbf{F}. \tag{2.120}$$

Furthermore, with (2.115) and (2.119),

$$\mathbf{G} \;=\; \mathbf{G} \cdot \mathbf{H} \cdot \mathbf{G} = \mathbf{G} \cdot (1 - \mathbf{F}) \tag{2.121}$$

and consequently

$$\mathbf{G} \cdot \mathbf{F} \;=\; 0. \tag{2.122}$$

Analogously, one shows that

$$\mathbf{F} \cdot \mathbf{H} \;=\; 0. \tag{2.123}$$

Now one defines

$$\mathbf{T} \;=\; \begin{pmatrix} (T^{(1,1)}_{n,m,n',m'}) & (T^{(1,2)}_{n,m,n',m'}) \\ (T^{(2,1)}_{n,m,n',m'}) & (T^{(2,2)}_{n,m,n',m'}) \end{pmatrix} \tag{2.124}$$

$$\mathcal{T} \;=\; \begin{pmatrix} (\mathcal{T}^{(1,1)}_{n,m,n',m'}) & (\mathcal{T}^{(1,2)}_{n,m,n',m'}) \\ (\mathcal{T}^{(2,1)}_{n,m,n',m'}) & (\mathcal{T}^{(2,2)}_{n,m,n',m'}) \end{pmatrix} \tag{2.125}$$

where it has already been mentioned that these two matrices are diagonal in the index m for spheroidal particles. The T-matrix relations in spherical and spheroidal coordinates can now be written in the compact form

$$\mathbf{p} \;=\; \mathbf{T} \cdot \mathbf{a} \tag{2.126}$$

$$\kappa \;=\; \mathcal{T} \cdot \alpha \tag{2.127}$$

With Eqs. (2.111). (2.112). (2.126). and (2.127). it follows that

$$\mathbf{T} = \mathbf{G} \cdot \mathcal{T} \cdot \mathbf{H}.$$ (2.128)

This is the desired transformation of the spheroidal into the spherical T-matrix. The explicit form of (2.128) is given by

$$
T^{(k,k')}_{n_1,m,n_2,m} =
$$
$$
i^{n_1-n_2} \sqrt{\frac{n_1(n_1+1)}{n_2(n_2+1)}}
$$
$$
\times \sum_{n=|m|,|m|+1}^{\infty}{}' \sum_{n'=|m|,|m|+1}^{\infty}{}' \sqrt{\frac{N_{m,n}}{N_{m,n'}}} \; i^{n'-n} \; f^{(m,n)}_{n_1-|m|}(c) \; f^{(m,n')*}_{n_2-|m|}(c) \; T^{(k,k')}_{n,m,n',m}
$$
(2.129)

After determining the spheroidal $\mathcal{T}$-matrix with the SVM as outlined in Section 2.3 and transforming it according to (2.129). the results of the SVM computation can be directly compared to the results of the computation of the spherical T-matrix with the EBCM. The usefulness of (2.129) is. however. not limited to allowing direct comparisons of results. The spherical functions are more practical for averaging analytically over orientation according to Mishchenko's method than any other set of functions including the spheroidal functions. The reason for this is explained in Section 2.5. Thus. the ill-conditioning of the EBCM for particles of higher aspect ratios can be circumvented with the SVM in the appropriate spheroidal coordinate system. while Mishchenko's method can still be applied for computing optical properties after transforming into the spherical coordinate system. The extra computer time necessary for the transformation (2.129) is negligible. especially since the coefficients in (2.129) have already been determined as part of the separation of variables solution.

2.5 Rotations of the coordinate system

In order to efficiently handle ensembles of randomly oriented particles. one needs to know how to transform the T-matrix under rotations. A unitary representation of the

rotation group $SO(3)$ is given by $\hat{U}(\vec{o}) = \exp(-i\mathbf{J}\cdot\vec{o})$, where $\mathbf{J}$ denotes the angular momentum operator, and $\vec{o}$ is a vector whose norm is equal to the rotation angle, and whose direction indicates the axis and the sense of rotation. Every general rotation can be decomposed into three rotations about the Euler angles α, β, γ. The corresponding representation of the $SO(3)$ is

$$\hat{U}(\alpha,\beta,\gamma) = e^{-iJ_z\alpha} e^{-iJ_y\beta} e^{-iJ_z\gamma}. \tag{2.130}$$

If applied to a vector field $\mathbf{P}(\mathbf{r})$, a rotation generally transforms both the field vector and the position vector in the argument of the function, i.e.

$$\hat{U}\mathbf{P}(\mathbf{r}) = \mathbf{P}'(\mathbf{r}'). \tag{2.131}$$

However, since the rotation operator commutes with the curl operator [50, 51], the solution functions $\mathbf{V}_{n,m}^{(j)}$ and $\mathbf{W}_{n,m}^{(j)}$ of the vector Helmholtz equation, (2.30) and (2.31), and their spherical analogs $\mathbf{M}_{n,m}^{(j)}$ and $\mathbf{N}_{n,m}^{(j)}$ simply transform according to

$$\hat{U}\mathbf{M}_{n,m}^{(j)} = \hat{U}\nabla \times (\mathbf{a}\cdot v_{n,m}^{(j)})$$
$$= \nabla \times (\mathbf{a}\cdot \hat{U}v_{n,m}^{(j)}). \tag{2.132}$$

and similarly for the other vector functions. Thus the problem is reduced to investigating the transformation behavior of the scalar functions. The angular part of the spherical wave functions is related to the spherical harmonics (2.23), which are the eigenfunctions of the operators $\hat{J}_z$ and $\hat{\mathbf{J}}^2$, i.e.

$$\hat{J}_z|j,m\rangle = m|j,m\rangle \tag{2.133}$$
$$\hat{\mathbf{J}}^2|j,m\rangle = j(j+1)|j,m\rangle \tag{2.134}$$

(where the units are chosen such that $\hbar = 1$). Since $\hat{\mathbf{J}}^2$ is a scalar operator, it is invariant under rotations. Consequently, a rotation of the function $|j,m\rangle$ can not alter the corresponding eigenvalue j. Thus, a rotated eigenfunction $|j,m\rangle$ can be written as a linear combination of eigenfunctions belonging to the same quantum number j, i.e.

$$\hat{U}(\alpha,\beta,\gamma)|j,m\rangle = \sum_{m'} D_{m',m}^{(j)}(\alpha,\beta,\gamma)|j,m'\rangle. \tag{2.135}$$

Thus. the subspace of functions characterized by a fixed value of j is an invariant subspace under rotations. and one can. in fact. not find any smaller invariant subspaces. This means that the Wigner D-matrices are an irreducible representation of the $SO(3)$ in the subspace characterized by a fixed value of j. They are given by

$$D^{(j)}_{m',m}(\alpha, \beta, \gamma) = \langle j, m' | \hat{U}(\alpha, \beta, \gamma) | j, m \rangle$$
$$= e^{-im'\alpha} d^{(j)}_{m',m}(\beta) e^{-im\gamma}. \tag{2.136}$$

where (2.133) has been used. and where the Wigner d-functions

$$d^{(j)}_{m',m}(\beta) = \langle jm' | e^{-iJ_y\beta} | jm \rangle \tag{2.137}$$

must not be confused with the expansion coefficients $d_r^{(m,n)}$ of the spheroidal functions. From (2.132) and (2.135), one obtains the transformation of the vector spherical functions in terms of the Wigner D-matrices. and from this one derives the transformation of the spherical T-matrix [32. 49]:

$$T^{(k,k')}_{n,m,n',m'}(\alpha, \beta, \gamma) =$$
$$\sum_{m_1=-n}^{n} \sum_{m_2=-n'}^{n'} D^{(n)}_{m,m_1}(\alpha, \beta, \gamma) T^{(k,k')}_{n,m_1,n',m_2}(0, 0, 0) (D^{-1})^{(n')}_{m_2,m'}(\alpha, \beta, \gamma). \tag{2.138}$$

In an analogous way. one can now derive a matrix representation of the $SO(3)$ in the basis of the angular spheroidal functions (2.22) by using (2.24):

$$\hat{U}(\alpha, \beta, \gamma) | Z_{n,m} \rangle = \sum_{n',m'} \mathcal{D}^{(n',n)}_{m',m}(\alpha, \beta, \gamma) | Z_{n',m'} \rangle. \tag{2.139}$$

where

$$\mathcal{D}^{(n',n)}_{m',m}(\alpha, \beta, \gamma) = \langle Z_{n',m'} | \hat{U}(\alpha, \beta, \gamma) | Z_{n,m} \rangle$$
$$= \sum_{q=|m|,|m|+1}^{\infty}{}' f^{(m',n')*}_{q-|m'|}(c) f^{(m,n)}_{q-|m|}(c) D^{(q)}_{m',m}(\alpha, \beta, \gamma). \tag{2.140}$$

The comparison of (2.135) and (2.139) shows that there is an extra infinite summation in the transformation of the spheroidal functions. The resulting transformation of the

spheroidal $\mathcal{T}$-matrix

$$\mathcal{T}^{(k,k')}_{n,m,n',m'}(\alpha,\beta,\gamma)$$

$$= \sum_{n_1,m_1} \sum_{n_2,m_2} \mathcal{D}^{(n,n_1)}_{m,m_1}(\alpha,\beta,\gamma)\, \mathcal{T}^{(k,k')}_{n_1,m_1,n_2,m_2}(0,0,0)\, (\mathcal{D}^{-1})^{(n',n_2)}_{m_2,m'}(\alpha,\beta,\gamma)$$

$$(2.141)$$

has an extra two infinite nested summations. Therefore. while spheroidal functions are more suitable for the micro-scale of the problem. i.e. for a single particle. the spherical functions turn out to be more advantageous on the macro-scale. i.e. when dealing with ensembles of many particles in random orientation. The reason is the close relation between the spherical harmonics and the generating observable of rotations $\hat{\mathbf{J}}$ according to the eigenvalue equations (2.133) and (2.134). and the related fact that one can find invariant subspaces of finite dimension in the basis of spherical harmonics. in which the matrix representation of the $SO(3)$ is irreducible. Instead of rotating the spheroidal $\mathcal{T}$-matrix. one can first transform it into the spherical basis according to (2.129). and then use it directly in connection with Mishchenko's method for analytical orientational averaging. for which. as it has become clear. spherical functions are more practical.

2.6 Numerical model tests

In this section a direct comparison is made between results obtained with the SVM and results obtained with the EBCM. The following test cases are considered:

1. Prolate spheroids with size parameter $x = 1$ and aspect ratio $a/b = 2$

2. Oblate spheroids with size parameter $x = 1$ and aspect ratio $a/b = 2$

3. Prolate spheroids with size parameter $x = 10$ and aspect ratio $a/b = 2$

4. Oblate spheroids with size parameter $x = 10$ and aspect ratio $a/b = 2$

5. Prolate spheroids with size parameter $x = 1$ and aspect ratio $a/b = 8.33$.
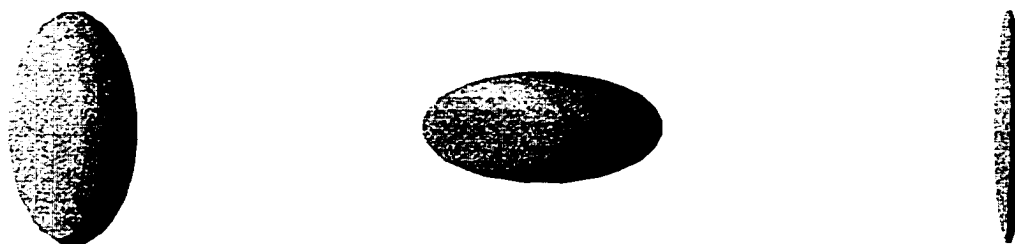
Figure 2.1. Prolate spheroids

In each of these cases the index of refraction is assumed to be $n = 1.33 + 0.05\,i$. The size parameter is defined as $x = 2\pi r_A/\lambda$. where r_A is the radius of an area-equivalent sphere and where λ is the wavelength of the incident light. Figure 2.1 shows spheroids with aspect ratios equal to the ones used in these test cases.

The accuracy of the SVM critically depends on how accurately one can compute the expansion coefficients $d_r^{(m,n)}$ from which the angular spheroidal functions are generated (cf. (2.15)). To check this, the following three preliminary tests relevant for the five test cases have been conducted:

(i) The radial spheroidal functions of the first and second kind, denoted by $R_{n,m}^{(1)}(c;\xi)$ and $R_{n,m}^{(2)}(c;\xi)$ [37]. are expanded in terms of the coefficients $d_r^{(m,n)}$. For several values of c and ξ corresponding to values of x and a/b close to those used in the five test cases. these two functions have been computed and the results have been compared to numerical values that can be found in the literature [52]. The agreement lay between 9 and 15 significant figures. The disadvantage of this testing method is that tabulated values are available only at discrete values of c and ξ. only for degrees $m = 0. 1.2$. and only for purely real and purely imaginary values of c. Thus. neither the correctness of the functions inside the scatterer. where c is complex. nor the accuracy for higher values of m. can be checked in this way.

(*ii*) The extinction cross section can be expressed in terms of the spherical T-matrix according to [3]

$$C_{ext} = -\frac{2\pi}{k^2} \operatorname{Re} \sum_{n=1}^{\infty} \sum_{m=-n}^{n} [T^{(1,1)}_{m,n,m,n} + T^{(2,2)}_{m,n,m,n}] \qquad (2.142)$$

which can be brought into the simple form

$$C_{ext} = -\frac{2\pi}{k^2} \operatorname{Re} \operatorname{Sp}(\mathbf{T}). \qquad (2.143)$$

Here Re denotes the real part. $\mathbf{T}$ is defined in (2.124). and Sp($\mathbf{T}$) denotes the trace of the spherical T-matrix. If a product of matrices appears in the argument of the trace. it is invariant under a cyclic permutation of the matrix factors. Thus. using (2.128) and (2.119). one obtains

$$\operatorname{Sp}(\mathbf{T}) = \operatorname{Sp}[(1 - \mathbf{F})\mathcal{T}] \qquad (2.144)$$

and consequently

$$C_{ext} = -\frac{2\pi}{k^2} \operatorname{Re} \operatorname{Sp}[(1 - \mathbf{F})\mathcal{T}]. \qquad (2.145)$$

As a test. one can compare numerical results for C_{ext} obtained by using the spheroidal $\mathcal{T}$-matrix in (2.145) with those obtained using the transformed spherical T-matrix in (2.143). Since the transformation in (2.128) depends on the $d_r^{(m,n)}$. this comparison provides a good practical test of the precision of the spheroidal expansion coefficients $d_r^{(m,n)}$. The results of this comparison are presented in Table 2.1. where the difference $\delta_2 C_{ext}$. defined by

$$\delta_2 C_{ext} := \frac{C_{ext}(spherical) - C_{ext}(spheroidal)}{C_{ext}(spherical)} \qquad (2.146)$$

is seen to be less than $4 \cdot 10^{-6}$ in all five test cases. These results further increase the confidence in the accuracy of the spheroidal expansion coefficients.

(*iii*) The completeness relation for the angular spheroidal functions. which can be expressed in terms of the coefficients $f_r^{(m,n)}$ (see Eq. (2.29)). which are related to

the $d_r^{(m,n)}$ by Eq. (2.20). can be used to undertake a more systematic study of the accuracy of these coefficients. One can investigate numerically to what precision this equation is satisfied for different lower indices s, t and for different degrees m. When using (2.29). one should be aware that the leading term in the set of coefficients $\{f_s^{(m,n)}\}$ is the coefficient $f_{n-|m|}^{(m,n)}$. The farther the subscript s deviates from $n - |m|$. the smaller the numerical value of the coefficient. If one checks numerically the condition

$$\sum_{n=|m|,|m|+1}^{\infty}{}' \; f_s^{(m,n)*}(c) \, f_t^{(m,n)}(c) \; = \; 0 \tag{2.147}$$

when s and t lie far apart. then the first factor will be very small when the second factor has its maximum value. and vice versa. Thus. even if this sum is close to zero when s and t lie far apart. one can not conclude very much about the precision of the coefficients $d_r^{(m,n)}$. Close attention should therefore be paid to the case $s = t$. i.e. a particularly useful numerical check is the condition

$$\sum_{n=|m|,|m|+1}^{\infty}{}' \; f_s^{(m,n)*}(c) \, f_s^{(m,n)}(c) \; = \; 1. \tag{2.148}$$

The truncation of the infinite sum should be such that the leading coefficient $f_s^{m,s+|m|}$ lies more or less in the middle of the summation interval.

The advantage of using (2.29) instead of the first testing method discussed above is that (2.29) can be used to check the accuracy of the coefficients also for complex values of c. for which no benchmark values can be found in the literature. In addition. one is not confined to discrete values of c and to low values of m. In principle. Eq. (2.21) could also be used to check the accuracy of the coefficients $d_r^{(m,n)}$. This equation expresses the normalization of the angular functions. However. since the coefficients $f_r^{(m,n)}$ contain the normalization factor $N_{m,n}$. and since the latter is computed from Eq. (2.19). which is not independent of the coefficients $d_r^{(m,n)}$. the use of (2.21) does not provide an independent test of the accuracy of the coefficients for $n = n'$. Consequently. it could only be used as an independent test for $n \neq n'$.

For this case. the same restrictions as discussed for (2.29) apply to (2.21) when s and t lie far apart.

The maximum order up to which the T-matrix and the coefficients $d_r^{(m,n)}$ are to be computed are chosen such that one obtains an accuracy in the computation of C_{ext}'. using (2.143). of at least 10^{-3}. This maximum expansion order varied from test case to test case. In each case. the coefficients $d_r^{(m,n)}$ or $f_r^{(m,n)}$ where tested up to the highest necessary order against (2.29). The observed agreement typically lay between 10^{-8} and 10^{-13}. but coefficients corresponding to complex values of c were consistently less accurate than those corresponding to real values.

For the five test cases of different shape and size. the T-matrix and optical properties were obtained using an existing SVM code based on the method of Asano and Yamamoto [19]. The code was modified by replacing the plane wave expansion coefficients in (2.42) and (2.43) by appropriate Kronecker-deltas (cf. (2.67)-(2.70)) so that the incoming waves become the vector spheroidal wave functions (as explained earlier). The solutions obtained in this manner are related to the desired $\mathcal{T}$-matrix (see (2.71)-(2.78) and (2.84) in connection with (2.79) and (2.89). as well as (2.88)). The spheroidal $\mathcal{T}$-matrix is transformed into the T-matrix in the spherical basis by using (2.129). Thus. the T-matrix in spherical coordinates obtained by transforming the $\mathcal{T}$-matrix computed in spheroidal coordinates by use of the SVM can be directly compared to the T-matrix obtained by use of the EBCM. To compute the latter. the EBCM routines contained in Mishchenko's T-matrix code have been used. Optical properties of an ensemble of randomly oriented particles. such as the extinction and scattering coefficients. the asymmetry parameter. and the scattering matrix were obtained by using Mishchenko's analytical procedure for orientational averaging. which is also contained in his T-matrix code package. The optical properties were calculated using both the T-matrix obtained with the SVM and the one obtained with the EBCM. and the results were compared.

For mildly aspherical particles. such as those in cases 1-4 with an aspect ratio of 2. one expects the EBCM to give fairly accurate results. so that direct comparisons

Table 2.1. Comparison SVM/EBCM

Case	1	2	3	4	5
$\delta \bar{T}(\text{abs})$	$5 \cdot 10^{-9}$	$2 \cdot 10^{-8}$	$3 \cdot 10^{-7}$	$4 \cdot 10^{-7}$	$5 \cdot 10^{-6}$
C'_{ext}	0.616701	0.599952	847.401	848.229	0.255740
C'_{sca}	0.227482	0.219721	547.401	556.409	0.219721
$\langle \cos\theta \rangle$	0.19031	0.18657	0.90125	0.90722	0.22005
$\delta_1 C'_{ext}$	$4 \cdot 10^{-7}$	$5 \cdot 10^{-6}$	$3 \cdot 10^{-6}$	$3 \cdot 10^{-3}$	$1 \cdot 10^{-2}$
$\delta_1 C'_{sca}$	$2 \cdot 10^{-8}$	$1 \cdot 10^{-6}$	$2 \cdot 10^{-6}$	$1 \cdot 10^{-3}$	$3 \cdot 10^{-2}$
$\delta_1 \langle \cos\theta \rangle$	$2 \cdot 10^{-8}$	$2 \cdot 10^{-6}$	$2 \cdot 10^{-6}$	$1 \cdot 10^{-3}$	$8 \cdot 10^{-2}$
$\delta_2 C'_{ext}$	$2 \cdot 10^{-8}$	$4 \cdot 10^{-6}$	$2 \cdot 10^{-6}$	$3 \cdot 10^{-6}$	$8 \cdot 10^{-11}$

of results from both methods should show a reasonably good agreement. In case 5. a prolate spheroid with an aspect ratio of 8.33 and a size parameter of 1 is investigated. The purpose of test case 5 is to make a comparison of both methods for spheroids departing farther from spherical shape.

The first row of Table 2.1 shows for the five test cases the average absolute difference $\delta \bar{T}$ between the T-matrix elements obtained with the EBCM and the SVM. The next three rows show the extinction and scattering cross section. C'_{ext}. C'_{sca}. and the asymmetry factor. $\langle \cos\theta \rangle$. computed with the SVM and Mishchenko's procedure for orientational averaging. The unit of the cross sections is μm^2. The following three rows show the relative deviation between these quantities and the corresponding results obtained with the EBCM. Thus, for instance.

$$\delta_1 C'_{ext} \quad := \quad \frac{C'_{ext}(SVM) - C'_{ext}(EBCM)}{C'_{ext}(SVM)} \tag{2.149}$$

and analogous expressions pertain to $\delta_1 C'_{sca}$ and $\delta_1 \langle \cos\theta \rangle$. The last row shows $\delta_2 C'_{ext}$ as defined in (2.146).

One can see that the agreement between the two methods is remarkably good for cases 1–3. In case 4. the agreement is of the same order as the required accuracy of

10^{-3}, whereas in case 5, the agreement is an order of magnitude below the required accuracy.

For an ensemble of randomly oriented particles with a plane of symmetry, the Stokes scattering matrix, which connects the scattered field Stokes vector to the incident field Stokes vector, is of the form [53]:

$$
\mathbf{F}_s(\Theta) \; = \; \begin{pmatrix} F_{11} & F_{12} & 0 & 0 \\ F_{12} & F_{22} & 0 & 0 \\ 0 & 0 & F_{33} & F_{34} \\ 0 & 0 & -F_{34} & F_{44} \end{pmatrix}.
\tag{2.150}
$$

Figure 2.2 shows the elements of the scattering matrix, computed with the SVM and the EBCM and Mishchenko's averaging procedure, for case 1. The curves are indistinguishable. Figure 2.3 shows the absolute difference between the elements of the scattering matrix obtained with the SVM and the EBCM in test case 1. Figures 2.4–2.11 depict analogous plots for test cases 2–5. By comparing Fig. 2.3 to Fig. 2.7 and Fig. 2.5 to Fig. 2.9, one can see that the absolute difference between the results of the two methods increases with increasing size parameter, which is in accordance to the difference of the optical properties in Table 2.1. The results for higher size parameters seem to differ more in the backscattering region (see Figs. 2.7 and 2.9). Note that the seemingly large difference of the phase functions F_{11} in Figs. 2.7 and 2.9 in the forward scattering direction is actually insignificant when expressed as a relative difference, due to the strong forward peak of the phase function (see Figs. 2.6 and 2.8 and note the logarithmic scale).

When comparing Fig. 2.3 to Fig. 2.5 and Fig. 2.7 to Fig. 2.9, one observes that the agreement of results is better for prolate spheroids of an aspect ratio of 2 than for oblate spheroids of the same aspect ratio, which again can be observed also in Table 2.1. A comparison of Figs. 2.3 and 2.11 and, with the columns for cases 1 and 5 in Table 2.1, respectively, clearly shows that the agreement between the two methods is decreasing when the spheroid departs too much from spherical shape.
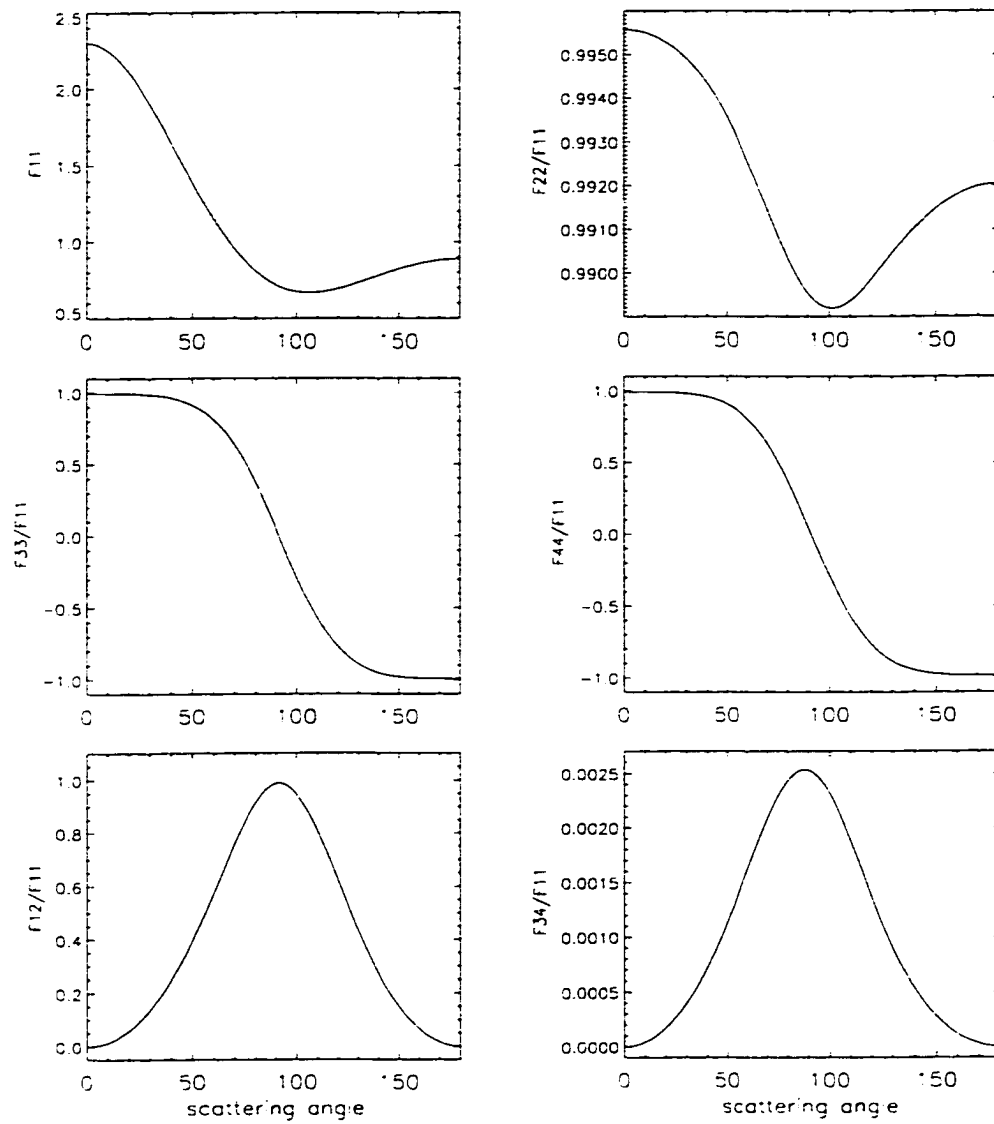
Figure 2.2. Stokes Scattering matrix for test case 1
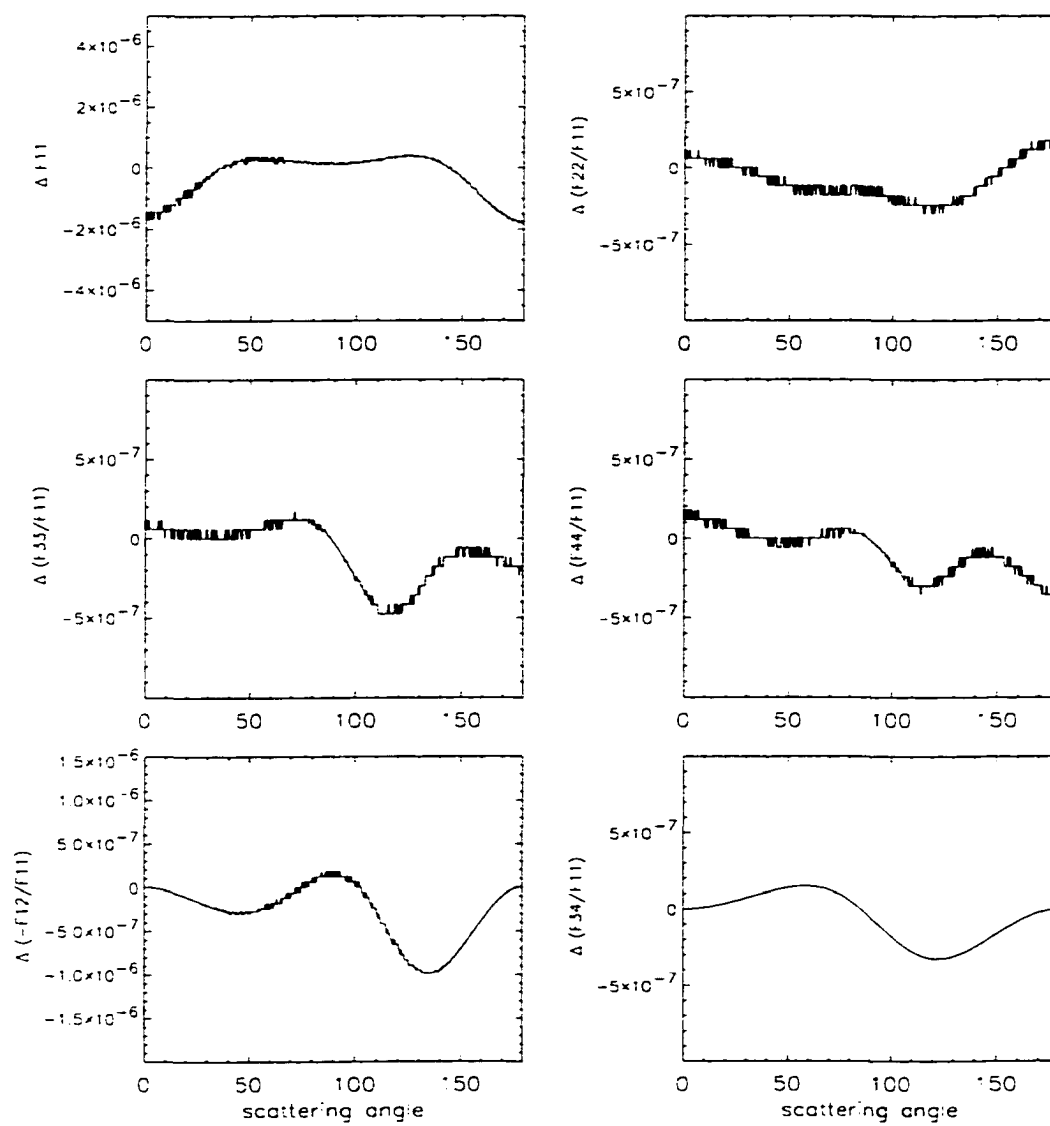
Figure 2.3. Difference between elements of the Stokes Scattering matrix in test case 1
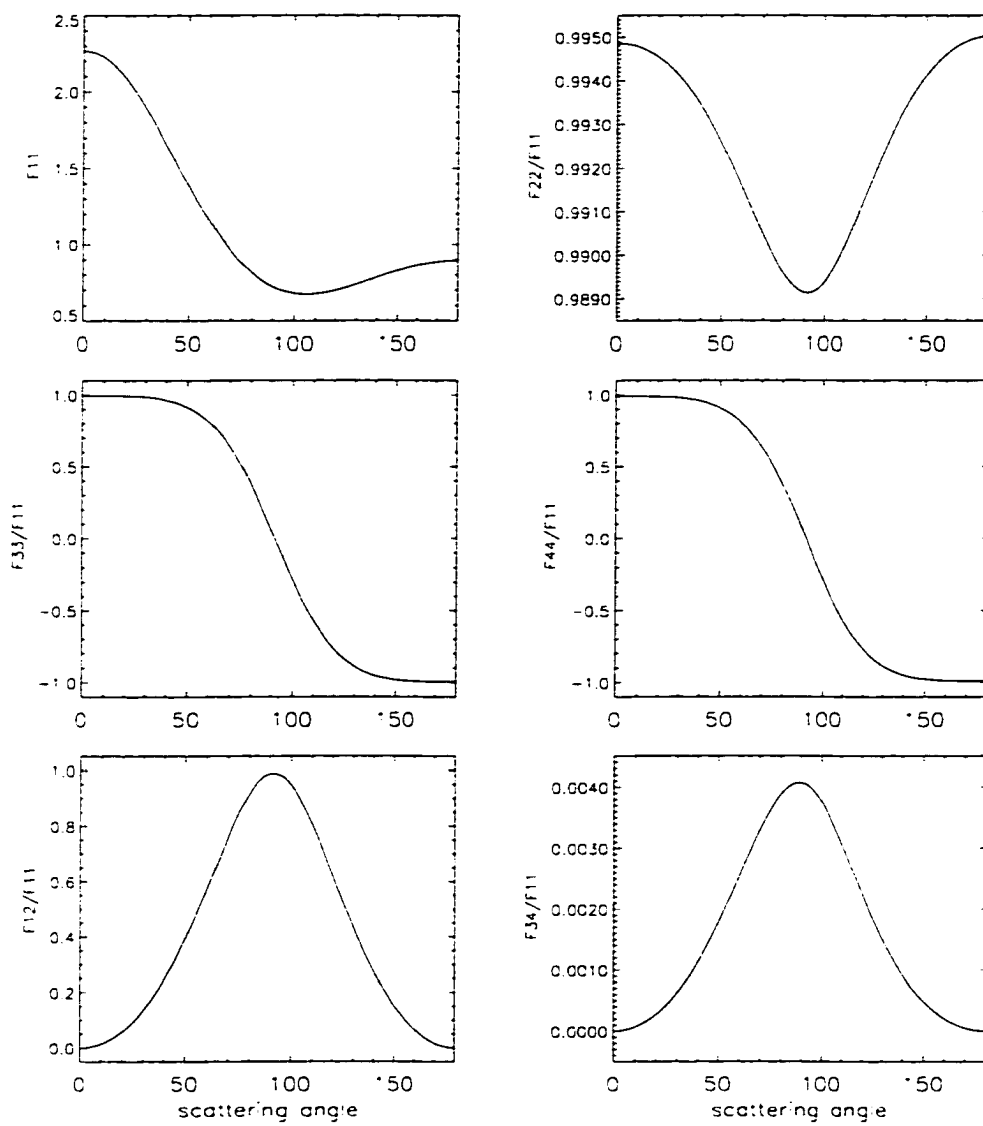
Figure 2.4. As Figure 2.2. but for test case 2.
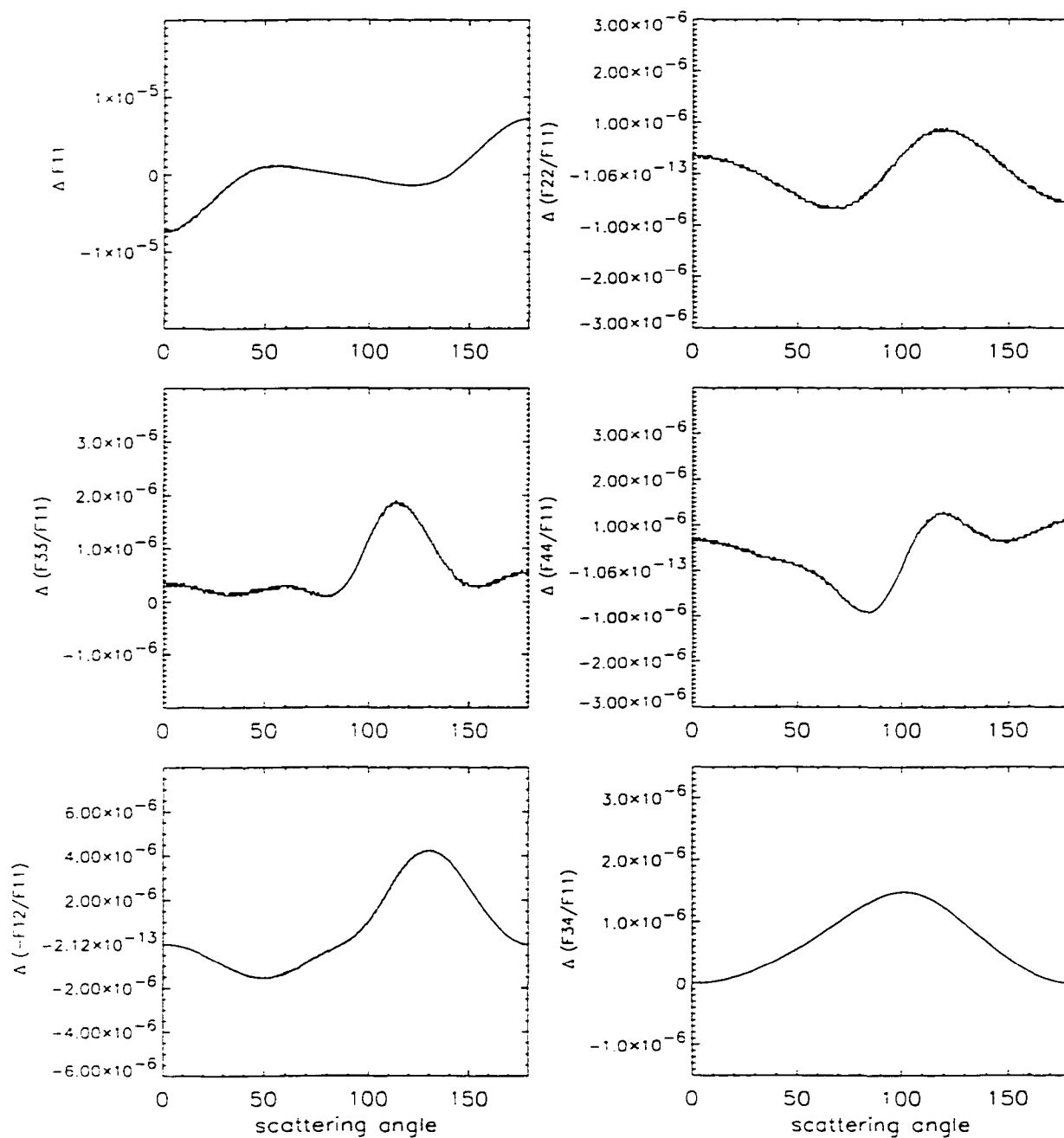
Figure 2.5. As Figure 2.3, but for test case 2.
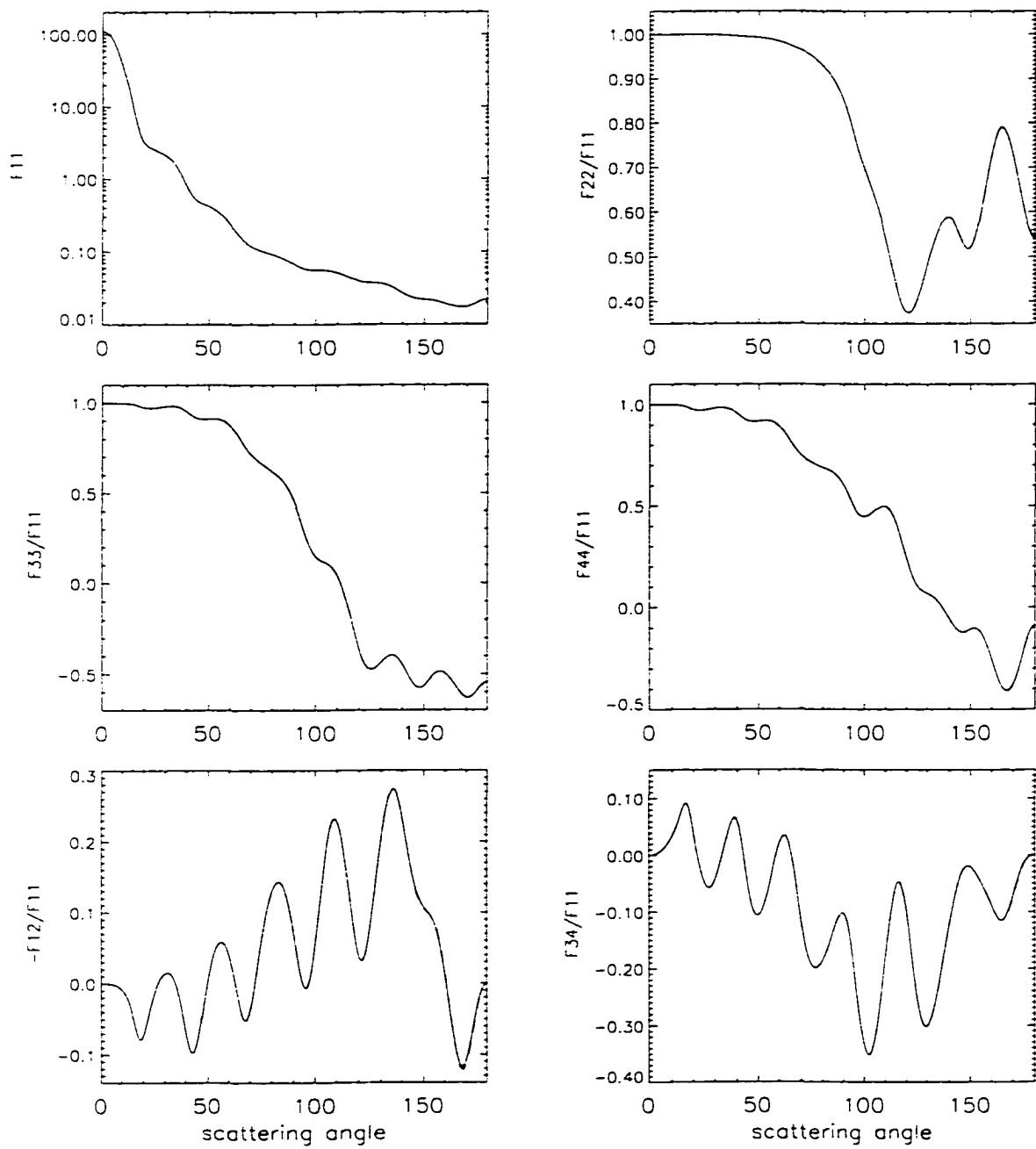
Figure 2.6. As Figure 2.2. but for test case 3.
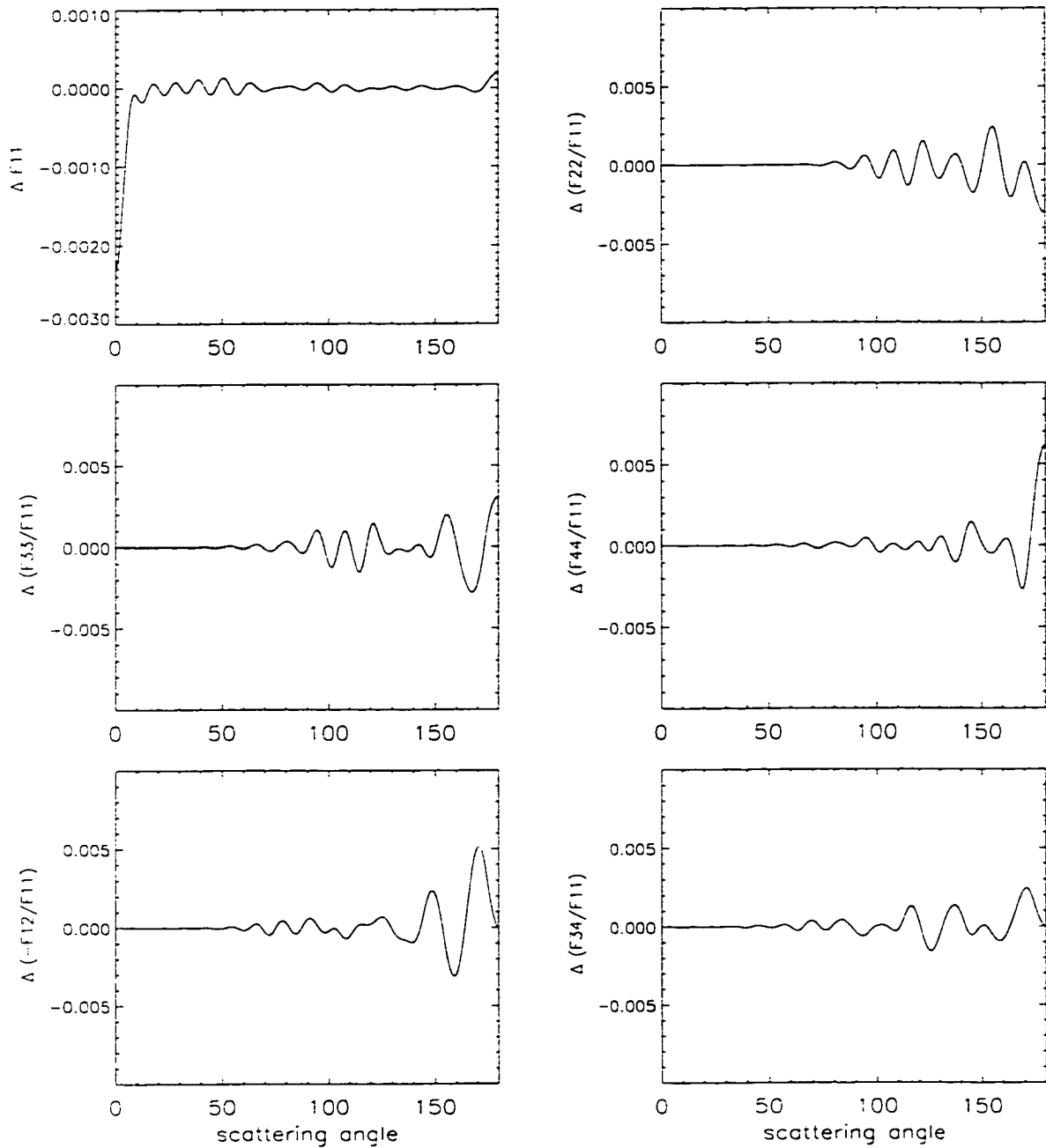
Figure 2.7. As Figure 2.3, but for test case 3.
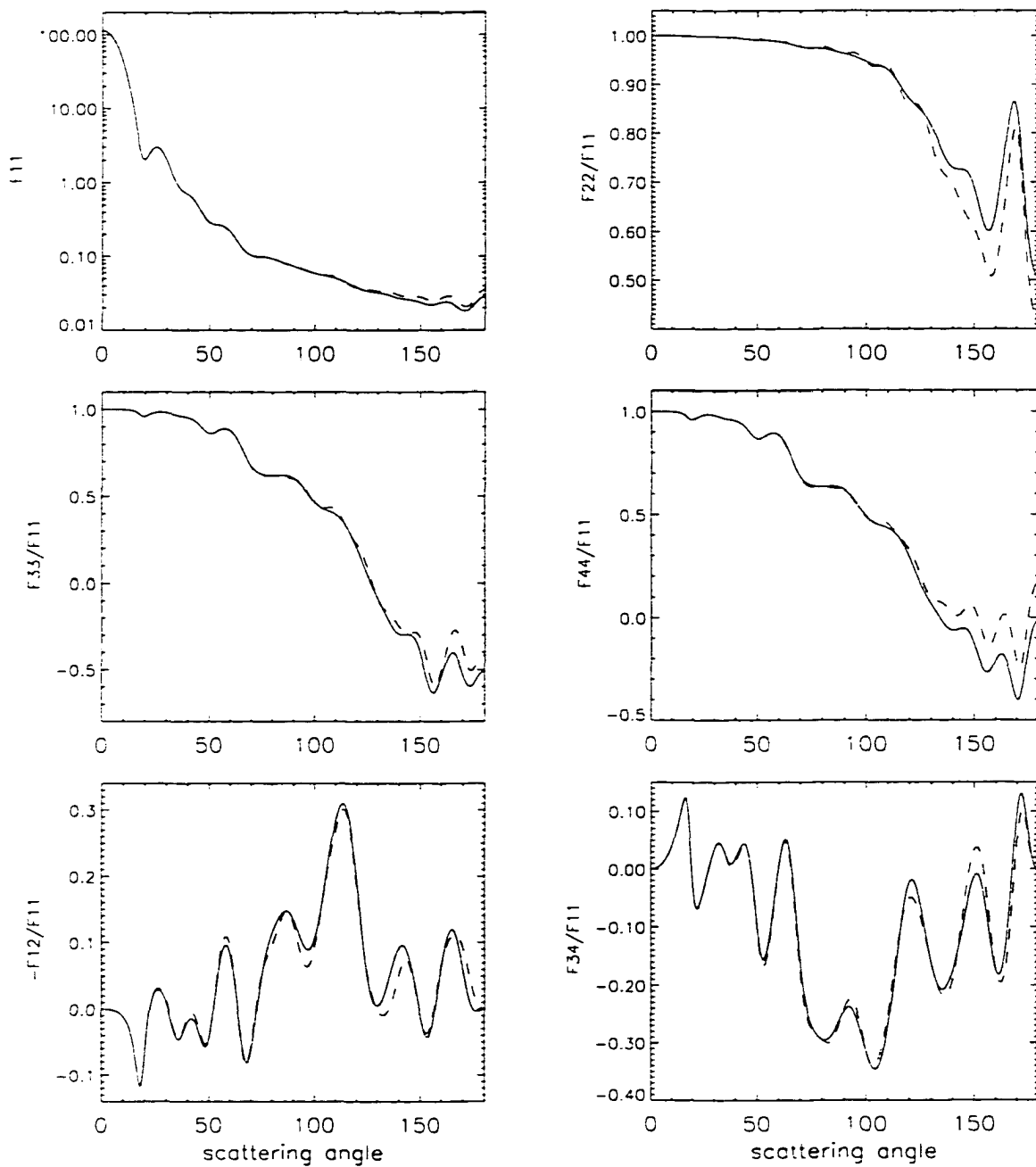
Figure 2.8. As Figure 2.2. but for test case 4.
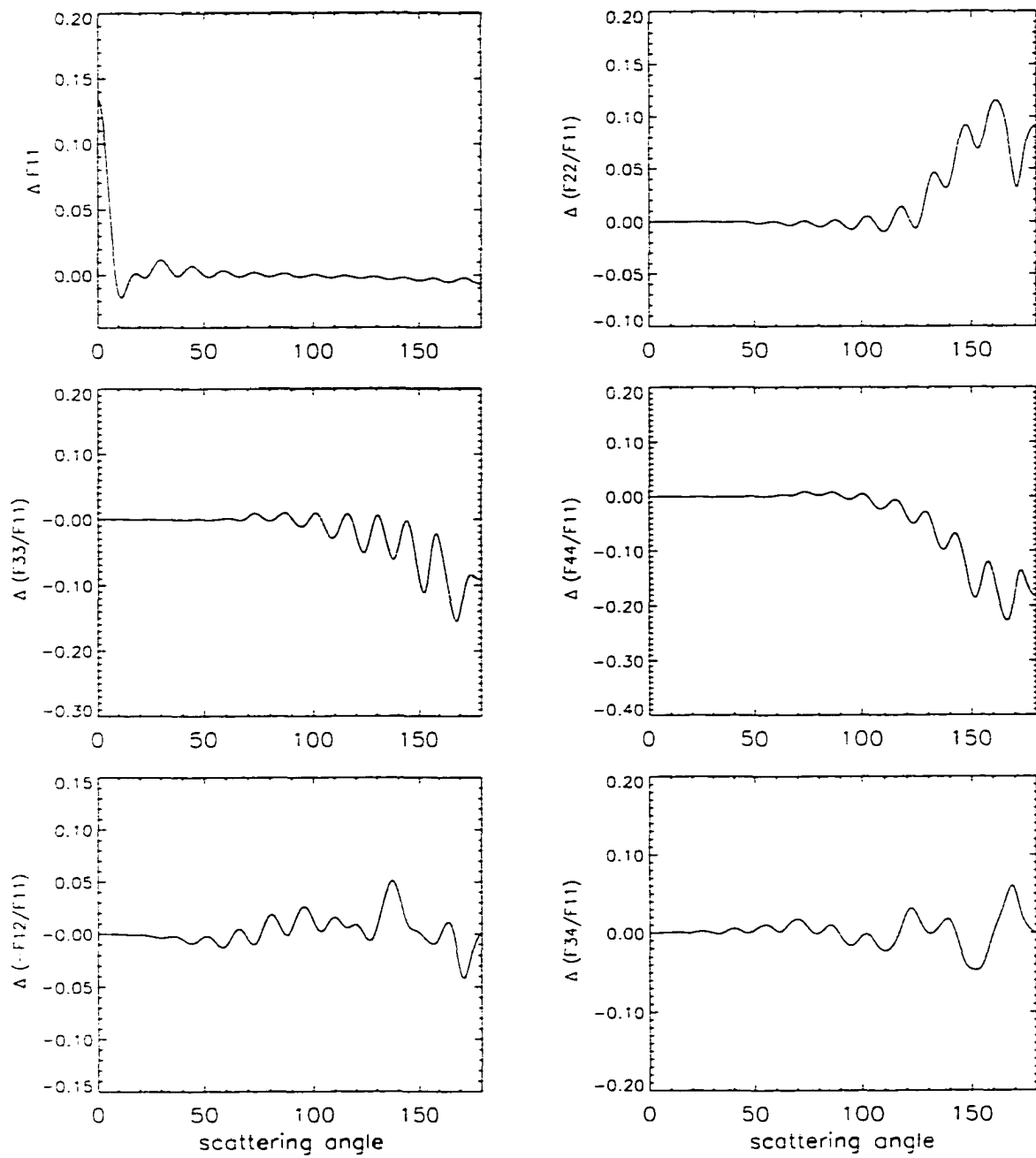
Figure 2.9. As Figure 2.3, but for test case 4.
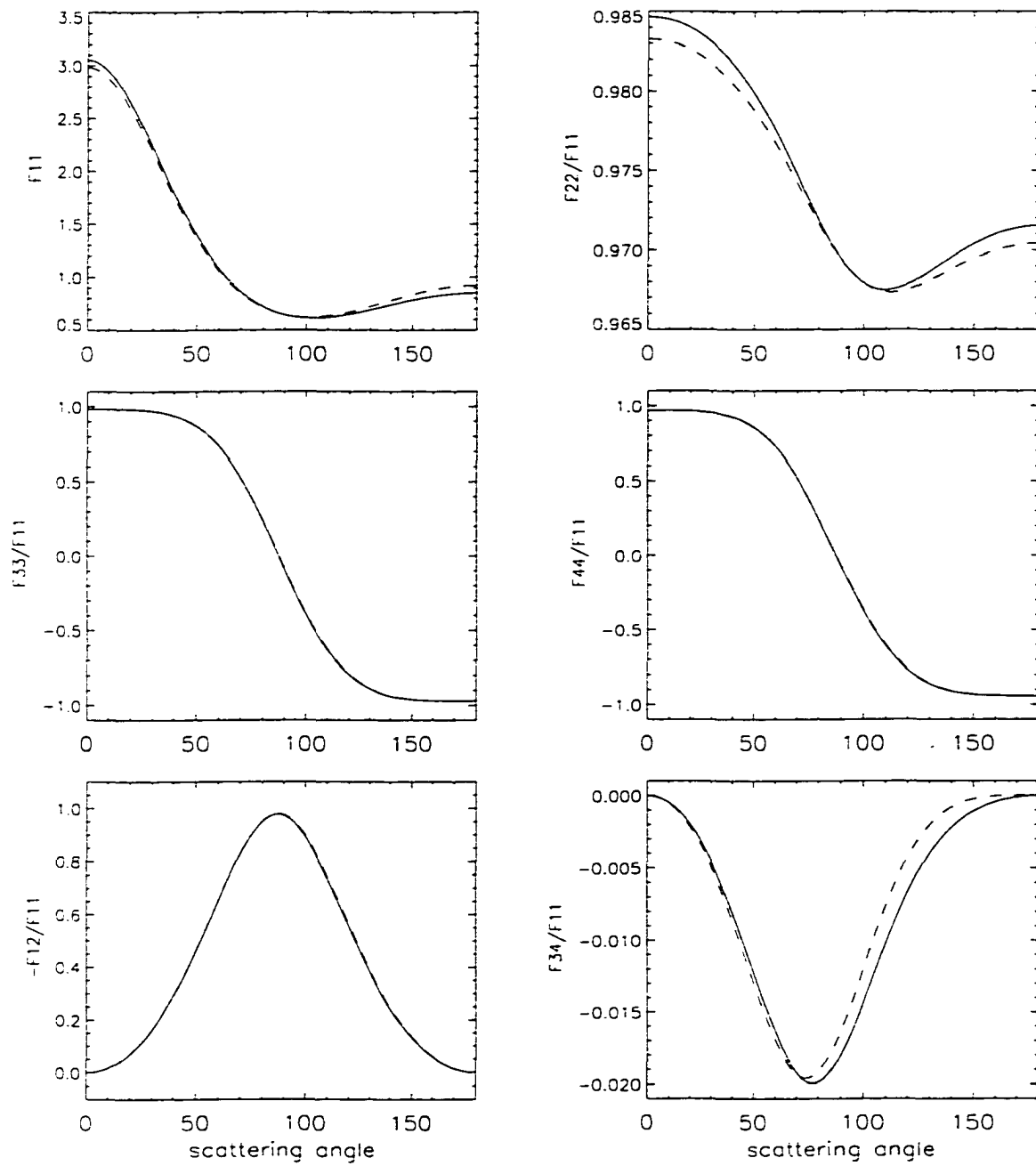
Figure 2.10. As Figure 2.2. but for test case 5.
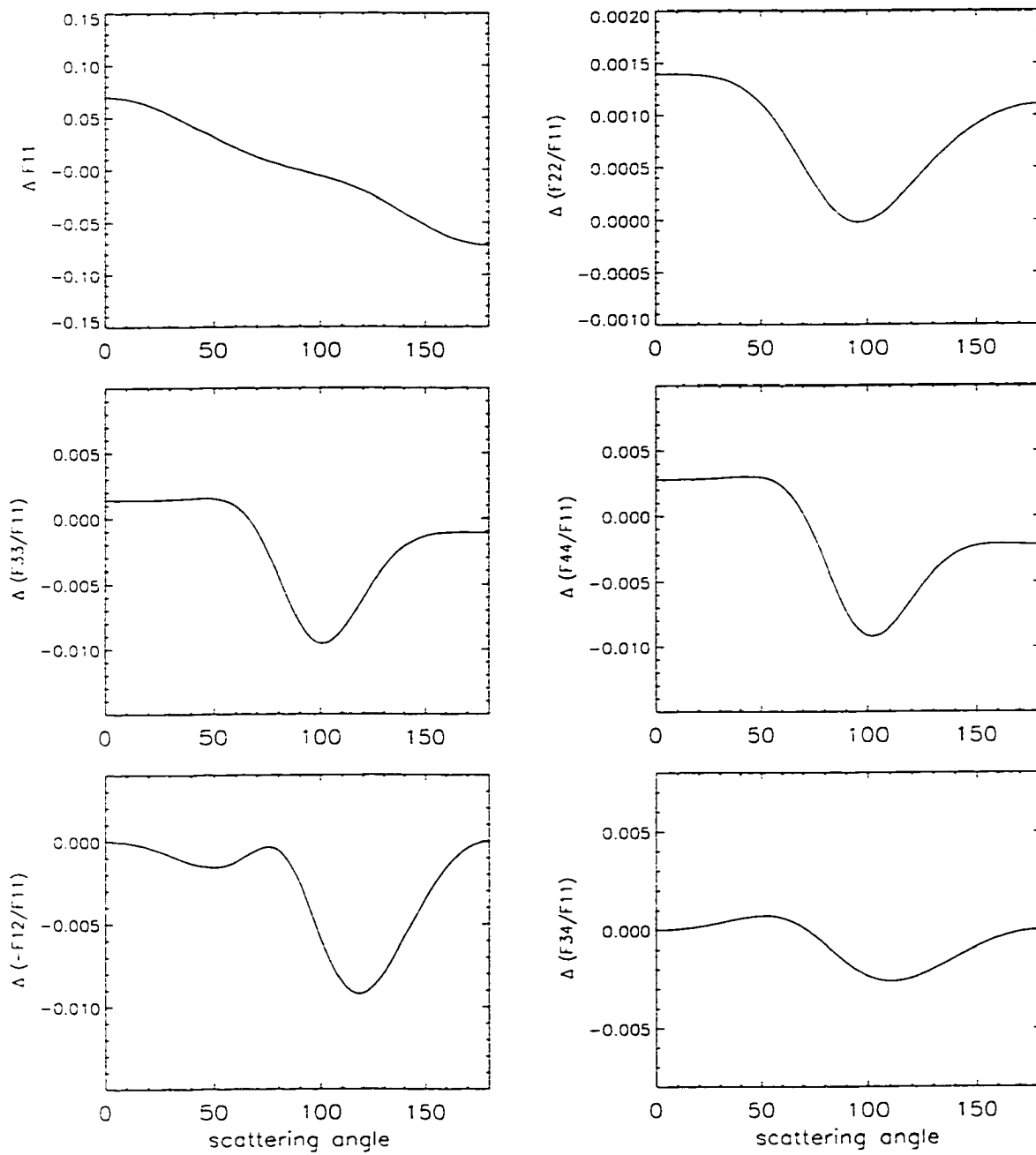
Figure 2.11. As Figure 2.3, but for test case 5.

It is well-known that the T-matrix method. within its range of applicability. is very advantageous in terms of computer time [41]. But for highly aspherical prolate or oblate spheroids. the SVM seems to be an interesting alternative to the EBCM for computing the T-matrix and derived optical properties. Also. very little work has been done in the past two decades to improve the procedures for calculating the spheroidal expansion coefficients $d_r^{(m,n)}$. These coefficients are. however. absolutely vital for the SVM. There is still a lot of potential for extending the usefulness of the SVM by finding improved procedures for calculating these coefficients. To this end. a promising approach is to extend the new method recently developed for computing eigenfunctions for scattering by elliptical cylinders [54].

2.7 Summary

The underlying concept of this chapter was the perception that the fundamental quantity that characterizes the light scattering properties of a particle is the T-matrix. and that a method for solving the single scattering problem should. if possible. be primarily targeted at computing the T-matrix rather than the scattered electromagnetic field. Based on this perception. the purpose of this chapter was to establish a new method to calculate the T-matrix for spheroidal particles with the separation of variables method (SVM). The strategy pursued in using the SVM was to circumvent the notorious ill-conditioning of the EBCM for highly aspherical particles by computing the T-matrix with the SVM in *spheroidal* coordinates instead of with the EBCM in *spherical* coordinates. The proposed modification of the SVM involving the vector spheroidal wave functions instead of plane waves as incident waves has one important advantage over the conventional SVM: The output is in form of the T-matrix. Thus. if one is interested in the fields. the SVM computations do not have to be redone for each new incident plane wave of interest. Instead. the T-matrix is obtained once and for all for a given wavelength as the fundamental property characterizing a particle in light scattering processes. and the scattered field can be obtained directly from the T-matrix for any incident field of the same wave-

length. When interested in the optical properties of ensembles of randomly oriented particles. the $\mathcal{T}$-matrix can be used to perform the integration over the orientational angles analytically. As explained in Section 2.5. this analytical step is most conveniently carried out in spherical coordinates. due to the close relation between the spherical functions and the angular momentum operator. which is the generating observable of the rotation group $SO(3)$.

A transformation. given in (2.129). has been developed to transform the $\mathcal{T}$-matrix from the spheroidal expansion basis into the spherical expansion basis. This allows for not only a direct comparison of the spheroidal and spherical T-matrices obtained with the SVM and the EBCM. respectively. It also enables one to use the spherical T-matrix. generated from the spheroidal $\mathcal{T}$-matrix obtained with the SVM. directly in Mishchenko's analytical procedure for calculating the optical properties of an ensemble of randomly oriented axisymmetric particles.

The relations in (2.21) and (2.29) that are derived in Section 2.2.1 for the coefficients of the spheroidal functions are useful analytical tools in the derivation of the T-matrix transformation in (2.129). In addition. (2.29) can be a useful practical tool for examining the numerical accuracy of techniques employed for the computation of the coefficients $d_r^{(m,n)}(c)$. The advantage of this method is that it can be applied to any value of r and m and for any value of c. including complex values.

Numerical comparisons have shown a remarkable agreement between T-matrices and derived optical properties obtained by use of the SVM and the EBCM. especially for small particles. although. as case 5 has shown. the agreement for larger aspect ratios is worse. There is also some indication that the agreement is better for prolate particles of a given aspect ratio than for oblate particles of the same aspect ratio.

The SVM seems to have the potential to fill an existing gap by providing useful results for prolate and oblate spheroids of extreme shapes. The range of applicability of the SVM critically depends on the range of accuracy of the spheroidal expansion coefficients $d_r^{(m,n)}(c)$. i.e. both the range of the indices and of the (in general complex)

parameter c. Further extensive studies will be necessary to investigate that range of accuracy. for which the testing methods proposed in this chapter should prove useful. The SVM may also greatly benefit from future improvements of the methods available or even the invention of new methods to compute these coefficients [54].

Chapter 3

Point Group Symmetries in Electromagnetic Scattering

In this chapter. a relation between point group symmetries of light scattering particles and symmetry relations for the electromagnetic scattering solution in the T-matrix formulation is developed [55]. A systematic derivation of a representation of symmetry operations is presented in the vector space on which the T-matrix operates. From this. the symmetry relations of the T-matrix corresponding to the various symmetry operations in point groups are derived. As examples. several symmetry groups relevant to modeling atmospheric particles are treated. such as the $\mathcal{K}$-group of spherical symmetry. the $\mathcal{C}_{\infty v}$-group of axisymmetric symmetry. and the $\mathcal{D}_{\infty h}$-group of dihedral axisymmetric symmetry. The $\mathcal{D}_{\infty h}$-symmetry relations for the $\mathcal{T}$-matrix in spheroidal coordinates are also derived. Previously known symmetry relations of the T-matrix for $\mathcal{D}_{\infty h}$- and $\mathcal{K}$-symmetry can be verified with the group theoretical approach developed here. A previously not discovered relation is found for $\mathcal{D}_{\infty h}$-symmetry. The full set of symmetry relations is presented for the T-matrix of particles with $\mathcal{D}_{Nh}$-symmetry. i.e. for the important case of particles with dihedral symmetry and an N-fold axis of rotation.

66

3.1 Introduction

The new SVM approach developed in the previous chapter relies on the use of spheroidal particles. For the $\mathcal{T}$-matrix of spheroidal particles, the symmetry relations (2.89) and (2.90) were found. Analogous symmetry relations have been reported for the T-matrix in spherical coordinates of axisymmetric particles [32]. The derivation in Ref. [32] was based on expressing the amplitude scattering matrix in terms of the T-matrix. and inferring symmetry relations of the T-matrix from the symmetry properties of the amplitude scattering matrix. Symmetry properties of the T-matrix greatly simplify the analytic expressions for the optical properties of ensembles of randomly oriented particles. and thus reduce the numerical computations.

While testing the modified SVM method described in the previous chapter against the EBCM. it was discovered that half of the computed T- and $\mathcal{T}$-matrix elements are actually zero. namely those for which $k + k' + n + n'$ is odd. This suggests additional symmetry relations of the T- and $\mathcal{T}$-matrix of spheroidal particles that have previously not been discovered. The objective of this chapter is to develop a systematic and general method for accounting for a particle's symmetry properties in practical T-matrix applications.

The appropriate framework to describe symmetries in physics is group theory. In the case of symmetric objects of finite extent. such as molecules in chemical physics or particles in the electromagnetic scattering problem. one is dealing with point groups. The name originates from the fact that there is one point in space which is always left invariant by the symmetry operations of a point group. because otherwise the group would also include translations. which can not be symmetry elements of objects of finite extent. The theory of point groups has been applied extensively and with great success in molecular physics. In electronic structure calculations. the molecular orbitals are first determined with the self-consistent field (SCF) method using the Hartree-Fock equation. Then. in the Configuration Interaction (CI) method. the electronic wave function of the ground state can be expanded in the basis of Slater determinants formed from the molecular

orbitals. This expansion includes an enormous number of terms. even for small molecules with only a few electrons. By exploiting the point group symmetries of a molecule. one can rule out a large number of terms and thus greatly reduce the number of terms in the CI-expansion.

The problem in electronic structure theory is mathematically entirely different from the electromagnetic scattering problem. The time-independent Schrödinger equation

$$\mathcal{H}v = Ev \qquad (3.1)$$

is an eigenvalue problem. in which the Hamiltonian operator $\mathcal{H}$ or its matrix representation in a particular basis is known (or at least. as in the SCF method. an initial guess for this operator exists which can be iteratively improved). The unknowns that are determined by solving this equation are the eigenvectors v and eigenvalues E. In the T-matrix formulation of electromagnetic scattering. the T-matrix $\mathbf{T}$ constitutes the linear relation between a vector. $\mathbf{p}$. containing the expansion coefficients of the scattered field in some basis of vector functions and a vector. $\mathbf{a}$. containing the expansion coefficients of the incident field. i.e.

$$\mathbf{p} = \mathbf{T} \cdot \mathbf{a}. \qquad (3.2)$$

This relation is obviously not an eigenvalue problem. The unknown quantity that has to be determined is. in contrast to the quantum mechanical eigenvalue problem. the matrix operator. i.e. $\mathbf{T}$. Although the mathematical problems are very different. one can nevertheless take advantage of point group symmetries in both cases. Just as the Hamiltonian of the electronic configuration in a molecule with given positions of the nuclei commutes with any symmetry operations that leave the geometry of the molecule invariant. so does the T-matrix commute with any symmetry operations that do not alter a particle's geometry. The relation between point group symmetries of a particular particle geometry and the corresponding symmetry relations for the T-matrix is the subject of this chapter. In Section 3.2. the symmetry relations of the T-matrix for different symmetry operations are derived. Section 3.3 deals with examples of point

groups which contain several of the symmetry elements treated in Section 3.2. The symmetry relations of the $\mathcal{T}$-matrix in spheroidal coordinates for spheroidal particles are derived in Section 3.4. Finally. Section 3.5 gives a summary of results.

3.2 Representation of point group elements in the space of the coefficient vectors

The first ground-breaking step when applying group theory to a new problem is to find a representation of the group in question in the particular vector space of interest. The T-matrix is a linear transformation that operates on the vector space of the coefficient vectors a and p with components $a_{n.m}^{(k)}$ and $p_{n.m}^{(k)}$. respectively. The transformation was given in Eq. (2.57): $\mathbf{p} = \mathbf{T} \cdot \mathbf{a}$. In order to find a representation of the elements of a point group in this particular vector space. one first has to investigate how the group elements operate on the vector spherical functions. which are again defined as

$$\mathbf{M}_{n.m}^{(j)} = \nabla \times (\mathbf{r} \cdot v_{n.m}^{(j)}). \tag{3.3}$$

$$\mathbf{N}_{n.m}^{(j)} = k^{-1} \cdot \nabla \times \mathbf{M}_{n.m}^{(j)}. \tag{3.4}$$

where $v_{n.m}^{(j)}$ are the scalar spherical wave functions of the jth kind. and where $\mathbf{r}$ is the position vector.

3.2.1 The reflection operation σ_h

As a first example. a reflection in the xy-plane is considered. The abstract group element is denoted by an operator σ_h. where the letter σ is commonly used for reflections (from German: *Spiegelung*). and where the subscript h stands for a "horizontal" plane of reflection. A Cartesian vector $(x.y.z)$ is transformed under σ_h into $(x.y.-z)$. Note that operators are denoted without a "hat" in this chapter to avoid confusion with unit vectors. Figure 3.1 shows that the effect of σ_h on a vector function $\mathbf{A}(\mathbf{r})$ is two-fold: Both the argument. i.e. the position vector $\mathbf{r}$. and the vector $\mathbf{A}$ are transformed. The
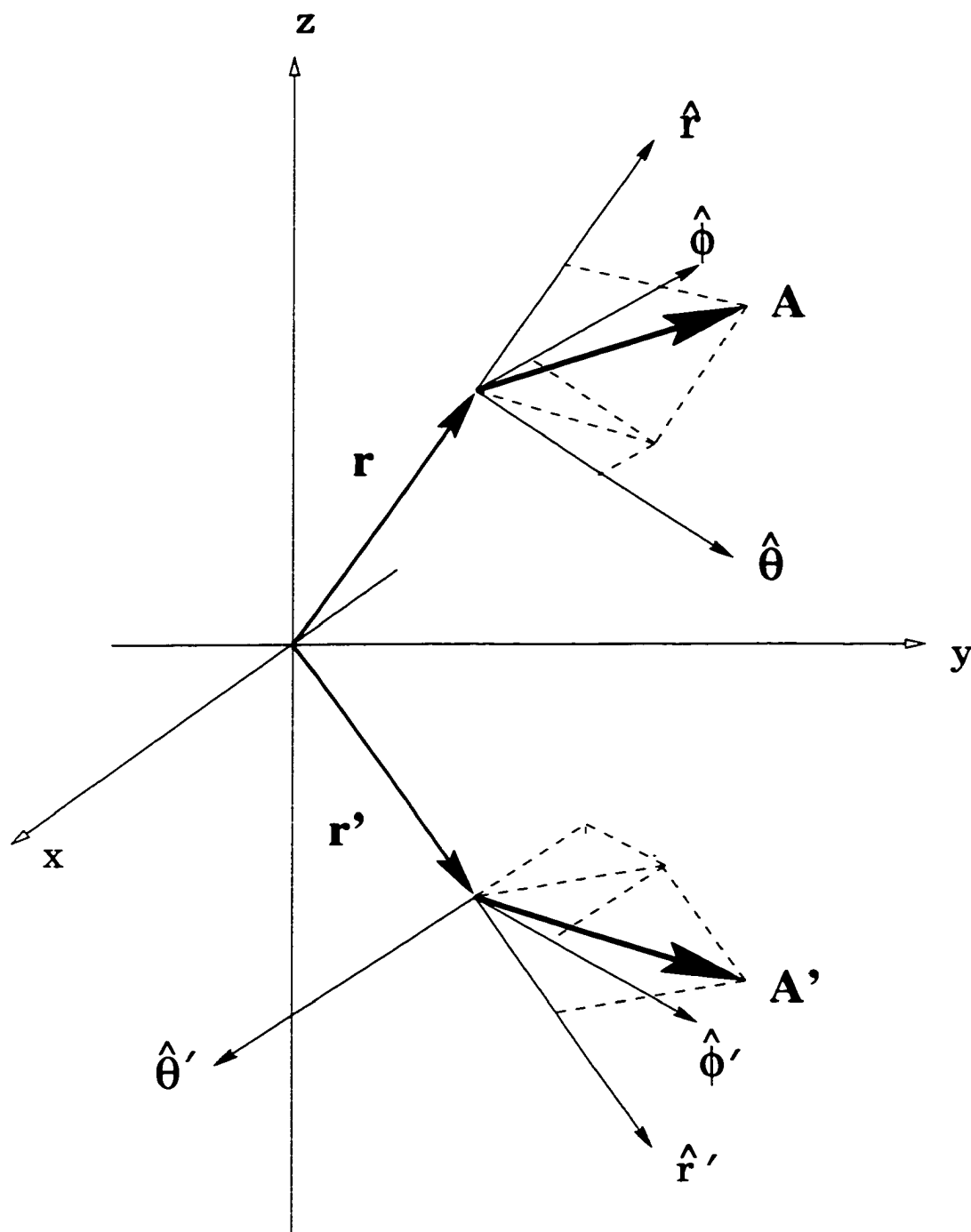
Figure 3.1. Transformation of a vector function under σ_{xy}

position vector $\mathbf{r} = (r, \theta, o)$ in spherical coordinates becomes $\mathbf{r}' = (r, \pi - \theta, o)$. The vector $\mathbf{A}$ is not a position vector and is expressed in *local* spherical coordinates, which are different at $\mathbf{r}$ and $\mathbf{r}'$. As can be seen in Fig. 3.1, the $\hat{r}$- and $\hat{o}$- components of $\mathbf{A}$ in the local coordinate systems are the same before and after the reflection, while the $\hat{\theta}$-component changes sign. Thus, the general rule for the transformation is

$$
\begin{pmatrix} A_r(r,\theta,o) \\ A_\theta(r,\theta,o) \\ A_o(r,\theta,o) \end{pmatrix} \xrightarrow{\sigma_h} \begin{pmatrix} A_r(r,\pi-\theta,o) \\ -A_\theta(r,\pi-\theta,o) \\ A_o(r,\pi-\theta,o) \end{pmatrix} \tag{3.5}
$$

The vector functions (3.3) and (3.4) are given explicitly by

$$
\mathbf{M}_{n,m}^{(3)}(kr) = \gamma_{n,m}\, h_n^{(1)}(kr)\exp(imo)\left(\hat{\theta}\, P_n^{(m)}(u)\,\frac{im}{\sin\theta} - \hat{o}\,\frac{dP_n^{(m)}(u)}{d\theta}\right) \tag{3.6}
$$

$$
\mathbf{N}_{n,m}^{(3)}(kr) = \gamma_{n,m}\,\exp(imo)\left\{\hat{r}\,\frac{n(n+1)}{kr}\,h_n^{(1)}(kr)\,P_n^{(m)}(u)\right.
$$

$$
\left.+\frac{1}{kr}\,[kr\,h_n^{(1)}(kr)]'\cdot\left[\hat{\theta}\,\frac{dP_n^{(m)}(u)}{d\theta} + \hat{o}\,P_n^{(m)}(u)\,\frac{im}{\sin\theta}\right]\right\}. \tag{3.7}
$$

Vector functions of the first kind are obtained from these expressions simply by replacing the spherical Hankel functions $h_n^{(1)}$ with the spherical Bessel functions j_n. When applied to (3.6), the transformation rule (3.5) yields

$$
\mathbf{M}_{n,m}^{(j)} \xrightarrow{\sigma_h} -(-1)^{n+m}\,\mathbf{M}_{n,m}^{(j)} \tag{3.8}
$$

where $P_n^{(m)}(-u) = (-1)^{n+m}\,P_n^{(m)}(u)$ has been used. Analogously, one obtains from (3.7)

$$
\mathbf{N}_{n,m}^{(j)} \xrightarrow{\sigma_h} (-1)^{n+m}\,\mathbf{N}_{n,m}^{(j)}. \tag{3.9}
$$

Thus, by substituting (3.8) and (3.9) into (2.52) and (2.53), one obtains the transformed electric field

$$
\mathbf{E}^i \xrightarrow{\sigma_h} \sum_{n=1}^{\infty}\sum_{m=-n}^{n}(-1)^{n+m}\,[-a_{n,m}^{(1)}\,\mathbf{M}_{n,m}^{(1)} + a_{n,m}^{(2)}\,\mathbf{N}_{n,m}^{(1)}] \tag{3.10}
$$

and analogously for the scattered field. The effect of σ_h can now be expressed as a transformation of the expansion coefficients rather than a transformation of the expansion functions. By comparing (2.52) and (3.10), one can see that

$$a_{n,m}^{(k)} \xrightarrow{\sigma_h} (-1)^{n+m+k} a_{n,m}^{(k)}. \tag{3.11}$$

In compact matrix notation, this can be written as $\mathbf{a} \xrightarrow{\sigma_h} \Sigma_h \cdot \mathbf{a}$, where Σ_h is a diagonal matrix with elements

$$(\Sigma_h)_{n,m,n',m'}^{k,k'} = (-1)^{n+m+k} \delta_{n,n'} \delta_{m,m'} \delta_{k,k'}. \tag{3.12}$$

This is the desired matrix representation of the abstract group element σ_h. The transformation of the T-matrix is then given by

$$\mathbf{T} \xrightarrow{\sigma_h} \Sigma_h \cdot \mathbf{T} \cdot \Sigma_h^{-1} \tag{3.13}$$

or explicitly

$$T_{n,m,n',m'}^{(k,k')} \xrightarrow{\sigma_h} (-1)^{n'+n} (-1)^{m'+m} (-1)^{k'+k} T_{n,m,n',m'}^{(k,k')}. \tag{3.14}$$

If σ_h is a symmetry element of the particle, then a reflection of the particle at the horizontal plane will produce an identical particle with identical light scattering properties. Consequently, σ_h leaves the T-matrix invariant, i.e.

$$\mathbf{T} = \Sigma_h \cdot \mathbf{T} \cdot \Sigma_h^{-1} \tag{3.15}$$

or

$$[\mathbf{T}, \Sigma_h] = 0 \tag{3.16}$$

where the brackets denote the commutator of the two matrices. Explicitly, one obtains from (3.14)

$$T_{n,m,n',m'}^{(k,k')} = 0 \quad \text{unless } (n' + n + m' + m + k' + k) \text{ even.} \tag{3.17}$$

This is the desired symmetry property of the T-matrix for a particle having σ_h-symmetry.

It is clear how to generalize the procedure outlined above to an arbitrary symmetry element g of some point group. One needs to find the transformation of the vector functions analogous to (3.8) and (3.9). in order to derive a representation $\mathbf{G}$ of the symmetry operation g in the vector space of the coefficient vectors analogous to (3.12). The symmetry relation $[\mathbf{T}.\mathbf{G}] = 0$ for the T-matrix can then be written out in explicit form for the symmetry operation g. In Subsections 3.2.2–3.2.5. results for some of the most important symmetry operations are presented.

3.2.2 The inverse operation i

An inversion at the origin. denoted by i. transforms $(x.y.z)$ into $(-x.-y.-z)$. For the transformation of the vector spherical functions under an inversion. one derives

$$\mathbf{M}_{n.m}^{(j)} \xrightarrow{i} -(-1)^n \, \mathbf{M}_{n.m}^{(j)} \tag{3.18}$$

$$\mathbf{N}_{n.m}^{(j)} \xrightarrow{i} (-1)^n \, \mathbf{N}_{n.m}^{(j)}. \tag{3.19}$$

If the T-matrix is invariant under the inversion. then one finds that

$$T_{n.m.n'.m'}^{(k.k')} = 0 \quad \text{unless } (n'+n+k'+k) \text{ even.} \tag{3.20}$$

3.2.3 The rotation operation C_N

Rotations are common symmetry elements of particles. For instance. a hexagonal column or plate that is rotated by $2\pi/6$ about an axis perpendicular to and through the center of the plane of the particle will be indistinguishable from the same particle before the rotation. The transformation of the T-matrix under rotations has been previously derived and applied in order to study ensembles of randomly oriented particles [49. 32]. The relevant transformation for the T-matrix in spherical coordinates has been given in Eq. (2.138). This transformation is used here in order to investigate rotational symmetry properties of the T-matrix.

In point groups. one usually deals with N-fold rotation axes. In the example of the hexagonal column or plate. the symmetry axis is 6-fold. i.e. a rotation by $2\pi/6$ yields an

identical particle. The abstract group element corresponding to a rotation by $2\pi/N$ is denoted by C_N. and. if the axis of rotation is chosen along the z-axis. the corresponding Euler angles are $\alpha = 2\pi/N$. $\beta = \gamma = 0$. Using the relation [56]

$$d^{(n)}_{m,m'}(0) = \delta_{m,m'}$$ (3.21)

Eq. (2.138) simplifies to

$$T^{(k,k')}_{n,m,n',m'}(2\pi/N.0.0) = \exp[-i2\pi(m-m')/N]\,T^{(k,k')}_{n,m,n',m'}(0.0.0).$$ (3.22)

If the particle has C_N-symmetry. then not only the group element C_N. but also C_N^2. C_N^3. .... C_N^{N-1} are symmetry elements of the particle. Thus. $T^{(k,k')}_{n,m,n',m'}(2\pi l/N.0.0) = T^{(k,k')}_{n,m,n',m'}(0.0.0)$. or $\exp(-i2\pi(m-m')l/N) = 1$. where $l = 1.2.\ldots.N-1$. Consequently. $(m-m')l/N$ must be an integer. In case of C_6 symmetry. for instance. this implies

$$l = 1 \quad : \quad (m-m') = 0.6.12.18\ldots.$$ (3.23)

$$l = 2 \quad : \quad (m-m') = 0.3.6.9\ldots$$ (3.24)

$$l = 3 \quad : \quad (m-m') = 0.2.4.6\ldots$$ (3.25)

$$l = 4 \quad : \quad (m-m') = 0.3.6.9\ldots$$ (3.26)

$$l = 5 \quad : \quad (m-m') = 0.6.12.18\ldots.$$ (3.27)

so

$$T^{(k,k')}_{n,m,n',m'} = 0 \quad \text{unless} \quad (m-m') \bmod 2 = 0$$

$$\text{or} \quad (m-m') \bmod 3 = 0$$ (3.28)

where $0 \bmod N = 0 \quad \forall N$.

Analogous to the previous case. one obtains for C_3-symmetry the symmetry relations

$$T^{(k,k')}_{n,m,n',m'} = 0 \quad \text{unless} \quad (m-m') \bmod 3 = 0.$$ (3.29)

More generally. if the scattering particle has C_N-symmetry. and if the set of all prime numbers that occur in the prime number decomposition of N is denoted by $\mathcal{M}$. then

$$T^{(k,k')}_{n,m,n',m'} = 0 \quad \text{unless} \quad (m-m') \bmod p = 0 \text{ for some } p \in \mathcal{M}.$$ (3.30)

A special case is the C_∞-symmetry of axisymmetric particles. such as spheroids. finite circular cylinders. and Chebyshev particles. In this case. one can replace the angle $2\pi/N$ in (3.22) by any angle α. Therefore. if a particle has C_∞-symmetry. then

$$
\begin{aligned}
T^{(k,k')}_{n,m,n',m'}(\alpha, 0, 0) &= \exp[-i(m - m')\alpha]\, T^{(k,k')}_{n,m,n',m'}(0, 0, 0) \\
&= T^{(k,k')}_{n,m,n',m'}(0, 0, 0) \quad \forall \alpha
\end{aligned}
\tag{3.31}
$$

which implies $m = m'$. Thus. one obtains for axisymmetric particles the symmetry property

$$
T^{(k,k')}_{n,m,n',m'} = \delta_{m,m'}\, T^{(k,k')}_{n,m,n',m}.
\tag{3.32}
$$

Often a particle has N additional C_2-symmetry axes perpendicular to the main symmetry axis. Spheroids. finite circular cylinders. and hexagonal plates and columns are common examples. If the y-axis of the coordinate system is chosen along one of these C_2-axes. then one obtains from (2.138)

$$
T^{(k,k')}_{n,m,n',m'}(0, \pi, 0) =
$$

$$
\sum_{m_1=-n}^{n} \sum_{m_2=-n'}^{n'} d^{(n)}_{m,m_1}(\pi)\, T^{(k,k')}_{n,m_1,n',m_2}(0, 0, 0)\, (d^{-1})^{(n')}_{m_2,m'}(\pi).
\tag{3.33}
$$

Using $(d^{-1})^{(n)}_{m,m'}(\beta) = d^{(n)}_{m',m}(\beta)$ and $d^{(n)}_{m,m'}(\pi) = (-1)^{n-m'}\delta_{-m,m'}$. one obtains

$$
T^{(k,k')}_{n,m,n',m'}(0, \pi, 0) =
$$

$$
(-1)^{n+n'+m+m'}\, T^{(k,k')}_{n,-m,n',-m'}(0, 0, 0).
\tag{3.34}
$$

The T-matrix of a particle with a C_2 symmetry axis perpendicular to the main symmetry axis therefore has the symmetry property

$$
T^{(k,k')}_{n,-m,n',-m'} = (-1)^{n+n'+m+m'}\, T^{(k,k')}_{n,m,n',m'}.
\tag{3.35}
$$

3.2.4 The reflection operation σ_v

Analogous to the reflection operation σ_h, one can investigate the effect of a reflection in the xz-plane. Reflections in planes containing the z axis are generally denoted by $\sigma_v, \sigma'_v, \ldots$ with a subscript v for a "vertical" plane of reflection. In particular, a reflection in the xz-plane transforms the Cartesian vector (x, y, z) into $(x, -y, z)$. To be more specific, this operation is denoted by σ_{xz}. In complete analogy to the reflection in a horizontal plane, one obtains for the transformation of the vector spherical functions

$$\mathbf{M}_{n,m}^{(j)} \xrightarrow{\sigma_{xz}} -(-1)^m \mathbf{M}_{n,-m}^{(j)} \tag{3.36}$$

$$\mathbf{N}_{n,m}^{(j)} \xrightarrow{\sigma_{xz}} (-1)^m \mathbf{N}_{n,-m}^{(j)}. \tag{3.37}$$

From these relations, one can easily derive the symmetry relation for the T-matrix of a particle having σ_{xz}-symmetry:

$$T_{n,-m,n',-m'}^{(k,k')} = (-1)^{m+m'}(-1)^{k+k'} T_{n,m,n',m'}^{(k,k')}. \tag{3.38}$$

A reflection in the yz-plane, denoted by σ_{yz}, transforms the Cartesian vector (x, y, z) into $(-x, y, z)$. The vector spherical functions transform under this operation according to

$$\mathbf{M}_{n,m}^{(j)} \xrightarrow{\sigma_{yz}} -\mathbf{M}_{n,-m}^{(j)} \tag{3.39}$$

$$\mathbf{N}_{n,m}^{(j)} \xrightarrow{\sigma_{yz}} \mathbf{N}_{n,-m}^{(j)}. \tag{3.40}$$

The resulting symmetry relation for the T-matrix is

$$T_{n,-m,n',-m'}^{(k,k')} = (-1)^{k+k'} T_{n,m,n',m'}^{(k,k')}. \tag{3.41}$$

Figure 3.2 illustrates that the reflection operation σ_{yz} can be represented by $\sigma_{yz} = C_4^{-1}\sigma_{xz}C_4$. By using Eqs. (3.38) and (3.22) for $N = 4$ one obtains

$$T_{n,m,n',m'}^{(k,k')} \xrightarrow{C_4^{-1}\sigma_{xz}C_4} \exp[i(-m+m')(-\pi/2)] (-1)^{m+m'k+k'}$$

$$\times \exp[i(m-m')\pi/2] T_{n,-m,n',-m'}^{(k,k')}$$

$$= (-1)^{k+k'} T_{n,-m,n',-m'}^{(k,k')} \tag{3.42}$$
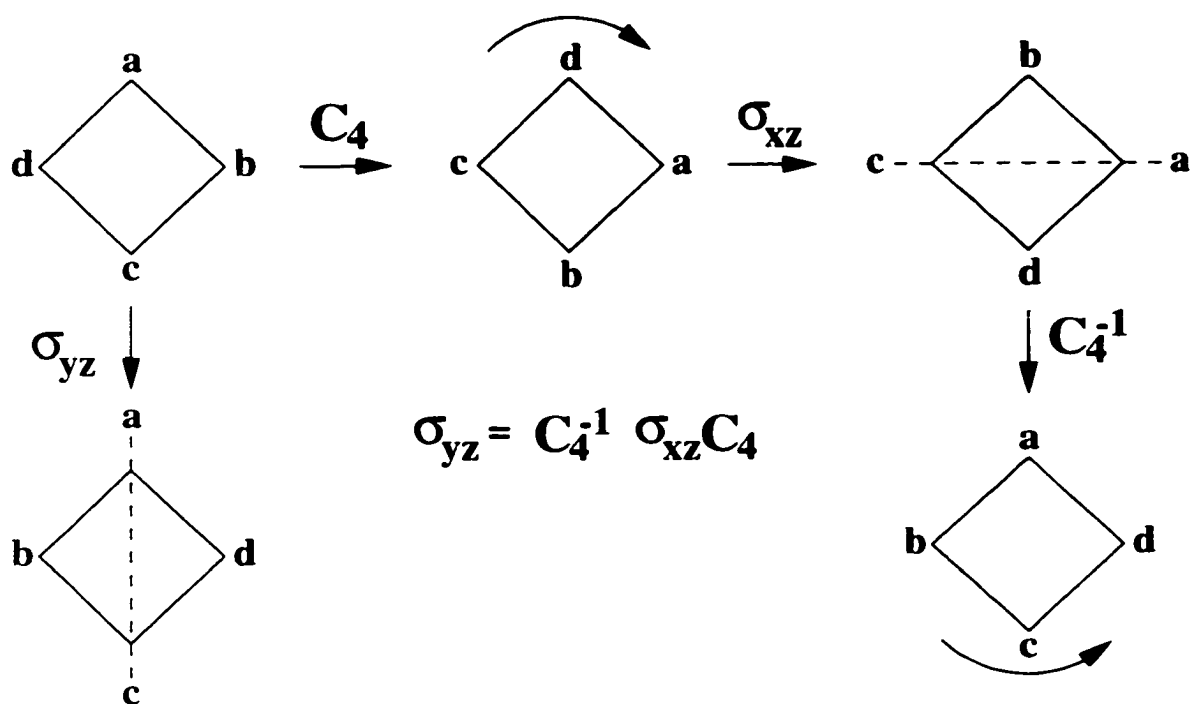
Figure 3.2. Decomposition of σ_{yz}

$$\sigma_{yz} = C_4^{-1} \, \sigma_{xz} C_4$$

which is identical. as expected. with (3.41).

The reflection operation σ'_v shown in Fig. 3.3 is given by $\sigma'_v = C_8^{-1}\sigma_{xz}C_8$. Using (3.38) and (3.22) for $N = 8$. one obtains

$$T^{(k,k')}_{n,m,n',m'} \xrightarrow{C_8^{-1}\sigma_{xz}C_8} i^{m-m'}(-1)^{m+m'+k+k'}T^{(k,k')}_{n,-m,n',-m'}. \tag{3.43}$$

In a similar fashion. one can obtain other rotated reflection planes by combining reflection and rotation operations in an adequate way.

3.2.5 The rotation-reflection operation S_N

A rotation-reflection operation S_N is obtained by first performing a rotation about an axis by $2\pi/N$. followed by a reflection in a plane perpendicular to the axis. If the rotation axis is along the z-axis. then one can write $S_N = C_N\sigma_h$. Consequently. if both C_N and σ_h are symmetry elements of the particle in question. then the group element S_N does not provide an independent symmetry relation for the T-matrix. Figure 3.4 shows a parallelepiped. It has identical rectangular top and bottom faces. $abcd$ and $efgh$. and two different kinds of faces at the sides. two rectangular ones. $adhe$ and $bcgf$. and two parallelograms. $abfe$ and $dcgh$. The operation C_2 in Figure 3.4 denotes in this case a rotation about the vertical z-axis and not. as usually in this chapter. a C_2 rotation perpendicular to the vertical axis. As can be seen in the figure. neither the rotation C_2 nor the reflection σ_h is a symmetry element of this particle's point group. However. the rotation-reflection operation $S_2 = \sigma_h C_2$ is.

The transformation of the T-matrix under the operation S_N can be obtained immediately by combining (3.14) and (3.22). The result is

$$T^{(k,k')}_{n,m,n',m'} \xrightarrow{S_N} \exp[-i2\pi(m-m')/N](-1)^{n'+n}(-1)^{m'+m}(-1)^{k'+k}T^{(k,k')}_{n,m,n',m'}. \tag{3.44}$$

Invariance of the T-matrix under a rotation-reflection operation S_N^l therefore requires that

$$\exp\{2\pi i[(n+n'+k+k'+m+m')/2+(m'-m)l/N]\} = 1 \tag{3.45}$$
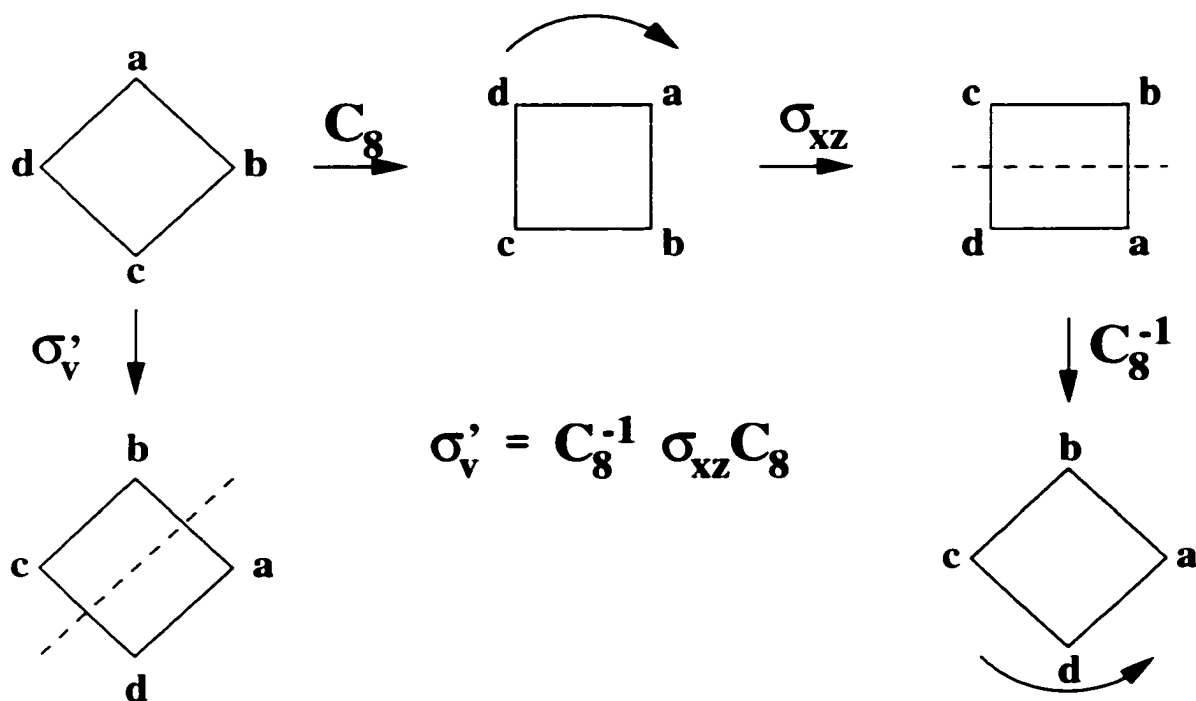
Figure 3.3. Decomposition of σ'_v

$$\sigma'_v = C_8^{-1}\, \sigma_{xz} C_8$$

$$S_2 = \sigma_h\, C_2$$
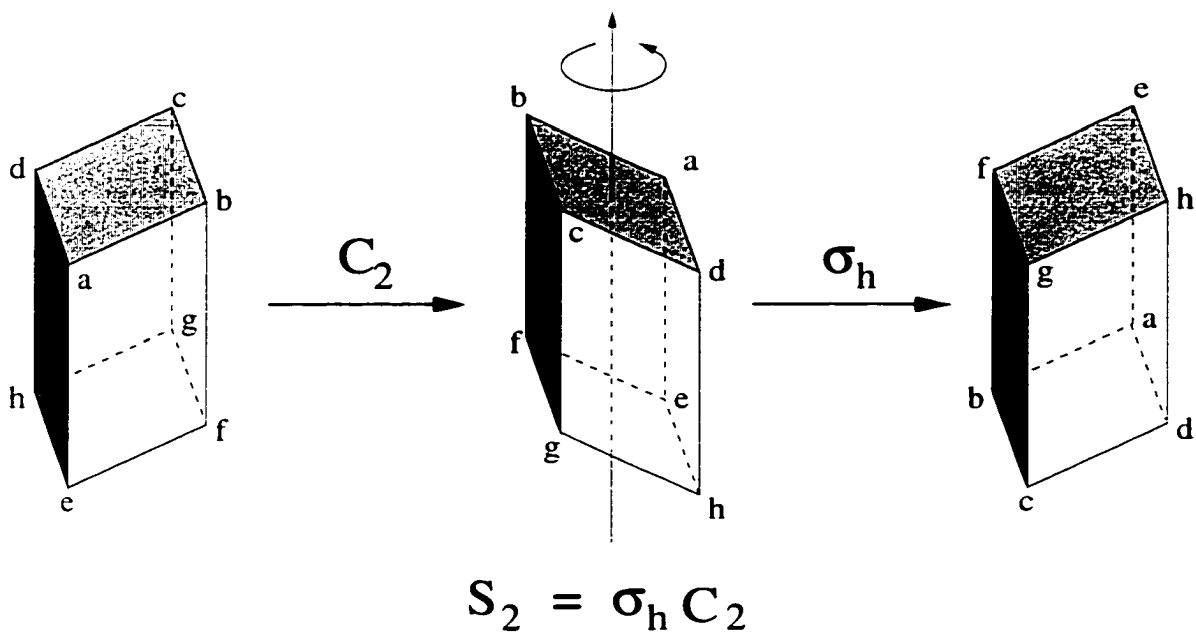
Figure 3.4. Decomposition of S_2

where S_N^l denotes a rotation by $2\pi l/N$ followed by a reflection σ_h. Note that an l-fold application of S_N. denoted by $(S_N)^l$. is not identical with S_N^l. Rather. $(S_N)^l$ is equal to $\sigma_h C_N^{'l}$ $(C_N^{'l})$ if l is odd (even). If the particle has S_N^l-symmetry. then (3.45) implies that the quantity

$$\frac{n + n' + k + k' + m + m'}{2} + (m' - m)\frac{l}{N}$$

must be an integer (including zero). where $l = 1, 2, \ldots, N - 1$. The T-matrix elements are zero for any combination of the indices for which this condition is not satisfied.

3.3 Examples of point groups

Up to this point. isolated symmetry operations have been considered. In this section. point groups of such operations are investigated. It will be found that in a group not all elements yield independent symmetry relations for the T-matrix.

3.3.1 The point group $\mathcal{K}$

Groups are denoted by caligraphic font to avoid confusion with the symmetry operations. A special case are spherical particles. which have $\mathcal{K}$-symmetry (from German *Kugelsymmetrie*). In this case. the calculation of the T-matrix by means of the extended boundary condition method can be carried out analytically. and the resulting T-matrix turns out to be diagonal in all indices [57]. This symmetry property can be easily verified with group theory. The spherical particle is invariant under any rotation. i.e.

$$T_{n,m,n',m'}^{(k,k')}(0, 0, 0) = T_{n,m,n',m'}^{(k,k')}(\alpha, \beta, \gamma) \quad \forall \alpha, \beta, \gamma. \tag{3.46}$$

One can substitute (2.138) and use (3.32). since spheres are in particular axisymmetric. This results in

$$T_{n,m,n',m}^{(k,k')}(0, 0, 0) = \sum_{m_1=-n}^{n} d_{m,m_1}^{(n)}(\beta) \, d_{m,m_1}^{(n')}(\beta) \, T_{n,m_1,n',m_1}^{(k,k')}(0, 0, 0) \quad \forall \beta. \tag{3.47}$$

Integration over ϑ and using the orthogonality property of the Wigner d-functions [56] yields

$$(2n + 1)\, T^{(k,k')}_{n,m,n',m} = \delta_{n,n'} \sum_{m_1=-n}^{n} T^{(k,k')}_{n,m_1,n,m_1}. \tag{3.48}$$

Since the right hand side contains a Kronecker-delta in n. the left hand side must contain one also. i.e. the T-matrix is diagonal in n. and since the right hand side is independent of m. the left hand side must be. too. Thus. $T^{(k,k')}_{n,m,n',m'} = \delta_{n,n'}\delta_{m,m'}T_n^{(k,k')}$. where the Kronecker-delta in m stems from (3.32). Finally. since spherical symmetry also includes i-symmetry. one obtains with (3.20) and the fact that k. k' only take on the values 1 and 2

$$T^{(k,k')}_{n,m,n',m'} = \delta_{k,k'}\, \delta_{n,n'}\, \delta_{m,m'}\, T_n \tag{3.49}$$

where T_n depends only on n. The diagonality of the T-matrix for spheres has previously been derived in the framework of the extended boundary condition method by evaluating several surface integrals over cross products of vector spherical functions. which is a moderately tedious exercise. This symmetry property of the T-matrix has been obtained here with hardly any analytical effort in the framework of group theory. which demonstrates how powerful the group theoretical approach is.

3.3.2 The point group $C_{\infty v}$

Groups with an N-fold rotational symmetry axis C_N are labeled with C_N. The additional subscript v indicates that N "vertical" reflection operations are contained in this symmetry group. Axisymmetric particles have an infinite number of reflection planes containing the symmetry axis. Chebyshev particles belong to this point group. According to (3.32). the T-matrix is diagonal in m

$$T^{(k,k')}_{n,m,n',m'} = \delta_{m,m'}\, T^{(k,k')}_{n,m,n',m}. \tag{3.50}$$

With this relation. Eq. (3.38) becomes

$$T^{(k,k')}_{n,-m,n',-m'} = (-1)^{k+k'}\, T^{(k,k')}_{n,m,n',m'} \tag{3.51}$$

which is equivalent to (3.41). These last two symmetry properties have been derived previously from the symmetry properties of the amplitude scattering matrix [32]. It is an encouraging result to be able to reproduce them with little effort in the more general and systematic framework of group theory.

3.3.3 The point group $\mathcal{D}_{\infty h}$

Point groups that have additional C_2 axes perpendicular to the main symmetry axis are called dihedral point groups and are labeled with a $\mathcal{D}$ instead of with a $\mathcal{C}$. The subscript h in $\mathcal{D}_{\infty h}$ denotes the existence of a "horizontal" (σ_h) reflection plane. i.e. a reflection plane perpendicular to the main symmetry axis. This point group also contains N "vertical" reflection planes containing the main symmetry axis. as well as the inverse operation i. The symmetry relation (3.17) due to the "horizontal" reflection plane becomes equivalent to the inversion symmetry (3.20). because T is diagonal in m. Thus. in addition to (3.50) and (3.51), there is one more symmetry property in the $\mathcal{D}_{\infty h}$-group. namely

$$T_{n,m,n'.m}^{(k,k')} \;\; = \;\; 0 \quad \text{unless} \; (n + n' + k + k') \; \text{even.} \tag{3.52}$$

Therefore. $n + n'$ and $k + k'$ must have the same parity. which makes the C_2-symmetry (3.35) equivalent to the σ_v-symmetry (3.51) in this symmetry group. The symmetry property (3.52) has not been discovered and exploited previously. It can be used to reduce the number of T-matrix elements to be computed by a factor of 2.

Examples of particles that belong to the $\mathcal{D}_{\infty h}$ point group are spheroids [3. 32. 39. 28] and finite circular cylinders [4. 40]. which play an important role in modeling the optical properties of ensembles of randomly oriented nonspherical particles. Note that both spheroids and finite circular cylinders have different shapes and consequently different T-matrices. but their T-matrices have nevertheless the same *symmetry properties* (3.50)-(3.52). simply because both types of particles belong to the same point group. Also. the symmetry properties are independent of the size or the refractive index of the particle. as long as the refractive index does not vary throughout the particle such that it would break the symmetry of the particle's geometry.

3.3.4 The point groups $\mathcal{D}_{Nh}$

Figure 3.5 shows a triangular column and a graphic representation of its symmetry elements σ_v, σ_h, C_3, and C_2. If the y-axis is chosen along C_2, then σ_v denotes in this case a reflection in the yz-plane. The inverse operation i is missing in this point group. Thus, the relevant symmetry relations of the T-matrix which apply in this case are (3.41), (3.17), (3.29), and (3.35). By comparing (3.41) and (3.35), one can see that $m + m' + n + n'$ must have the same parity as $k + k'$, which is equivalent to (3.17). One is therefore left with three independent symmetry relations:

$$T^{(k,k')}_{n,m,n',m'} = 0 \quad \text{unless } (m - m') = 0, 3, 6, 9, \ldots \tag{3.53}$$

$$T^{(k,k')}_{n,m,n',m'} = 0 \quad \text{unless } (n + n' + m + m' + k + k') \quad \text{even} \tag{3.54}$$

$$T^{(k,k')}_{n,-m,n',-m'} = (-1)^{k+k'} T^{(k,k')}_{n,m,n',m'}. \tag{3.55}$$

Consequently, not all of the four symmetry operations (3.41), (3.17), (3.29), and (3.35) provide independent symmetry relations, similar to the case of the $\mathcal{D}_{\infty h}$ point group. Also, the rotation-reflection operations in the $\mathcal{D}_{3h}$ and $\mathcal{D}_{\infty h}$ group have not been considered. The phenomenon of interdependence of symmetry relations will now be investigated in a more systematic way. Three symmetry operations Q, R, S and their matrix representations $\mathbf{Q}, \mathbf{R}, \mathbf{S}$ in the space of the coefficient vectors are considered. The symmetry relations of the T-matrix are

$$\mathbf{T} = \mathbf{Q}\mathbf{T}\mathbf{Q}^{-1} \tag{3.56}$$

$$\mathbf{T} = \mathbf{R}\mathbf{T}\mathbf{R}^{-1} \tag{3.57}$$

$$\mathbf{T} = \mathbf{S}\mathbf{T}\mathbf{S}^{-1}. \tag{3.58}$$

If in additional a relation holds of the form

$$\mathbf{S} = \mathbf{R}\mathbf{Q} \tag{3.59}$$

then the three relations (3.56)–(3.58) are not independent, since one obtains for instance from (3.56) and (3.57) $\mathbf{R}^{-1}\mathbf{T}\mathbf{R} = \mathbf{Q}\mathbf{T}\mathbf{Q}^{-1}$, and by multiplying with $\mathbf{Q}^{-1}$ from the left
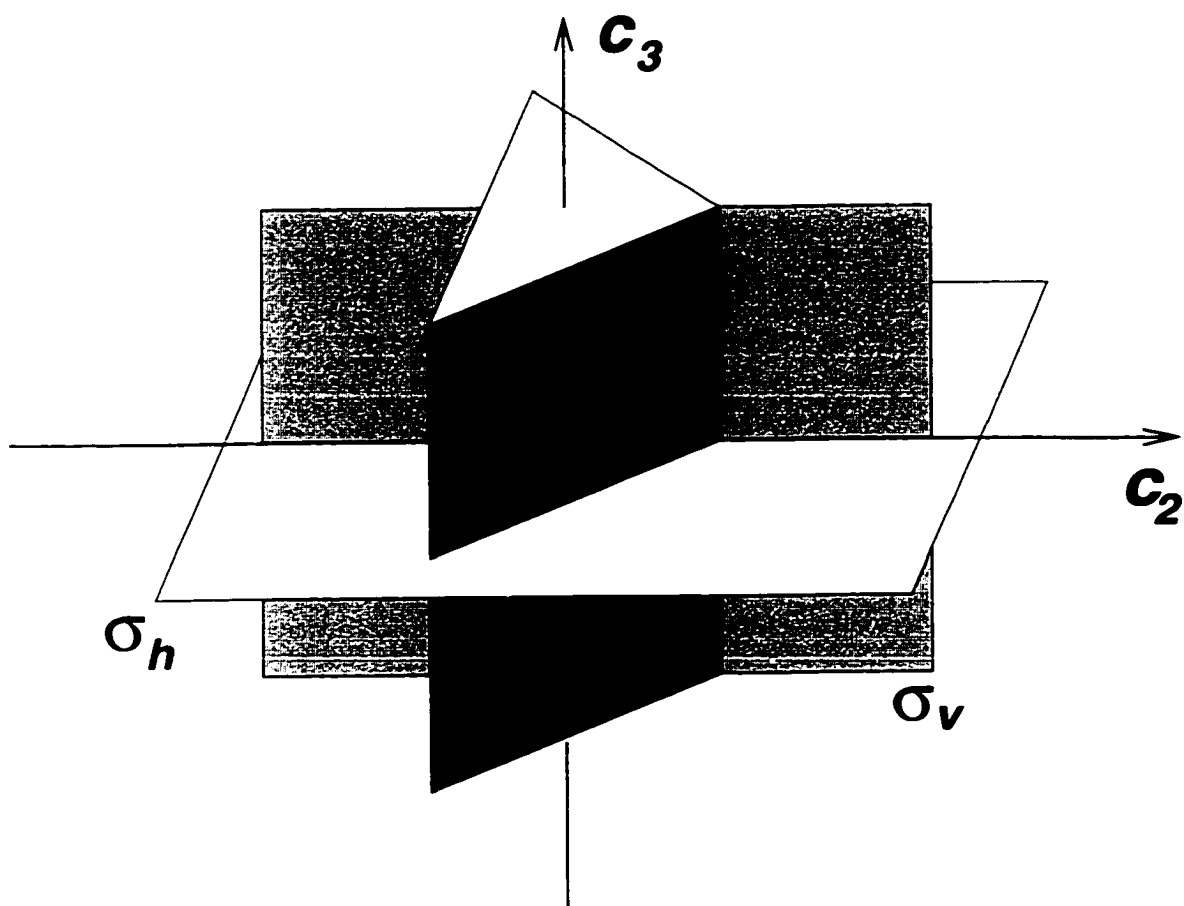
Figure 3.5. Symmetry elements of a triagonal column

and with **Q** from the right. one immediately obtains (3.58). With this result in mind. one can inspect the group multiplication table of the $\mathcal{D}_{3h}$-group. which lists all possible combinations of the elements in this point group (Table 3.1). The element E is the identity operation. The table is to be interpreted as follows: In the column of σ_v' and the row of S_3. for instance. one finds the element C_2. This means that $S_3\sigma_v' = C_2$. where the column element σ_v' is applied first and the row element S_3 second. One can see that from the elements C_3. C_2. σ_h. one can obtain the elements E. C_3^2. C_2''. S_3. σ_v. σ_v'. and from those plus the original three group elements one obtains the remaining elements C_2'. σ_v''. and S_3^2. One can easily verify that one can not find a smaller set than the original three elements C_3. C_2. σ_h for constructing all the other elements. Thus. the *essential* group elements are C_3. C_2. and σ_h. and all other group elements can be obtained from these. With the above remark. it follows that only C_3. C_2. and σ_h give independent symmetry relations for the T-matrix. namely the relations (3.53)–(3.55). In particular. it is clear that any rotation C_N^l can be obtained by an l-fold application of C_N. Thus. C_N is the only essential group elements among all C_N^l in any C_N- or $\mathcal{D}_N$-type point group. and consequently. the symmetry relation (3.30) reported above for C_N symmetry can actually be reduced to

$$T^{(k,k')}_{n,m,n',m'} = 0 \quad \text{unless} \quad (m - m') \bmod N = 0. \tag{3.60}$$

From this one obtains that for $N \to \infty$. (3.60) becomes identical with (3.32). Also. in groups having both a C_N element and a σ_h element. the rotation-reflection operations $S_N. S_N^2. \ldots \ldots S_N^{N-1}$ can be obtained from $C_N. C_N^2. \ldots \ldots C_N^{N-1}$ in connection with σ_h.

The choice of the essential group elements is not unique and therefore a matter of convenience. but the resulting symmetry relations of the T-matrix are independent of that choice.

Similarly to the $\mathcal{D}_{3h}$ group considered above. one can write down the symmetry relations of the T-matrix for a particle belonging to the $\mathcal{D}_{4h}$-group

$$T^{(k,k')}_{n,m,n',m'} = 0 \quad \text{unless} \ (m - m') = 0, 4, 8, 12 \ldots \tag{3.61}$$

Table 3.1. Group multiplication table of the dihedral point group $\mathcal{D}_{3h}$

	E	C_3	C_3^2	C_2	C_2'	C_2''	σ_h	S_3	S_3^2	σ_v	σ_v'	σ_v''
E	E	C_3	C_3^2	C_2	C_2'	C_2''	σ_h	S_3	S_3^2	σ_v	σ_v'	σ_v''
C_3	C_3	C_3^2	E	C_2''	C_2	C_2'	S_3	S_3^2	σ_h	σ_v''	σ_v	σ_v'
C_3^2	C_3^2	E	C_3	C_2'	C_2''	C_2	S_3^2	σ_h	S_3	σ_v'	σ_v''	σ_v
C_2	C_2	C_2''	C_2'	E	C_3	C_3^2	σ_v	σ_v'	σ_v''	σ_h	S_3	S_3^2
C_2'	C_2'	C_2	C_2''	C_3^2	E	C_3	σ_v'	σ_v''	σ_v	S_3^2	σ_h	S_3
C_2''	C_2''	C_2'	C_2	C_3	C_3^2	E	σ_v''	σ_v	σ_v'	S_3	S_3^2	σ_h
σ_h	σ_h	S_3	S_3^2	σ_v	σ_v'	σ_v''	E	C_3	C_3^2	C_2	C_2'	C_2''
S_3	S_3	S_3^2	σ_h	σ_v''	σ_v	σ_v'	C_3	C_3^2	E	C_2''	C_2	C_2'
S_3^2	S_3^2	σ_h	S_3	σ_v'	σ_v''	σ_v	C_3^2	E	C_3	C_2'	C_2''	C_2
σ_v	σ_v	σ_v'	σ_v''	σ_h	S_3	S_3^2	C_2	C_2'	C_2''	E	C_3	C_3^2
σ_v'	σ_v'	σ_v''	σ_v	S_3^2	σ_h	S_3	C_2'	C_2''	C_2	C_3^2	E	C_3
σ_v''	σ_v''	σ_v	σ_v'	S_3	S_3^2	σ_h	C_2''	C_2	C_2'	C_3	C_3^2	E

$$T_{n,m,n',m'}^{(k,k')} = 0 \quad \text{unless } (n + n' + k + k') \quad \text{even} \tag{3.62}$$

$$T_{n,-m,n',-m'}^{(k,k')} = (-1)^{k+k'} T_{n,m,n',m'}^{(k,k')}. \tag{3.63}$$

The $\mathcal{D}_{4h}$ point group can be of special interest when attempting to model size-shape distributions of randomly oriented particles. It is advantageous. as became clear in Chapter 2. to use a particle geometry in which the Helmholtz equation is separable. because one can then use the separation of variables method (SVM) for solving the single scattering problem. which is capable of producing accurate results even for particles of extreme elongated or flat shapes. The extended boundary condition method (EBCM). on the other hand. with which a lot of progress in the study of scattering by nonspherical particles could be made. is limited to only mildly aspherical particles. The SVM solution for spheroidal particles has been investigated in several studies [19. 2. 20. 21. 22]. With the SVM approach developed in Chapter 2. it is possible to obtain the optical properties of size-shape distributions of randomly oriented particles analytically [28] by use of the analytical-averaging formalism originally developed in connection with the EBCM [32]. The modified SVM approach is not restricted to spheroidal particles. It could easily be applied to bricks. The Helmholtz equation is also separable in rectangular coordinates. In fact. the corresponding eigenfunctions in Cartesian coordinates are even significantly easier to calculate than the spheroidal eigenfunctions. The question that has not been addressed in the pertinent literature is why spheroids are preferable to bricks in modeling size-shape distributions of randomly oriented particles. The justification for using spheroids rather than bricks can be found by comparing the point group symmetries of both particles. Bricks with two equal sides belong to the $\mathcal{D}_{4h}$ point group . When comparing the relations (3.61)-(3.63) to the ones of $\mathcal{D}_{\infty h}$-symmetry. Eqs. (3.50)-(3.52). one immediately sees that particles belonging to the $\mathcal{D}_{\infty h}$ group have a higher symmetry than those belonging to the $\mathcal{D}_{4h}$ group. since significantly more elements of the T-matrix of a $\mathcal{D}_{\infty h}$-particle are zero. Thus. the computation of the T-matrix. which takes considerably more time than the computation of the eigenfunctions of the Helmholtz equation in a particular coordinate system. is greatly reduced for spheroidal (or other axisymmet-

ric particles) as compared to bricks. This is the reason why spheroids are indeed the simplest choice within the SVM for modeling nonspherical particles if a spherical particle model produces not accurate enough results.

The T-matrix symmetry relations for $\mathcal{D}_{6h}$-symmetry can be obtained in an analogous way

$$T^{(k,k')}_{n,m,n',m'} = 0 \quad \text{unless } (m-m') = 0.6.12.18\ldots \tag{3.64}$$

$$T^{(k,k')}_{n,m,n',m'} = 0 \quad \text{unless } (n+n'+k+k') \quad \text{even} \tag{3.65}$$

$$T^{(k,k')}_{n,-m,n',-m'} = (-1)^{k+k'} T^{(k,k')}_{n,m,n',m'} \tag{3.66}$$

and it is clear how to generalize these relations to any $\mathcal{D}_{Nh}$ point group

$$T^{(k,k')}_{n,m,n',m'} = 0 \quad \text{unless } (m-m') = 0.N.2N.3N\ldots \tag{3.67}$$

$$T^{(k,k')}_{n,m,n',m'} = 0 \quad \text{unless } (n+n'+m+m'+k+k') \quad \text{even} \tag{3.68}$$

$$T^{(k,k')}_{n,-m,n',-m'} = (-1)^{k+k'} T^{(k,k')}_{n,m,n',m'}. \tag{3.69}$$

The symmetry relations for the $\mathcal{D}_{6h}$ point group can be useful in future applications of the T-matrix method for calculating the optical properties of hexagonal columns or plates, which are commonly observed geometries in laboratory clouds that develop under controlled conditions. These shapes also occur in natural cirrus clouds, although irregular ice-crystal shapes are by far the most common [29].

Current models for scattering by size-shape distributions of randomly oriented non-spherical particles rely on the use of model shapes that are axisymmetric [32. 28. 27. 58. 59]. In future applications, one may also wish to drop this restriction and rather use model particles that have different dimensions along all three coordinate axes. such as bricks with sides x, y, z. $x \neq y \neq z$. or ellipsoids with axes $a, b, c, a \neq b \neq c$. For both classes of particles. the T-matrix could be calculated with the SVM in rectangular and ellipsoidal coordinates. respectively. thus avoiding possible ill-conditioning problems of the EBCM for highly aspherical shapes. From the above considerations. one can immediately predict which model would be more efficient. Since both classes of particles

belong to the $\mathcal{D}_{2h}$ group. the T-matrices would have the same symmetry properties. and both choices of particles would therefore be equally good from this perspective. However. since the rectangular eigenfunctions are much simpler than the ellipsoidal eigenfunctions. rectangular particles would be computationally more efficient.

3.4 The $\mathcal{T}$-matrix in spheroidal coordinates

Up to this point. the assumption was that the expansion functions of the incident and scattered fields are the vector spherical functions (3.3) and (3.4). In this section. the symmetry properties of the spheroidal $\mathcal{T}$-matrix. which was derived in the previous chapter with the SVM using vector spheroidal functions $\mathbf{V}_{n,m}^{(j)}$ and $\mathbf{W}_{n,m}^{(j)}$. is investigated. In analogy to Eq. (3.5). one obtains for the transformation of a vector functions in spheroidal coordinates under the operation σ_h

$$\begin{pmatrix} A_\eta(\eta.\xi.o) \\ A_\xi(\eta.\xi.o) \\ A_o(\eta.\xi.o) \end{pmatrix} \xrightarrow{\sigma_h} \begin{pmatrix} -A_\eta(\pi-\eta.\xi.o) \\ A_\xi(\pi-\eta.\xi.o) \\ A_o(\pi-\eta.\xi.o) \end{pmatrix}. \tag{3.70}$$

Only the property $P_n^{(m)}(-u) = (-1)^{n+m} P_n^{(m)}(u)$ of the associated Legendre functions was used in the derivation of the symmetry relation (3.17) from (3.5). It is straightforward to show that an analogous property holds for the angular spheroidal functions $S_{nm}(c;\eta)$. Thus. the derivation of the symmetry property of the spheroidal $\mathcal{T}$-matrix corresponding to σ_h-symmetry is completely analogous to that of the spherical T-matrix. The result is

$$T_{n,m,n',m'}^{(k,k')} = 0 \quad \text{unless } (n'+n+m'+m+k'+k) \text{ even.} \tag{3.71}$$

Similarly. one can show in close analogy to the investigation of the spherical T-matrix that σ_v-symmetry implies

$$T_{n,-m,n',-m'}^{(k,k')} = (-1)^{m+m'}(-1)^{k+k'} T_{n,m,n',m'}^{(k,k')}. \tag{3.72}$$

For i-symmetry, one obtains

$$T^{(k,k')}_{n,m,n',m'} = 0 \quad \text{unless} \ (n' + n + k' + k) \ \text{even.} \tag{3.73}$$

The transformation of the spheroidal T-matrix under rotations is given by (2.141). The rotation matrices in spheroidal coordinates are given in Eq. (2.140), and the inverse matrices are

$$(\mathcal{D}^{-1})^{(n',n_2)}_{m_2,m'}(\alpha,\beta,\gamma) = \mathcal{D}^{(n',n_2)}_{m_2,m'}(-\gamma,-\beta,-\alpha). \tag{3.74}$$

Since one is interested in spheroidal particles, one has to consider rotations about the z-axis. i.e. $\beta = \gamma = 0$. Substituting (2.140) and (3.74) into (2.141) and using (2.136) and (3.21), one obtains

$$T^{(k,k')}_{n,m,n',m'}(\alpha,0,0)$$

$$= \sum_{n_1,n_2} \sideset{}{'}\sum_{q=|m|,|m|+1}^{\infty} \sideset{}{'}\sum_{q'=|m'|,|m'|+1}^{\infty} f^{(m,n)*}_{q-|m|} f^{(m,n_1)}_{q-|m|} f^{(m',n')}_{q'-|m'|} f^{(m',n_2)*}_{q'-|m'|}$$

$$\times \exp[-i(m-m')\alpha] T^{(k,k')}_{n_1,m,n_2,m'}(0,0,0) \tag{3.75}$$

which reduces with Eq. (2.21) to

$$T^{(k,k')}_{n,m,n',m'}(\alpha,0,0) = \exp[-i(m-m')\alpha] \, T^{(k,k')}_{n,m,n',m'}(0,0,0) \quad \forall \alpha \tag{3.76}$$

in complete analogy to (3.31). Consequently, C_∞-symmetry implies for the T-matrix

$$T^{(k,k')}_{n,m,n',m'} = \delta_{m,m'} \, T^{(k,k')}_{n,m,n',m} \tag{3.77}$$

which should be compared to (3.32). The relations (3.71), (3.72), and (3.73) can be summarized into the relations

$$T^{(k,k')}_{n,-m,n',-m'} = (-1)^{k+k'} \, T^{(k,k')}_{n,m,n',m'} \tag{3.78}$$

$$T^{(k,k')}_{n,m,n',m'} = 0 \quad \text{unless} \ (n' + n + k' + k) \ \text{even.} \tag{3.79}$$

The relations (3.77)–(3.79) are the symmetry relations for the T-matrix in spheroidal coordinates for a particle in the $\mathcal{D}_{\infty h}$ point group. The relations (3.77) and (3.78) have

been derived in the previous chapter (see Eqs. (2.89) and (2.90)) with the modified SVM approach. and they could be reproduced here in the framework of group theory. The symmetry relation (3.79) is newly discovered here.

3.5 Summary

The relation between point group symmetries of a light scattering particle with a given geometry and the symmetry properties of the particle's T-matrix has been established. For the example of the σ_h operation. it has been shown in detail how to proceed in order to obtain from the transformation behavior of the vector spherical functions a representation of the point group elements (symmetry operations) in the vector space of the coefficient vectors. The components of these vectors are the expansion coefficients of the incident and scattered electromagnetic fields. and they are related by a linear transformation represented by the T-matrix. Thus. one can obtain from the representation of the point group elements in the vector space of the coefficient vectors the corresponding transformation of the T-matrix under the various operations. From these relations. one can derive the symmetry relations of the T-matrix which apply if a particular operation is a symmetry operation of the particle. In this case. the matrix representation of the symmetry operation commutes with the particle's T-matrix.

The symmetry relations of the T-matrix for the reflection operations σ_h. σ_v. i. C_N. C_2 and S_N have been derived. Subsequently. these symmetry operations have been compiled in point groups. and the set of symmetry relations for the T-matrix has been reduced to a minimum set of independent relations. which were related to the point group's essential symmetry elements. In particular. the well-known diagonality-property of the T-matrix of spherical particles has been verified. as well as two well-known symmetry properties of axisymmetric particles. These results constituted two important test cases for the group theoretical approach. An additional symmetry property for particles with a horizontal plane of reflection. such as spheroids or finite circular cylinders. could be derived. which can be used in practical T-matrix computations to reduce the number of elements com-

puted by a factor of two. As a further example. the complete set of symmetry relations for particles with $\mathcal{D}_{Xh}$-symmetry. explicitly with $\mathcal{D}_{3h}$-. $\mathcal{D}_{4h}$- and $\mathcal{D}_{6h}$-symmetry. has been obtained. These relations can be used in future applications. both to save a considerable amount of computer time and to test the accuracy of the computations by verifying that the numerical computations satisfy the symmetry relations.

The two symmetry relations for the $\mathcal{T}$-matrix in spheroidal coordinates for spheroidal particles were verified. which were derived in the previous chapter. and an additional symmetry relation has been discovered for spheroids. which is due to the horizontal reflection symmetry σ_h. in analogy to the investigation of $\mathcal{D}_{\infty h}$-symmetry of the T-matrix in spherical coordinates.

In addition to the practical aspect of reducing computational efforts. this group theoretical investigation of electromagnetic scattering also provides a deeper theoretical insight into the structure of the T-matrix. A more profound understanding of the symmetry structure of the T-matrix allows one to answer fundamental questions of practical importance. As one example. it was argued on the ground of symmetry considerations that the use of spheroidal particles instead of bricks for modeling size-shape distributions of randomly oriented particles with the SVM is more advantageous. because of the significantly higher symmetry of the T-matrix of a particle belonging to the $\mathcal{D}_{\infty h}$ point group as compared to one belonging to the $\mathcal{D}_{4h}$ point group. As another example. a possible extension of current nonspherical particle models was discussed that introduces two instead one shape parameter. such as the aspect ratios x/y and x/z (a/b and a/c)in a brick (ellipsoid) with sides x. y. z (a. b. c). It was found that bricks would give a computationally more efficient model due to the fact that ellipsoids belong to the same point group. whereas the ellipsoidal eigenfunctions are significantly more complicated than those in rectangular coordinates.

The remarkably small analytical effort in the group theoretical calculations demonstrates the power of group theory. Also. the fact that the point group symmetries of a particle's geometry can be readily translated into symmetry relations of the T-matrix

clearly shows the advantage of characterizing a particle's light scattering properties in terms of the T-matrix, rather than in terms of the scattered field as a function of the incident field. Thus, the T-matrix is much more than just a by-product of the extended boundary condition method. It is, as stated earlier, the fundamental property characterizing a particle's light scattering properties. It has to be considered a great advantage of a single scattering method if it is capable of determining the particle's T-matrix. So far, only the extended boundary condition method and, according to the results of the previous chapter, the separation of variables method have that capability.

Chapter 4

A Vector Discrete Ordinate Radiative Transfer Model (VDISORT)

At this point, one is in a position to efficiently calculate the ensemble-averaged optical properties of size-shape distributions of randomly oriented spheroidal particles from first principles. These single-scattering optical properties (Stokes scattering matrix and single scattering albedo) will be used in a radiative transfer model which accounts for multiple scattering and which computes the intensity and polarization of the radiation field in a vertically inhomogeneous plane parallel medium. This radiative transfer model [36] is treated in the current chapter.

A previously developed model for vector discrete ordinate radiative transfer in vertically inhomogeneous plane parallel media has been tested for both Rayleigh and Mie scattering phase matrices. A few errors were found in the implementation of the model that seriously impaired the model output. An improved version of the model, described in this chapter, has been created in which the errors have been corrected. In addition, the procedure for computing the Fourier components of the phase matrix, required as input

94

to the radiative transfer routines, has been replaced by a more efficient and more accurate procedure. While the original version of the model was limited to phase matrices of spherical particles or to scatterers much smaller than the wavelength of the incident light (Rayleigh limit), the new version presented here is valid for a much broader range of applications including scattering by an ensemble of nonspherical particles. Extensive tests of the model in the Rayleigh limit as well as for unpolarized and polarized beam source applications in the Mie regime demonstrate the significant improvements in accuracy and efficiency achieved with the new version.

4.1 Introduction

The interest in interpreting the polarization of atmospheric radiation measured by instruments deployed at the ground as well as on aircraft, balloons, and satellites, has increased rapidly in recent years [60, 61, 62, 63, 64, 65, 66, 67]. Polarimetric measurements can be used to retrieve atmospheric aerosol properties [4, 61, 68], distinguish between atmospheric and surface contributions to the total reflectance of the planet [62], discriminate between ice and water clouds [1], and determine the shape of the scattering particles [3]. Polarization measurements have a number of essential advantages as compared to standard photometry experiments [69]. The accuracy of polarization measurements is high ($\sim 0.1\%$ for the linear polarization), since it is a relative measure and consequently does not require absolute calibration. The relative errors of polarization measurements can be kept much smaller than the polarization features of radiation scattered by small particles. Also, radiation scattered by air molecules (Rayleigh scattering) shows polarization characteristics that are distinctly different from those exhibited by radiation scattered by aerosols and cloud particles. The degree of polarization (linear and circular) produced by cloud and aerosol particles is more sensitive than the intensity to size, shape, and refractive index of polydispersed small scattering particles. The intensity as a function of the polar angle also has a stronger tendency, as compared to the corresponding polarization characteristics, to be smeared out in an optically thick

medium with a correspondingly higher multiple scattering probability.

The high experimental precision of polarimetric data can be fully exploited only if accurate results from a vector radiative transfer model are available for the retrieval and interpretation of the observations. The discrete ordinate radiative transfer model (DISORT) has proven to be an accurate. versatile. and reliable method for solution of the scalar radiative transfer problem in plane-parallel. vertically inhomogeneous media [70].

Recently. an extension of the scalar discrete ordinate theory to solve the 4-vector problem for the complete set of Stokes parameters has been reported [71]. The approach to the solution of the problem adopted for the vector case is completely analogous to that for the scalar case (see Section 4.2 and compare to [70]). The computer code for the vector problem can therefore rely on the same well-tested routine to obtain the algebraic eigenvalues and eigenvectors (see Section 4.2) as the one used in the scalar version (DISORT). Also. the same scaling transformation [72] can be applied to circumvent the notorious ill-conditioning problem that occurs when one applies boundary and layer interface continuity conditions [71]. The remaining numerical computations are done by using standard computational library subroutines. The main practical problem that remains for the implementation is the "book-keeping" part involved in preparing the input to the numerical routines.

In this chapter. an improved solution to the full 4-vector problem is reported. in which a few errors in the numerical implementation of the model described in Ref. [71] have been corrected. These errors severely impaired the accuracy of the results for beam source applications. In addition. the procedure to compute the Fourier components of the phase matrix has been replaced by a different and more efficient method. These changes have led to significant improvements of the accuracy of the computed results. The superior performance of the upgraded vector version of DISORT is demonstrated by testing it against benchmark results and comparing it to the performance of the original version. The present version of the code has both the accuracy and the reliability needed

to make it a useful tool for a variety of applications which require the interpretation of polarization measurements. A complete description of the theoretical approach is given in the next section.

4.2 Theory

One method to solve the integro-differential radiative transfer equation is the discrete ordinate method. which has been applied with great success to the scalar radiative transfer problem. The basic idea of the discrete ordinate method is to discretize the integral term and to recast the radiative transfer equation in the form of an algebraic eigenvalue equation for the radiation field at discretized polar angles. This section describes the discrete ordinate method generalized to the full 4-vector problem.

4.2.1 Discretization of the vector radiative transfer equation

The basic integro-differential equation of the vector radiative transfer problem is

$$u\frac{d\,\mathbf{I}(\tau.\,u.\,o)}{d\tau} \;=\; \mathbf{I}(\tau.\,u.\,o) - \mathbf{J}(\tau.\,u.\,o) \tag{4.1}$$

where

$$\mathbf{I} \;=\; \begin{pmatrix} I_l \\ I_r \\ U \\ V \end{pmatrix}$$

$$\mathbf{J} \;=\; \frac{a(\tau)}{4\pi}\int_0^{2\pi} do'\int_{-1}^1 du'\,\mathbf{M}(\tau.\,u.\,o;\,u'.\,o')\mathbf{I}(\tau.\,u'.\,o') \;+\; \mathbf{Q}(\tau.\,u.\,o).$$

$$\tag{4.2}$$

I denotes the Stokes vector of the diffuse radiation. u is the cosine of the polar angle. o denotes the azimuth angle. and τ denotes the optical thickness in a plane-parallel. vertically inhomogeneous medium. The first term contributing to the source term $\mathbf{J}$ is

the multiple scattering term. $\mathbf{M}$ is the phase matrix. a denotes the single scattering albedo. and

$$\mathbf{Q}(\tau. u. o) = \frac{a(\tau)}{4\pi} \mathbf{M}(\tau. u. o: -\mu_0. o_0) \mathbf{S}_b(\tau) \exp(-\tau/\mu_0)$$
$$+ [1 - a(\tau)] \mathbf{S}_t(\tau).$$

$$(4.3)$$

The first term on the rhs describes the incident beam $\mathbf{S}_b$ (which for an unpolarized beam would have the form $[I_0/2. I_0/2. 0. 0]^T$). attenuated at depth τ by a factor $\exp(-\tau/\mu_0)$ and undergoing single scattering into the direction $(u. o)$. The second term is the thermal emission. which is unpolarized. i.e. $\mathbf{S}_t(\tau) = [B(T(\tau))/2. B(T(\tau))/2. 0. 0]^T$. and B is the Planck function. It was set $\mu_0 := |u_0| := |\cos\theta_0|$. where θ_0 is the polar angle of the beam source. To isolate the azimuthal dependence from the radiative transfer equation. one performs the following Fourier expansions:

$$\mathbf{M}(\tau. u. o: u'. o') = \sum_{m=0}^{2N-1} \left\{ \mathbf{M}_m^c(\tau. u. u') \cos m(o' - o) \right.$$
$$\left. + \mathbf{M}_m^s(\tau. u. u') \sin m(o' - o) \right\}$$

$$(4.4)$$

$$\mathbf{I}(\tau. u. o) = \sum_{m=0}^{2N-1} \left\{ \mathbf{I}_m^c(\tau. u) \cos m(o_0 - o) \right.$$
$$\left. + \mathbf{I}_m^s(\tau. u) \sin m(o_0 - o) \right\}$$

$$(4.5)$$

$$\mathbf{Q}(\tau. u. o) = \sum_{m=0}^{2N-1} \left\{ \mathbf{Q}_m^c(\tau. u) \cos m(o_0 - o) \right.$$
$$\left. + \mathbf{Q}_m^s(\tau. u) \sin m(o_0 - o) \right\}.$$

$$(4.6)$$

Substitution of (4.4) into (4.3) and comparison with (4.6) yields:

$$\mathbf{Q}_m^c(\tau. u) = \frac{a(\tau)}{4\pi} \mathbf{M}_m^c(\tau. u. -\mu_0) \cdot \mathbf{S}_b(\tau) \exp(-\tau/\mu_0)$$

$$+ \delta_{0m} \left[1 - a(\tau)\right] \mathbf{S}_t(\tau)$$

$$\text{(4.7)}$$

$$\mathbf{Q}_m^s(\tau, u) = \frac{a(\tau)}{4\pi} \mathbf{M}_m^s(\tau, u, -\mu_0) \cdot \mathbf{S}_b(\tau) \exp(-\tau/\mu_0) \qquad \text{(4.8)}$$

By substituting (4.4) - (4.6) into (4.1) and (4.2), performing the integration over ϕ in the multiple scattering term, and comparing Fourier terms of equal order, one obtains a transfer equation for each Fourier component:

$$u \frac{d\mathbf{I}_m^c(\tau, u)}{d\tau} = \mathbf{I}_m^c(\tau, u) - \frac{a(\tau)}{4} \int_{-1}^{1} du' \left\{ \mathbf{M}_m^c(\tau, u, u') \mathbf{I}_m^c(\tau, u') (1 + \delta_{0m}) \right.$$

$$\left. - \mathbf{M}_m^s(\tau, u, u') \mathbf{I}_m^s(\tau, u') (1 - \delta_{0m}) \right\} - \mathbf{Q}_m^c(\tau, u) \qquad \text{(4.9)}$$

$$u \frac{d\mathbf{I}_m^s(\tau, u)}{d\tau} = \mathbf{I}_m^s(\tau, u) - \frac{a(\tau)}{4} \int_{-1}^{1} du' \left\{ \mathbf{M}_m^c(\tau, u, u') \mathbf{I}_m^s(\tau, u') (1 + \delta_{0m}) \right.$$

$$\left. + \mathbf{M}_m^s(\tau, u, u') \mathbf{I}_m^c(\tau, u') (1 - \delta_{0m}) \right\} - \mathbf{Q}_m^s(\tau, u). \qquad \text{(4.10)}$$

The cosine modes start at $m = 0$, and the sine modes start at $m = 1$. i.e. $\mathbf{I}_m^s$ and $\mathbf{M}_m^s$ vanish for $m = 0$. Thus, one can omit the Kronecker-deltas in (4.10), as well as the second Kronecker-delta in (4.9). Subsequently, the remaining integration over u is replaced by a discrete sum by introducing the Gaußian quadrature points u_j and corresponding weights w_j. One obtains for each Fourier component:

$$u_i \frac{d\mathbf{I}_m^c(\tau, u_i)}{d\tau} = \mathbf{I}_m^c(\tau, u_i)$$

$$- \frac{a(\tau)}{4} \sum_{\substack{j=-N \\ j \neq 0}}^{N} w_j \left\{ (1 + \delta_{0m}) \mathbf{M}_m^c(\tau, u_i, u_j) \mathbf{I}_m^c(\tau, u_j) \right.$$

$$\left. - \mathbf{M}_m^s(\tau, u_i, u_j) \mathbf{I}_m^s(\tau, u_j) \right\} - \mathbf{Q}_m^c(\tau, u_i) \qquad \text{(4.11)}$$

$$u_i \frac{d\mathbf{I}_m^s(\tau, u_i)}{d\tau} = \mathbf{I}_m^s(\tau, u_i)$$

$$- \frac{a(\tau)}{4} \sum_{\substack{j=-N \\ j \neq 0}}^{N} w_j \left\{ \mathbf{M}_m^c(\tau, u_i, u_j) \mathbf{I}_m^s(\tau, u_j) \right.$$

$$\left. + \mathbf{M}_m^s(\tau, u_i, u_j) \mathbf{I}_m^c(\tau, u_j) \right\} - \mathbf{Q}_m^s(\tau, u_i), \qquad \text{(4.12)}$$

$$m = 0, \ldots, 2N - 1$$

$$i = \pm 1, \ldots, \pm N.$$

The convention for the indices of the quadrature points is such that $u_j < 0$ for $j < 0$, and $u_j > 0$ for $j > 0$. These points are distributed symmetrically about zero, i.e. $u_{-j} = -u_j$. The corresponding weights are equal, i.e. $w_{-j} = w_j$. In a plane parallel atmosphere it is convenient to consider the two hemispheres defined by $u < 0$ (downwelling radiation) and $u > 0$ (upwelling radiation) separately, and to introduce the quantity $\mu := |u|$. Furthermore, as a consequence of certain symmetry relations, the Fourier components of the phase matrix have the following form [73]:

$$\mathbf{M}_m^c = \begin{pmatrix} M_{11m}^c & M_{12m}^c & 0 & 0 \\ M_{21m}^c & M_{22m}^c & 0 & 0 \\ 0 & 0 & M_{33m}^c & M_{34m}^c \\ 0 & 0 & M_{43m}^c & M_{44m}^c \end{pmatrix} =: \begin{pmatrix} \mathbf{M}_{1m}^c & \mathbf{0} \\ \mathbf{0} & \mathbf{M}_{2m}^c \end{pmatrix}$$

$$\mathbf{M}_m^s = \begin{pmatrix} 0 & 0 & M_{13m}^s & M_{14m}^s \\ 0 & 0 & M_{23m}^s & M_{24m}^s \\ M_{31m}^s & M_{32m}^s & 0 & 0 \\ M_{41m}^s & M_{42m}^s & 0 & 0 \end{pmatrix} =: \begin{pmatrix} \mathbf{0} & \mathbf{M}_{1m}^s \\ \mathbf{M}_{2m}^s & \mathbf{0} \end{pmatrix}$$

where (2×2) block matrices have been introduced for notational convenience. If one further defines

$$\mathbf{I}_m^c = \begin{pmatrix} I_{m,l}^c \\ I_{m,r}^c \\ U_m^c \\ V_m^c \end{pmatrix} := \begin{pmatrix} \mathbf{I}_{1m}^c \\ \mathbf{I}_{2m}^c \end{pmatrix} \quad : \quad \mathbf{I}_m^s = \begin{pmatrix} I_{m,l}^s \\ I_{m,r}^s \\ U_m^s \\ V_m^s \end{pmatrix} := \begin{pmatrix} \mathbf{I}_{1m}^s \\ \mathbf{I}_{2m}^s \end{pmatrix}$$

then the combination of the first two components of (4.11) and the last two components of (4.12) gives

$$\pm \mu_i \frac{d}{d\tau} \begin{pmatrix} \mathbf{I}_{1m}^c(\tau, \pm \mu_i) \\ \mathbf{I}_{2m}^s(\tau, \pm \mu_i) \end{pmatrix} = \begin{pmatrix} \mathbf{I}_{1m}^c(\tau, \pm \mu_i) \\ \mathbf{I}_{2m}^s(\tau, \pm \mu_i) \end{pmatrix}$$

$$
-\frac{a(\tau)}{4} \sum_{j=1}^{N} \left(\begin{array}{cc} w_{-j}(1+\delta_{0m})\mathbf{M}_{1m}^{c} & -w_{-j}\mathbf{M}_{1m}^{s} \\ w_{-j}\mathbf{M}_{2m}^{s} & w_{-j}\mathbf{M}_{2m}^{c} \end{array} \right) \Bigg|_{\tau, \pm\mu_{i}, -\mu_{j}} \cdot \left(\begin{array}{c} \mathbf{I}_{1m}^{c}(\tau, -\mu_{j}) \\ \mathbf{I}_{2m}^{s}(\tau, -\mu_{j}) \end{array} \right)
$$

$$
-\frac{a(\tau)}{4} \sum_{j=1}^{N} \left(\begin{array}{cc} w_{j}(1+\delta_{0m})\mathbf{M}_{1m}^{c} & -w_{j}\mathbf{M}_{1m}^{s} \\ w_{j}\mathbf{M}_{2m}^{s} & w_{j}\mathbf{M}_{2m}^{c} \end{array} \right) \Bigg|_{\tau, \pm\mu_{i}, +\mu_{j}} \cdot \left(\begin{array}{c} \mathbf{I}_{1m}^{c}(\tau, +\mu_{j}) \\ \mathbf{I}_{2m}^{s}(\tau, +\mu_{j}) \end{array} \right)
$$

$$
- \left(\begin{array}{c} Q_{m,l}^{c} \\ Q_{m,r}^{c} \\ Q_{m,u}^{s} \\ Q_{m,v}^{s} \end{array} \right) \tag{4.13}
$$

where now $i = 1, \ldots, N$. and where the upper and lower signs pertain to the upper and lower hemisphere, respectively.

Now the radiative transfer equation has been brought into a form that can be written in a much more compact way by combining the 4-vector components of the vectors in (4.13) at the various quadrature points into $4N$-vectors for the up and downwelling radiation, respectively:

$$
\mathcal{I}_{m-}^{c} := \left(\begin{array}{c} I_{m,l}^{c}(\tau, -\mu_{i}) \\ I_{m,r}^{c}(\tau, -\mu_{i}) \\ U_{m}^{s}(\tau, -\mu_{i}) \\ V_{m}^{s}(\tau, -\mu_{i}) \end{array} \right)_{1 \times 4N} \quad : \quad \mathcal{I}_{m+}^{c} := \left(\begin{array}{c} I_{m,l}^{c}(\tau, +\mu_{i}) \\ I_{m,r}^{c}(\tau, +\mu_{i}) \\ U_{m}^{s}(\tau, +\mu_{i}) \\ V_{m}^{s}(\tau, +\mu_{i}) \end{array} \right)_{1 \times 4N} . \tag{4.14}
$$

where caligraphic letters were used for the $4N$-vectors to avoid confusion with the corresponding 4-vector quantities. Explicitly, the $4N$-vectors are of the form

$$
\mathcal{I}_{m-}^{c} = [I_{m,l}^{c}(\tau, -\mu_{N}), I_{m,l}^{c}(\tau, -\mu_{N-1}), \ldots I_{m,l}^{c}(\tau, -\mu_{1}),
$$

$$
I_{m,r}^{c}(\tau, -\mu_{N}), I_{m,r}^{c}(\tau, -\mu_{N-1}), \ldots I_{m,r}^{c}(\tau, -\mu_{1}),
$$

$$
U_{m}^{s}(\tau, -\mu_{N}), U_{m}^{s}(\tau, -\mu_{N-1}), \ldots U_{m}^{s}(\tau, -\mu_{1}),
$$

$$
V_{m}^{s}(\tau, -\mu_{N}), V_{m}^{s}(\tau, -\mu_{N-1}), \ldots V_{m}^{s}(\tau, -\mu_{1})]^{T}.
$$

$$
\mathcal{I}_{m+}^{c} = [I_{m,l}^{c}(\tau, +\mu_{1}), I_{m,l}^{c}(\tau, +\mu_{2}), \ldots I_{m,l}^{c}(\tau, +\mu_{N}),
$$

$$I^c_{m,r}(\tau, +\mu_1),\ I^c_{m,r}(\tau, +\mu_2),\ \ldots\ldots\ I^c_{m,r}(\tau, +\mu_N).$$

$$U^s_m(\tau, +\mu_1),\ U^s_m(\tau, +\mu_2),\ \ldots\ldots\ U^s_m(\tau, +\mu_N).$$

$$V^s_m(\tau, +\mu_1),\ V^s_m(\tau, +\mu_2),\ \ldots\ldots\ V^s_m(\tau, +\mu_N)]^T.$$

By summarizing the phase matrix elements at the various quadrature angles in (4.13), new ($4N \times 4N$) matrices are defined that correspond to the $4N$-vectors in Eq. (4.14):

$$\mathcal{A}^c_{11m}(\tau) \quad := \quad -w_j\,\frac{a(\tau)}{4}\left(\begin{array}{cc} (1+\delta_{0m})\mathbf{M}^c_{1m} & -\mathbf{M}^s_{1m} \\[2mm] \mathbf{M}^s_{2m} & \mathbf{M}^c_{2m} \end{array}\right)_{4N\times4N}\Bigg|_{\tau,-\mu_i,-\mu_j:\,i,j=1\ldots N} \tag{4.15}$$

$$\mathcal{A}^c_{12m}(\tau) \quad := \quad -w_j\,\frac{a(\tau)}{4}\left(\begin{array}{cc} (1+\delta_{0m})\mathbf{M}^c_{1m} & -\mathbf{M}^s_{1m} \\[2mm] \mathbf{M}^s_{2m} & \mathbf{M}^c_{2m} \end{array}\right)_{4N\times4N}\Bigg|_{\tau,-\mu_i,+\mu_j:\,i,j=1\ldots N} \tag{4.16}$$

$$\mathcal{A}^c_{21m}(\tau) \quad := \quad -w_j\,\frac{a(\tau)}{4}\left(\begin{array}{cc} (1+\delta_{0m})\mathbf{M}^c_{1m} & -\mathbf{M}^s_{1m} \\[2mm] \mathbf{M}^s_{2m} & \mathbf{M}^c_{2m} \end{array}\right)_{4N\times4N}\Bigg|_{\tau,+\mu_i,-\mu_j:\,i,j=1\ldots N} \tag{4.17}$$

$$\mathcal{A}^c_{22m}(\tau) \quad := \quad -w_j\,\frac{a(\tau)}{4}\left(\begin{array}{cc} (1+\delta_{0m})\mathbf{M}^c_{1m} & -\mathbf{M}^s_{1m} \\[2mm] \mathbf{M}^s_{2m} & \mathbf{M}^c_{2m} \end{array}\right)_{4N\times4N}\Bigg|_{\tau,+\mu_i,+\mu_j:\,i,j=1\ldots N} \tag{4.18}$$

where $w_{-j} = w_j$ has been used.

Then the radiative transfer equation (4.13) becomes

$$\mathcal{U}_-\frac{d\mathcal{I}^c_{m-}}{d\tau} \quad = \quad (\mathcal{E}+\mathcal{A}^c_{11m})\,\mathcal{I}^c_{m-} + \mathcal{A}^c_{12m}\,\mathcal{I}^c_{m+} - \mathcal{S}^c_{m-} \tag{4.19}$$

$$\mathcal{U}_+\frac{d\mathcal{I}^c_{m+}}{d\tau} \quad = \quad \mathcal{A}^c_{21m}\,\mathcal{I}^c_{m-} + (\mathcal{E}+\mathcal{A}^c_{22m})\,\mathcal{I}^c_{m+} - \mathcal{S}^c_{m+} \tag{4.20}$$

where

$$\mathcal{S}^c_{m\pm} \quad := \quad \left(\begin{array}{c} Q^c_{m,l}(\tau,\pm\mu_i) \\[2mm] Q^c_{m,r}(\tau,\pm\mu_i) \\[2mm] Q^s_{m,u}(\tau,\pm\mu_i) \\[2mm] Q^s_{m,v}(\tau,\pm\mu_i) \end{array}\right)_{1\times4N} \tag{4.21}$$

$$\mathcal{U}_{\pm} = \begin{pmatrix} \pm\mu_i & 0 & 0 & 0 \\ 0 & \pm\mu_i & 0 & 0 \\ 0 & 0 & \pm\mu_i & 0 \\ 0 & 0 & 0 & \pm\mu_i \end{pmatrix}_{4N \times 4N} \tag{4.22}$$

and $\mathcal{E}$ denotes the $4N$-unit matrix. To combine the equations of the positive and negative hemisphere. one defines

$$\mathcal{U} := \begin{pmatrix} \mathcal{U}_- & 0 \\ 0 & \mathcal{U}_+ \end{pmatrix}_{8N \times 8N} \quad ; \quad \mathcal{I}_m^c := \begin{pmatrix} \mathcal{I}_{m-}^c(\tau) \\ \mathcal{I}_{m+}^c(\tau) \end{pmatrix}_{1 \times 8N}$$

$$\mathcal{A}_m^c := \begin{pmatrix} \mathcal{A}_{11m}^c & \mathcal{A}_{12m}^c \\ \mathcal{A}_{21m}^c & \mathcal{A}_{22m}^c \end{pmatrix}_{8N \times 8N} \quad ; \quad \mathcal{S}_m^c := \begin{pmatrix} \mathcal{S}_{m-}^c \\ \mathcal{S}_{m+}^c \end{pmatrix}_{1 \times 8N} .$$

Then Eqs. (4.19) and (4.20) can be written in compact form as

$$\mathcal{U}\frac{d\mathcal{I}_m^c}{d\tau} = (\mathcal{E} + \mathcal{A}_m^c)\mathcal{I}_m^c - \mathcal{S}_m^c. \tag{4.23}$$

where $\mathcal{E}$ now denotes the $8N$-unit matrix. The components of the $8N$-vectors are denoted by lower case letters. Thus the kth component of $\mathcal{I}_m^c$ will be denoted by $i_m^c(\tau, k)$. where $k = 1, \ldots, 8N$.

Equation (4.23) for the $8N$-cosine mode vectors was arrived at by first combining the first two components of (4.11) and the last two components of (4.12) into new 4-vectors. and by then combining the 4-vectors at different quadrature angle arguments into $4N$ and eventually $8N$ vectors. In a similar way. an equation for $8N$-vector sine modes can be obtained by combining the first two components of (4.12) with the last two components of (4.11). In complete analogy. one defines new $8N$-vector and matrix quantities $\mathcal{I}_m^s$. $\mathcal{S}_m^s$. $\mathcal{A}_m^s$. where the latter consists of the four $4N$-block matrices

$$\mathcal{A}_{11m}^s(\tau) := -w_j \frac{a(\tau)}{4} \begin{pmatrix} \mathbf{M}_{1m}^c & \mathbf{M}_{1m}^s \\ -\mathbf{M}_{2m}^s & (1 + \delta_{0m})\mathbf{M}_{2m}^c \end{pmatrix}_{4N \times 4N} \Bigg|_{\tau, -\mu_i, -\mu_j; i, j = 1 \ldots N} \tag{4.24}$$

$$\mathcal{A}_{12m}^s(\tau) := -w_j \frac{a(\tau)}{4} \begin{pmatrix} \mathbf{M}_{1m}^c & \mathbf{M}_{1m}^s \\ -\mathbf{M}_{2m}^s & (1 + \delta_{0m})\mathbf{M}_{2m}^c \end{pmatrix}_{4N \times 4N} \Bigg|_{\tau, -\mu_i, +\mu_j; i, j = 1 \ldots N} \tag{4.25}$$

$$\mathcal{A}_{21m}^s(\tau) \quad := \quad -w_j \, \frac{a(\tau)}{4} \begin{pmatrix} \mathbf{M}_{1m}^c & \mathbf{M}_{1m}^s \\ -\mathbf{M}_{2m}^s & (1+\delta_{0m})\mathbf{M}_{2m}^c \end{pmatrix}_{4N\times4N} \Bigg|_{\tau+\mu_i,-\mu_j \, : \, i,j=1......N} \qquad (4.26)$$

$$\mathcal{A}_{22m}^s(\tau) \quad := \quad -w_j \, \frac{a(\tau)}{4} \begin{pmatrix} \mathbf{M}_{1m}^c & \mathbf{M}_{1m}^s \\ -\mathbf{M}_{2m}^s & (1+\delta_{0m})\mathbf{M}_{2m}^c \end{pmatrix}_{4N\times4N} \Bigg|_{\tau+\mu_i,+\mu_j \, : \, i,j=1......N} \qquad (4.27)$$

One arrives at an equation of exactly the same form as for the $8N$ dimensional cosine mode vectors:

$$\mathcal{U} \frac{d\mathcal{I}_m^s}{d\tau} = (\mathcal{E} + \mathcal{A}_m^s)\,\mathcal{I}_m^s \, - \, \mathcal{S}_m^s. \qquad (4.28)$$

4.2.2 General solution to the homogeneous radiative transfer equation

The vector radiative transfer equation is of the same form for all cosine and all sine modes. Substitution of the ansatz

$$\mathcal{I}_m(\tau) \quad = \quad \mathcal{G}_m \exp(-\lambda_m \cdot \tau) \qquad (4.29)$$

into the homogeneous equation corresponding to (4.23) or (4.28) leads to

$$-\lambda_m \mathcal{U}\,\mathcal{G}_m = (\mathcal{E} + \mathcal{A}_m)\,\mathcal{G}_m$$

or

$$(\mathcal{E} + \mathcal{A}_m + \lambda_m \mathcal{U})\,\mathcal{G}_m = 0.$$

Solving this eigenvalue equation yields $8N$ eigenvalues $\lambda_{m1}.....\lambda_{m8N}$ with corresponding eigenvectors $\mathcal{G}_{m1}.....\mathcal{G}_{m8N}$. So the general solution to the homogeneous equation is a linear combination of $8N$ linearly independent solutions of the form of Eq. (4.29). For the case of a vertically inhomogeneous atmosphere. one can just subdivide the atmosphere into L horizontal layers labeled by a layer index p that are assumed to be homogeneous also in the vertical direction. i.e. the optical properties. such as the phase matrix and the single scattering albedo. are constant in each layer. The radiative transfer equation is then solved in each layer separately. The general solution to the homogeneous part of

the radiative transfer equations (4.23) or (4.28) in layer p is then

$$\mathcal{I}_{mp}(\tau) \;=\; \sum_{j=1}^{8N} C'_{jmp}\mathcal{G}_{jmp}\exp(-\lambda_{jmp}\cdot\tau) \tag{4.30}$$

j : eigenvalue index

$p = 1,\ldots,L$ (index of atmospheric layer)

$m = 0,\ldots,2N-1$ (index of Fourier mode).

4.2.3 Particular solutions to the inhomogeneous radiative transfer equation

From (4.7) and (4.8), it can be seen that the source term in the inhomogeneous equations (4.23) and (4.28) is of the form $\mathcal{S}_m = \mathcal{F}_m\,\exp(-\tau/\mu_0)+\mathcal{F}_t$. Particular solutions $\mathcal{Z}_m$ and $\mathcal{X}_m$ are therefore found separately for the beam source term $\mathcal{F}_m$ and the thermal source term $\mathcal{F}_t$, respectively, and for the cosine and sine modes, by making an appropriate ansatz in either case, quite like in the scalar problem. The $8N$-beam source term is obtained from (4.7), (4.8), and (4.21):

$$\mathcal{F}^c_{bm} \;=\; \begin{pmatrix} F^c_{b,l} \\ F^c_{b,r} \\ F^s_{b,u} \\ F^s_{b,v} \end{pmatrix}_{1\times 8N} = \frac{a(\tau)}{4\pi}\begin{pmatrix} M^c_{11m} & M^c_{12m} & 0 & 0 \\ M^c_{21m} & M^c_{22m} & 0 & 0 \\ M^s_{31m} & M^s_{32m} & 0 & 0 \\ M^s_{41m} & M^s_{42m} & 0 & 0 \end{pmatrix}_{8N\times 8N}\cdot\begin{pmatrix} S_{b,l} \\ S_{b,r} \\ S_{b,u} \\ S_{b,v} \end{pmatrix}_{1\times 8N}$$

$$= \frac{a(\tau)}{4\pi}\cdot\mathcal{M}^c_m \tag{4.31}$$

where

$$\mathcal{M}_m^c := \begin{pmatrix} M_{11m}^c(\tau. -\mu_i. -\mu_0)S_{b.l} + M_{12m}^c(\tau. -\mu_i. -\mu_0)S_{b.r} \\ M_{21m}^c(\tau. -\mu_i. -\mu_0)S_{b.l} + M_{22m}^c(\tau. -\mu_i. -\mu_0)S_{b.r} \\ M_{31m}^s(\tau. -\mu_i. -\mu_0)S_{b.l} + M_{32m}^s(\tau. -\mu_i. -\mu_0)S_{b.r} \\ M_{41m}^s(\tau. -\mu_i. -\mu_0)S_{b.l} + M_{42m}^s(\tau. -\mu_i. -\mu_0)S_{b.r} \\ M_{11m}^c(\tau. +\mu_i. -\mu_0)S_{b.l} + M_{12m}^c(\tau. +\mu_i. -\mu_0)S_{b.r} \\ M_{21m}^c(\tau. +\mu_i. -\mu_0)S_{b.l} + M_{22m}^c(\tau. +\mu_i. -\mu_0)S_{b.r} \\ M_{31m}^s(\tau. +\mu_i. -\mu_0)S_{b.l} + M_{32m}^s(\tau. +\mu_i. -\mu_0)S_{b.r} \\ M_{41m}^s(\tau. +\mu_i. -\mu_0)S_{b.l} + M_{42m}^s(\tau. +\mu_i. -\mu_0)S_{b.r} \end{pmatrix}_{1\times 8N}$$

and likewise

$$\mathcal{F}_{bm}^s = \frac{a(\tau)}{4\pi}.\mathcal{M}_m^s \tag{4.32}$$

where

$$\mathcal{M}_m^s := \begin{pmatrix} M_{13m}^s(\tau. -\mu_i. -\mu_0)S_{b.u} + M_{14m}^s(\tau. -\mu_i. -\mu_0)S_{b.v} \\ M_{23m}^s(\tau. -\mu_i. -\mu_0)S_{b.u} + M_{24m}^s(\tau. -\mu_i. -\mu_0)S_{b.v} \\ M_{33m}^c(\tau. -\mu_i. -\mu_0)S_{b.u} + M_{34m}^c(\tau. -\mu_i. -\mu_0)S_{b.v} \\ M_{43m}^c(\tau. -\mu_i. -\mu_0)S_{b.u} + M_{44m}^c(\tau. -\mu_i. -\mu_0)S_{b.v} \\ M_{13m}^s(\tau. +\mu_i. -\mu_0)S_{b.u} + M_{14m}^s(\tau. +\mu_i. -\mu_0)S_{b.v} \\ M_{23m}^s(\tau. +\mu_i. -\mu_0)S_{b.u} + M_{24m}^s(\tau. +\mu_i. -\mu_0)S_{b.v} \\ M_{33m}^c(\tau. +\mu_i. -\mu_0)S_{b.u} + M_{34m}^c(\tau. +\mu_i. -\mu_0)S_{b.v} \\ M_{43m}^c(\tau. +\mu_i. -\mu_0)S_{b.u} + M_{44m}^c(\tau. +\mu_i. -\mu_0)S_{b.v} \end{pmatrix}_{1\times 8N}$$

The source term (4.32) "drives" the sine modes of the first two and the cosine modes of the last two Stokes vector components, i.e. if the incident beam source has no U and V component, as in atmospheric applications, then these modes vanish. Substitution of the ansatz

$$\mathcal{I}_m^{c.s}(\tau) = \mathcal{Z}_m^{c.s} \exp(-\tau/\mu_0) \tag{4.33}$$

into the inhomogeneous radiative transfer equations (4.23) and (4.28) with $\mathcal{S}_m^{c,s} = \mathcal{F}_{bm}^{c,s}$ leads to

$$(\frac{1}{\mu_0}\mathcal{U} + \mathcal{E} + \mathcal{A}_m^{c,s})\,\mathcal{Z}_m^{c,s} \;=\; \mathcal{F}_{bm}^{c,s}. \tag{4.34}$$

from which the particular solution vectors $\mathcal{Z}_m^{c,s}$ with components $z_m^{c,s}(k)$ are determined.

From the thermal source term, there is only a contribution to the 0th cosine mode, as can be seen from (4.7) and (4.8). To get an approximate particular solution to the radiative transfer equation associated with the thermal source, one can make a polynomial approximation of both the Planck function and the source vector $\mathcal{F}_t$:

$$B(T(\tau)) \;=\; \sum_{l=0}^{K} b_l \tau^l$$

and

$$\mathcal{F}_t \;=\; (1 - a(\tau))\,\delta_{0m}\sum_{l=0}^{K}\mathcal{D}_l \tau^l \tag{4.35}$$

where

$$\mathcal{D}_l \;:=\; \begin{pmatrix} \mathcal{D}_{1l} \\ \mathcal{D}_{0l} \\ \mathcal{D}_{1l} \\ \mathcal{D}_{0l} \end{pmatrix}_{1\times 8N} \quad,\quad \mathcal{D}_{1l} \;:=\; \begin{pmatrix} b_l \\ \vdots \\ b_l \end{pmatrix}_{1\times 2N} \quad,\quad \mathcal{D}_{0l} \;:=\; \begin{pmatrix} 0 \\ \vdots \\ 0 \end{pmatrix}_{1\times 2N} \tag{4.36}$$

At this point it was taken into account that the thermal source is unpolarized. The ansatz

$$\mathcal{I}_m^c(\tau) \;:=\; \delta_{0m}\sum_{l=0}^{K}\mathcal{X}_l \tau^l \tag{4.37}$$

substituted into (4.23) with $\mathcal{S}_m^c = \delta_{0m}\mathcal{F}_t$ yields

$$\delta_{0m}\,\mathcal{U}\sum_{l=1}^{K} l\mathcal{X}_l \tau^{l-1} \;=\; \delta_{0m}\,(\mathcal{E}+\mathcal{A}_m^c)\sum_{l=0}^{K}\mathcal{X}_l \tau^l - \delta_{0m}\,(1-a(\tau))\sum_{l=0}^{K}\mathcal{D}_l \tau^l$$

$$= \delta_{0m}\,(\mathcal{E}+\mathcal{A}_m^c)\sum_{l=1}^{K+1}\mathcal{X}_{l-1}\tau^{l-1} - \delta_{0m}\,(1-a(\tau))\sum_{l=1}^{K+1}\mathcal{D}_{l-1}\tau^{l-1}.$$

Equating equal powers of τ, one finds

$$l < K+1 \quad : \quad \mathcal{U}l\mathcal{X}_l = (\mathcal{E}+\mathcal{A}_0^c)\,\mathcal{X}_{l-1} - (1-a(\tau))\mathcal{D}_{l-1}$$

$$l = K + 1 \quad : \quad 0 = (\mathcal{E} + \mathcal{A}_0^c)\, \mathcal{X}_K - (1 - a(\tau))\, \mathcal{D}_K.$$

So to a first order approximation, the procedure is as follows:

1. Find $\mathcal{X}_1$ from

$$(\mathcal{E} + \mathcal{A}_0^c)\, \mathcal{X}_1 \;=\; (1 - a(\tau))\, \mathcal{D}_1$$

$$(4.38)$$

2. Then find $\mathcal{X}_0$ from

$$(\mathcal{E} + \mathcal{A}_0^c)\, \mathcal{X}_0 \;=\; (1 - a(\tau))\, \mathcal{D}_0 + \mathcal{U}\, \mathcal{X}_1.$$

$$(4.39)$$

The combination of the general homogeneous solution (4.30) and the particular inhomogeneous solutions then gives the final result for each layer p:

$$\mathcal{I}_{m,p}^{c,s}(\tau) = \sum_{j=1}^{8N} C_{jmp}^{c,s}\, \mathcal{G}_{jmp}^{c,s}\, \exp(-\lambda_{jmp}^{c,s} \cdot \tau) \;+\; \mathcal{T}_{mp}^{c,s}(\tau).$$

or in components:

$$i_{m,p}^{c,s}(\tau, k) \;=\; \sum_{j=1}^{8N} C_{jmp}^{c,s}\, g_{jmp}^{c,s}(k)\, \exp(-\lambda_{jmp}^{c,s} \cdot \tau) \;+\; t_{mp}^{c,s}(\tau, k). \qquad (4.40)$$

where

$$t_{mp}^{c}(\tau, k) \;:=\; z_{mp}^{c}(k)\exp(-\tau/\mu_0) \;+\; \delta_{0m}[x_{0p}(k) + x_{1p}(k)\cdot\tau].$$

$$t_{mp}^{s}(\tau, k) \;:=\; z_{mp}^{s}(k)\exp(-\tau/\mu_0).$$

$$k = 1,\dots,8N \quad \text{(index of vector component).}$$

$$p = 1,\dots,L \quad \text{(layer index).}$$

$$m = 0,\dots,2N - 1 \quad \text{(index of Fourier mode).}$$

$$j : \text{index of eigenvalue.}$$

4.2.4 Boundary Conditions

The coefficients $C^{c,s}_{jmp}$ now have to be determined from the boundary and layer interface conditions.

In terms of the 4-Stokes vectors, the radiation at the top of the horizontal slab is

$$\mathbf{I}(\tau_0. -\mu. o) = \mathbf{I}_i(\tau_0) + \mathbf{I}_t(\tau_0).$$

where $\mathbf{I}_i$ and $\mathbf{I}_t$ denote a possible source of isotropic radiation incident from above the medium and the thermal emission from the upper boundary itself. respectively. Since both are isotropic. these vectors only have a cosine Fourier component for $m = 0$. Furthermore. they are both unpolarized. i.e. $\mathbf{I}_i = [I_i/2. I_i/2. 0. 0]^T$ and $\mathbf{I}_t = [I_t/2. I_t/2. 0. 0]^T$. Thus. in terms of the $8N$-vectors. one must require that the radiation at the upper boundary be equal to

$$i^c_m(\tau_0. k) := \begin{cases} \delta_{0m} \, (I_i(\tau_0) + I_t(\tau_0))/2 & : \quad k = 1 \ldots \ldots N \\[4pt] \delta_{0m} \, (I_i(\tau_0) + I_t(\tau_0))/2 & : \quad k = N + 1 \ldots \ldots 2N \\[4pt] 0 & : \quad k = 2N + 1 \ldots \ldots 3N \\[4pt] 0 & : \quad k = 3N + 1 \ldots \ldots 4N \\[4pt] 0 & : \quad k = 4N + 1 \ldots \ldots 5N \\[4pt] 0 & : \quad k = 5N + 1 \ldots \ldots 6N \\[4pt] 0 & : \quad k = 6N + 1 \ldots \ldots 7N \\[4pt] 0 & : \quad k = 7N + 1 \ldots \ldots 8N \end{cases} \tag{4.41}$$

and

$$i^s_m(\tau_0. k) = 0 \qquad \forall k.$$

The radiation field at the lower boundary taken here to be the surface of a planet is given in 4-vector form by

$$\begin{aligned} \mathbf{I}(\tau_L. \mu. o) &= \mathbf{E}_t(\mu) \, \mathbf{S}_t(\tau_L) \\ &+ \frac{1}{\pi} \int_0^{2\pi} do' \int_0^1 d\mu' \, \mu' \, \mathbf{A}(\mu. o: -\mu'. o') \, \mathbf{I}(\tau_L. -\mu'. o') \\ &+ \mathbf{A}(\mu. o: -\mu_0. o_0) \frac{\mu_0}{\pi} \mathbf{S}_b \, \exp(-\tau_L/\mu_0). \end{aligned} \tag{4.42}$$

The three terms on the rhs are the thermal emission of the surface. the reflection of diffuse light by the surface. and the reflection of direct sunlight. respectively.

$$\mathbf{E}_t := \begin{pmatrix} \epsilon_{11} & 0 & 0 & 0 \\ 0 & \epsilon_{22} & 0 & 0 \\ 0 & 0 & 0 & 0 \\ 0 & 0 & 0 & 0 \end{pmatrix}$$

denotes the matrix of the unpolarized surface emittance. and

$$\mathbf{A} := \begin{pmatrix} a_{11} & a_{12} & a_{13} & a_{14} \\ a_{21} & a_{22} & a_{23} & a_{24} \\ a_{31} & a_{32} & a_{33} & a_{34} \\ a_{41} & a_{42} & a_{43} & a_{44} \end{pmatrix}$$

is the bidirectional reflectance matrix. The azimuthal dependency is again eliminated by a Fourier expansion which. after integration over o and Gaußian quadrature leads to:

$$
\mathbf{I}_m^c(\tau_L. +\mu_i) = \delta_{0m}\, \mathbf{E}_t(+\mu_i)\, \mathbf{S}_t(\tau_L)
$$

$$
+ \sum_{j=1}^{N} w_j \mu_j \Big\{ (1+\delta_{0m})\, \mathbf{A}_m^c(\mu_i. -\mu_j)\, \mathbf{I}_m^c(\tau_L. -\mu_j)
$$

$$
- \mathbf{A}_m^s(\mu_i. -\mu_j)\, \mathbf{I}_m^s(\tau_L. -\mu_j) \Big\}
$$

$$
+ \frac{\mu_0}{\pi}\, \exp(-\tau_L/\mu_0)\, \mathbf{A}_m^c(\mu_i. -\mu_0)\, \mathbf{S}_b. \qquad i=1\ldots\ldots N \qquad (4.43)
$$

$$
\mathbf{I}_m^s(\tau_L. +\mu_i) =
$$

$$
= \sum_{j=1}^{N} w_j \mu_j \{ \mathbf{A}_m^c(\mu_i. -\mu_j)\, \mathbf{I}_m^s(\tau_L. -\mu_j)
$$

$$
+ \mathbf{A}_m^s(\mu_i. -\mu_j)\, \mathbf{I}_m^c(\tau_L. -\mu_j) \}
$$

$$
+ \frac{\mu_0}{\pi}\, \exp(-\tau_L/\mu_0)\, \mathbf{A}_m^s(\mu_i. -\mu_0)\, \mathbf{S}_b. \qquad i=1\ldots\ldots N \qquad (4.44)
$$

Eqs. (4.43) and (4.44) also have to be translated into $8N$-vector form. The first term on

the rhs of (4.43) takes on the form

$$
i_{t,m}^c(\tau_L, k) \;:=\; \delta_{0m}\,\frac{B(T(\tau_L))}{2}\cdot
\begin{cases}
\epsilon_{11}(\mu_{k-4N}) & : \ \text{for } k = 4N+1\ldots\ldots5N \\[4pt]
\epsilon_{22}(\mu_{k-5N}) & : \ \text{for } k = 5N+1\ldots\ldots6N \\[4pt]
0 & : \ \text{for } k = 6N+1\ldots\ldots7N \\[4pt]
0 & : \ \text{for } k = 7N+1\ldots\ldots8N
\end{cases}
$$

$$(4.45)$$

If one assumes that the elements of the reflectance matrix have the same symmetry properties with respect to $\phi' - \phi$ as those of the phase matrix, i.e.

$$
\mathbf{A}_m^c = \begin{pmatrix}
a_{11m}^c & a_{12m}^c & 0 & 0 \\
a_{21m}^c & a_{22m}^c & 0 & 0 \\
0 & 0 & a_{33m}^c & a_{34m}^c \\
0 & 0 & a_{43m}^c & a_{44m}^c
\end{pmatrix}
=: \begin{pmatrix}
\mathbf{A}_{1m}^c & \mathbf{0} \\
\mathbf{0} & \mathbf{A}_{2m}^c
\end{pmatrix}
$$

$$
\mathbf{A}_m^s = \begin{pmatrix}
0 & 0 & a_{13m}^s & a_{14m}^s \\
0 & 0 & a_{23m}^s & a_{24m}^s \\
a_{31m}^s & a_{32m}^s & 0 & 0 \\
a_{41m}^s & a_{42m}^s & 0 & 0
\end{pmatrix}
=: \begin{pmatrix}
\mathbf{0} & \mathbf{A}_{1m}^s \\
\mathbf{A}_{2m}^s & \mathbf{0}
\end{pmatrix}.
$$

then the combination of the I_l- and I_r- components of the third term in (4.43) with the corresponding U- and V-components in (4.44) becomes in $8N$-vector form:

$$
i_{b,m}^{\ }(\tau_L, k) \;:=\; \frac{\mu_0}{\pi}\,\exp(-\tau_L/\mu_0)
$$

$$
\times
\begin{cases}
a_{11m}^c(\mu_{k-4N}, -\mu_0)\,S_{b,l} + a_{12m}^c(\mu_{k-4N}, -\mu_0)\,S_{b,r} & : \ k = 4N+1\ldots\ldots5N \\[4pt]
a_{21m}^c(\mu_{k-5N}, -\mu_0)\,S_{b,l} + a_{22m}^c(\mu_{k-5N}, -\mu_0)\,S_{b,r} & : \ k = 5N+1\ldots\ldots6N \\[4pt]
a_{31m}^s(\mu_{k-6N}, -\mu_0)\,S_{b,l} + a_{32m}^s(\mu_{k-6N}, -\mu_0)\,S_{b,r} & : \ k = 6N+1\ldots\ldots7N \\[4pt]
a_{41m}^s(\mu_{k-7N}, -\mu_0)\,S_{b,l} + a_{42m}^s(\mu_{k-7N}, -\mu_0)\,S_{b,r} & : \ k = 7N+1\ldots\ldots8N
\end{cases}
$$

$$(4.46)$$

With the definition

$$
\mathcal{R}^c \;:=\; (r_{ij}^c) \;:=\; w_j\mu_{+j}
\begin{pmatrix}
(1 + \delta_{0m})\mathbf{A}_{1m}^c & -\mathbf{A}_{1m}^s \\
\mathbf{A}_{2m}^s & \mathbf{A}_{2m}^c
\end{pmatrix}_{4N\times 4N}\Bigg|_{+\mu_i, -\mu_j\,;\,i,j=1\ldots\ldots N}
$$

$$(4.47)$$

the combination of the I_l - and I_r - components of the second term on the rhs of (4.43) and the corresponding U - and V - components of (4.44) becomes

$$i_{d,m}^c(\tau_L, k) = \sum_{n=1}^{4N} r_{k-4N,n} \, i_m^c(\tau_L, n) \, , \quad k = 4N + 1, \ldots, 8N.$$

Finally, substitution of (4.40) for $i_m^c(\tau_L, n)$ yields two terms:

$$i_{dg,m}^c(\tau_L, k) := \sum_{j=1}^{8N} C_{jmL}^{'c} \left\{ \sum_{n=1}^{4N} r_{k-4N,n}^c \, g_{jmL}^c(n) \right\} \exp(-\lambda_{jmL}^c \cdot \tau_L)$$

$$k = 4N + 1, \ldots, 8N \tag{4.48}$$

and

$$i_{dp,m}^c(\tau_L, k) := \sum_{n=1}^{4N} r_{k-4N,n}^c \, t_{m,L}^c(\tau_L, n) \, , \quad k = 4N + 1, \ldots, 8N \, .$$

$$\tag{4.49}$$

So at the lower boundary, the condition is that the intensity components be equal to

$$i_{m+}^c(\tau_L, k) := i_{t,m}^c(\tau_L, k) + i_{b,m}^c(\tau_L, k) + i_{dg,m}^c(\tau_L, k) + i_{dp,m}^c(\tau_L, k)$$

$$k = 4N + 1, \ldots, 8N \tag{4.50}$$

where the different terms are defined in (4.45) – (4.49).

In complete analogy, the components of the $8N$-sine mode Stokes vectors have to be equal to

$$i_{m+}^s(\tau_L, k) := i_{b,m}^s(\tau_L, k) + i_{dg,m}^s(\tau_L, k) + i_{dp,m}^s(\tau_L, k)$$

$$k = 4N + 1, \ldots, 8N \tag{4.51}$$

where

$$i_{b,m}^s(\tau_L, k) := \frac{\mu_0}{\pi} \exp(-\tau_L/\mu_0)$$

$$\times \begin{cases} a_{13m}^s(\mu_{k-4N}, -\mu_0) \, S_{b,u} + a_{14m}^s(\mu_{k-4N}, -\mu_0) \, S_{b,v} & : \quad k = 4N + 1, \ldots, 5N \\ a_{23m}^s(\mu_{k-5N}, -\mu_0) \, S_{b,u} + a_{24m}^s(\mu_{k-5N}, -\mu_0) \, S_{b,v} & : \quad k = 5N + 1, \ldots, 6N \\ a_{33m}^c(\mu_{k-6N}, -\mu_0) \, S_{b,u} + a_{34m}^c(\mu_{k-6N}, -\mu_0) \, S_{b,v} & : \quad k = 6N + 1, \ldots, 7N \\ a_{43m}^c(\mu_{k-7N}, -\mu_0) \, S_{b,u} + a_{44m}^c(\mu_{k-7N}, -\mu_0) \, S_{b,v} & : \quad k = 7N + 1, \ldots, 8N \end{cases}$$

$$\tag{4.52}$$

$$i^s_{dg,m}(\tau_L, k) \; := \; \sum_{j=1}^{8N} C'^s_{jmL} \left\{ \sum_{n=1}^{4N} r^s_{k-4N,n} \, g^s_{jmL}(n) \right\} \exp(-\lambda^s_{jmL} \cdot \tau_L)$$

$$k = 4N + 1, \ldots, 8N. \tag{4.53}$$

$$i^s_{dp,m}(\tau_L, k) \; := \; \sum_{n=1}^{4N} r^s_{k-4N,n} \, t^s_{m,L}(\tau_L, n) \,, \quad k = 4N + 1, \ldots, 8N. \tag{4.54}$$

and

$$\mathcal{R}^s \; := \; (r^s_{ij}) \; := \; w_j \mu_{+j} \left(\begin{array}{cc} \mathbf{A}^c_{1m} & \mathbf{A}^s_{1m} \\ -\mathbf{A}^s_{2m} & (1 + \delta_{0m})\mathbf{A}^c_{2m} \end{array} \right)_{4N \times 4N} \Bigg|_{+\mu_i, -\mu_j; i,j=1,\ldots,N} \tag{4.55}$$

So if one requires continuity of $i^{c,s}_m$ at the upper and lower boundaries as well as across interfaces of layers, then

$$i^{c,s}_{m,1}(\tau_0, k) \; = \; i^{c,s}_{m-}(\tau_0, k) \quad .$$

$$k = 1, \ldots, 4N; \; m = 0, \ldots, 2N - 1$$

$$i^{c,s}_{m,p}(\tau_p, k) \; = \; i^{c,s}_{m,p+1}(\tau_p, k) \quad .$$

$$k = 1, \ldots, 8N; \; p = 1, \ldots, L - 1; \; m = 0, \ldots, 2N - 1$$

$$i^{c,s}_{m,L}(\tau_L, k) \; = \; i^{c,s}_{m+}(\tau_L, k) \quad .$$

$$k = 4N + 1, \ldots, 8N; \; m = 0, \ldots, 2N - 1. \tag{4.56}$$

Substitution of (4.40) finally yields:

$$\sum_{j=1}^{8N} C^{c,s}_{jm1} \, g^{c,s}_{jm1}(k) \, \exp(-\lambda^{c,s}_{jm1} \cdot \tau_0) = i^{c,s}_{m-}(\tau_0, k) - t^{c,s}_{m1}(\tau_0, k) \quad .$$

$$k = 1, \ldots, 4N$$

$$\sum_{j=1}^{8N} \left\{ C^{c,s}_{jmp} \, g^{c,s}_{jmp}(k) \, \exp(-\lambda^{c,s}_{jmp} \cdot \tau_p) \right.$$

$$\left. - C^{c,s}_{jm,p+1} \, g^{c,s}_{jm,p+1}(k) \, \exp(-\lambda^{c,s}_{jm,p+1} \cdot \tau_p) \right\}$$

$$= r^{c,s}_{m,p+1}(\tau_p, k) - r^{c,s}_{mp}(\tau_p, k) \quad k = 1, \ldots, 8N \; : \quad p = 1, \ldots, L - 1$$

$$\sum_{j=1}^{8N} C_{jmL}^{c,s} \, a_{jmL}^{c,s}(k) \, \exp(-\lambda_{jmL}^{c,s} \cdot \tau_L) \; = \; i_{g,m}^{c,s}(\tau_L, k) \; - \; t_{m,L}^{c,s}(\tau_L, k)$$

$$k = 4N + 1, \ldots, 8N$$

where $\quad i_{g,m}^{c} := i_{t,m}^{c} + i_{b,m}^{c} + i_{dp,m}^{c} \cdot i_{g,m}^{s} := i_{b,m}^{s} + i_{dp,m}^{s}$

and $\quad a_{jmL}^{c,s}(k) := g_{jmL}^{c,s}(k) - \sum_{n=1}^{4N} r_{k-4N,n} \, g_{jmL}^{c,s}(n)$.

$$(4.57)$$

So the boundary conditions yield a system of $8N \times L$ equations (at fixed m) for the $8N \times L$ unknown coefficients C_{jmp}' for each Fourier mode. Solving these equations and back substituting the determined coefficients into (4.40) solves the vector radiative transfer problem.

As in the discrete ordinate solution of the scalar radiative transfer problem, the determination of the constants of integration of the discrete ordinate solution (4.40) by means of the system of linear equations (4.57) may be a numerically ill-conditioned problem due to the occurrence of positive and negative exponentials in the coefficient matrix. In complete analogy to the scalar problem, this numerical obstacle is removed by the scaling transformation

$$C_{jmp}'^{c,s} \; = \; \bar{C}_{jmp}'^{c,s} \, \exp(\lambda_{jmp}^{c,s} \tau_{p-1}) \quad : \quad \lambda_{jmp}^{c,s} \geq 0$$

$$C_{jmp}'^{c,s} \; = \; \bar{C}_{jmp}'^{c,s} \, \exp(\lambda_{jmp}^{c,s} \tau_p) \quad : \quad \lambda_{jmp}^{c,s} < 0. \qquad (4.58)$$

After substituting (4.58) into (4.57), one can solve for $\bar{C}_{jmp}'^{c,s}$ and later transform back to obtain the constants of integration $C_{jmp}'^{c,s}$.

4.3 Rayleigh scattering tests

The vector version of DISORT (hereafter VDISORT) has so far been tested only for a few cases of Rayleigh scattering as well as for scattering by spherical particles in the microwave region [74]. Extensive additional tests for a Rayleigh scattering, non-absorbing atmosphere have been conducted in this work by generating new results for several val-

ues of optical thickness. surface albedo, and solar zenith angle. and comparing them to benchmark values found in the literature [75]. For many test cases. the agreement between the literature values and the numerical results produced by the original code turned out to be very poor. Figure 4.1 gives a typical example of the problems encountered. The intensity I obtained with the original version of VDISORT is shown as a function of the cosine of the polar angle μ (dashed line). both at the top and at the bottom of the atmosphere for an atmosphere of optical depth $\tau = 1$. an underlying black surface (albedo $\alpha = 0$). the sun incident at $\mu_0 = 0.8$. and the azimuth between the sun and the direction of observation $\phi - \phi_0 = 90°$. The benchmark values are marked by the circles. A close investigation revealed a few errors in the implementation of the procedures specific to the vector problem. No errors were found in the numerical core routines of VDISORT. which had been adopted from the scalar version of the code [70]. After eliminating the technical errors in the code. the tests were repeated for an optical thickness $\tau = 1$. surface albedos $\alpha = 0$. 0.25. and 0.8. and the beam source incident at $\mu_0 = 0.2$. 0.6. and 0.8. Benchmark values can be found in the literature for I. Q. and U at the top and bottom of the Rayleigh scattering atmosphere for most combinations of these parameters [75] (the Stokes component V vanishes in a purely Rayleigh scattering atmosphere). No further problems were encountered in reproducing the benchmark values. As an example. Fig. 4.2 shows the Stokes components I. Q. and U of the downwelling radiation at the bottom. and of the upwelling radiation at the top of the medium as a function of μ. obtained with the corrected code. and with the input exactly as in Fig. 4.1. Comparison of Figs. 4.1 and 4.2 shows that the problem has been eliminated.

The Stokes parameters in Figs. 4.1 and 4.2 have been obtained at the computational quadrature angles. When interpolating between the quadrature angles to the angles of the tabulated literature values with a standard spline procedure. the direct comparison between the benchmark and the interpolated VDISORT-values shows an agreement that is typically better than 99.5 %.

4.4 Fourier decomposition of the phase matrix—spherical particles

In the theoretical development of the vector discrete ordinate radiative transfer theory it is convenient to choose the Stokes vector representation $\mathbf{I} = [I_l. I_r. U. V]^T$. In terms of the complex transverse electric field components of the radiation field $E_l = |E_l|e^{-i\epsilon_1}$ and $E_r = |E_r|e^{-i\epsilon_2}$. these Stokes vector components are given by

$$I_l = E_l E_l^*$$

$$I_r = E_r E_r^*$$

$$U = 2|E_l||E_r|\cos\delta$$

$$V = 2|E_l||E_r|\sin\delta \qquad (4.59)$$

where $\delta = \epsilon_1 - \epsilon_2$. The connection with the most commonly used representation $\mathbf{I}_s = [I.Q.U.V]^T$ is given by

$$\mathbf{I}_s = \mathbf{D} \cdot \mathbf{I} \qquad (4.60)$$

where

$$\mathbf{D} := \begin{pmatrix} 1 & 1 & 0 & 0 \\ 1 & -1 & 0 & 0 \\ 0 & 0 & 1 & 0 \\ 0 & 0 & 0 & 1 \end{pmatrix}.$$

The scattered transverse electric field $[E_l. E_r]^T$ can be obtained in terms of the incident field $[E_{l0}. E_{r0}]^T$ by a linear transformation:

$$\begin{pmatrix} E_l \\ E_r \end{pmatrix} = \mathbf{A} \cdot \begin{pmatrix} E_{l0} \\ E_{r0} \end{pmatrix}$$

where $\mathbf{A}$ is a 2×2 matrix. The corresponding linear transformation connecting the incident and scattered Stokes vectors in the scattering plane is called the Mueller matrix (in the case of a single scattering event). For scattering by a small volume containing

an ensemble of particles. the ensemble-averaged Mueller matrix is referred to as the scattering matrix **F**. Finally. when transforming from the scattering plane to a fixed laboratory frame. the corresponding matrix is referred to as the phase matrix **M**.

For the case of scattering by particles with a size parameter comparable to the wavelength of the incident light. certain assumptions are usually made concerning the ensemble of scattering particles. which have consequences for the scattering matrix. In particular. the matrix **A** is diagonal for homogeneous spherical particles [76]. and the scattering matrix in the Stokes vector representation (4.60) is of the following form [53]:

$$
\mathbf{F}_s(\Theta) \;=\; \begin{pmatrix} a_1 & b_1 & 0 & 0 \\ b_1 & a_1 & 0 & 0 \\ 0 & 0 & a_3 & b_2 \\ 0 & 0 & -b_2 & a_3 \end{pmatrix}
\tag{4.61}
$$

where each of the four independent components $a_1 . a_3 . b_1 . b_2$ is a function of the scattering angle Θ.

4.5 Generalization to nonspherical particles

The original version of VDISORT assumes a scattering matrix of the form (4.61). and the four independent components are expanded in Legendre polynomials [71]. Consequently. the original VDISORT version is strictly limited to scattering by *spherical* particles. commonly referred to as Mie scattering. However. for the broad field of atmospheric and other applications. more general phase matrices often have to be considered. In order to expand the scope of VDISORT to more general applications including scattering by nonspherical particles. a phase matrix of the same form as the one considered by Hovenier

[53] is considered:

$$\mathbf{F}_s(\Theta) \; = \; \begin{pmatrix} a_1 & b_1 & 0 & 0 \\ b_1 & a_2 & 0 & 0 \\ 0 & 0 & a_3 & b_2 \\ 0 & 0 & -b_2 & a_4 \end{pmatrix}.$$ (4.62)

This scattering matrix with six independent elements is valid if any of the following assumptions is satisfied [73]:

1. Each particle in the ensemble has a plane of symmetry (e.g. homogeneous spheroids. which include homogeneous spheres). and the particles are randomly oriented: or

2. the ensemble contains particles and their mirror particles in equal number and in random orientation: or

3. the particles are much smaller than the wavelength (Rayleigh limit).

The elements of (4.62) are most conveniently expanded in generalized spherical functions. The procedure for expanding a scattering matrix of the form (4.62) in this basis was added to the original version of VDISORT. Thus. the generality of VDISORT has been significantly enhanced to apply to cases satisfying any one of the above three assumptions.

4.6 Mie scattering test

A well-studied and documented test case for Mie scattering is based on the use of a Gamma-size distribution for the scattering particles

$$N(r) \; = \; \frac{1}{(ab)^{(\frac{1}{b}-2)} \, \Gamma\left(\frac{1}{b} - 2\right)} \cdot r^{\frac{1}{b}-3} \cdot \exp\left(-\frac{r}{ab}\right)$$ (4.63)

with the choices $a = 0.2\mu$m and $b = 0.07$. and an index of refraction of the particles of $n = 1.44$ with vanishing imaginary part. The Fourier components of the phase matrix

have been computed up to the 13th order for the wavelength $\lambda = 0.951\mu$m. For this reason, this case has been referred to as the $L = 13$ case, and the expansion coefficients of the scattering matrix in the basis of the generalized spherical functions can be found in the literature [77]. Benchmark values for the Stokes vector components have been computed for beam incidence by Garcia and Siewert with the F_N method [34, 78] by using this particular scattering matrix, but then allowing for some absorption by setting the single scattering albedo to $a = 0.99$. The surface albedo was assumed to be $\alpha = 0.1$, the total optical thickness $\tau = 1$, the cosine of the solar zenith angle $\mu_0 = 0.2$, and the Stokes vector of the incident beam source term $\mathbf{S}_b = \pi[1, 0, 0, 0]^T$ in the representation (4.60). The benchmark values of Garcia and Siewert could initially not be reproduced with the original version of VDISORT, not even after the errors found while performing the Rayleigh scattering tests had been corrected. Some major changes were necessary in the theoretical approach as well as those parts of the code that prepare the input to the VDISORT core routines in the Mie scattering case. Again, these changes affected only routines specific to the *vector* version. In order to obtain the Fourier components of the phase matrix (as required by the discrete ordinate method, see Section 4.2) from the expansion coefficients of the scattering matrix, the original approach consisted of an expansion of the scattering matrix in Legendre polynomials (in the newly substituted procedure, the generalized spherical functions are chosen as the expansion basis). Subsequently, the scattering matrix was transformed into the phase matrix by rotating it from the scattering plane into the laboratory frame. The Fourier components were finally obtained in Weng's original approach by applying a numerical Fast Fourier Transform routine to the phase matrix. So in order to get from one set of expansion coefficients to another set in a different expansion basis, this procedure relies on a detour via the scattering matrix and the phase matrix. The expansion, rotation, and particularly the Fast Fourier Transformation involved in that detour are quite costly in terms of computing time. The poor results one obtains in the $L = 13$ test case also suggest that the implementation of this procedure is not error-free.

A much more efficient method was developed by Siewert [79, 80] and successfully implemented and applied in connection with the doubling/adding method [35, 73]. In this method, the expansion coefficients of the scattering matrix in the basis of generalized spherical functions are directly and analytically transformed into the Fourier components of the phase matrix. No unnecessary detour via the scattering matrix and the phase matrix is involved, and the time consuming Fourier transformation procedure is rendered unnecessary. Another advantage is that the expressions for the Fourier components in terms of the generalized spherical functions are purely analytical. The numerical implementation basically relies on a few simple recurrence relations for the generalized spherical functions, as described in detail elsewhere [35, 80].

Upon replacing the original Fast Fourier Transform (FFT) package including the expansion and transformation routines for the scattering matrix, this method has been adopted for the upgraded version of VDISORT. Siewert's method [79, 80] for the Fourier decomposition of the phase matrix pertains to a scattering matrix of the same form as in (4.62) and is thus valid for ensembles of nonspherical particles satisfying any of the assumptions mentioned above. CPU time comparisons in the $L = 13$ test case showed that the new procedure is about 16 times as fast as the FFT method used in the original version of VDISORT.

The improvement in accuracy achieved by the new procedure can be seen in Figs. 4.3 and 4.4, showing the Stokes vector components I, Q, and U, as well as the degree of polarization $P = \sqrt{Q^2 + U^2 + V^2}/I$ for the $L = 13$ case at the top and bottom of the medium, respectively. The dashed line represents the numerical values obtained with the original version of VDISORT after correcting the errors detected in the Rayleigh scattering tests, but still using the original FFT method. The solid line represents the results from the corrected and improved version of VDISORT using Siewert's method. The circles indicate the benchmark values from Garcia and Siewert's F_N method [78].

4.7 Polarized incident beam test

The first two Stokes components I and Q of the scattered field are symmetric in $o - o'$, while the last two, U and V are antisymmetric, unless the Stokes vector of the incident beam source has a U- or V-component (see Section 4.2), which is not the case in atmospheric applications. Therefore, after performing a Fourier expansion of all vector and matrix quantities pertinent to the radiative transfer equation and boundary conditions, only the cosine modes contribute to I and Q, and only the sine modes to U and V. VDISORT is, however, capable of handling also the general case of an arbitrarily polarized incident beam source. To test the performance of those routines computing the sine modes of I and Q and the cosine modes of U and V, a polarized beam source term $S_b = \pi \cdot [1, 0.4, 0.2, 0.05]^T$ is chosen as input; all other parameters are as in the $L = 13$ case.

For comparison, the Stokes parameters I, Q, U, and the degree of polarization P for this test case have been computed with the General Adding Program (GAP) described by de Haan et al. [35]. (In the $L = 13$ case with an unpolarized beam source, as considered in the previous section, the test of GAP gave an agreement with the results published by Garcia and Siewert that was typically better than 99.999 % .)

The particular VDISORT routines responsible for the computation of the sine modes of I and Q and the cosine modes of U and V also needed some corrections. The comparison in Fig. 4.5 of the results obtained with the new VDISORT version for the case of a polarized beam source to the values obtained with GAP in this test case show that the routines in question are now working correctly.

4.8 Summary

An extension of the scalar discrete ordinate radiative transfer model to the 4-vector problem including polarization has been tested for Rayleigh and Mie scattering. The tests for Rayleigh scattering revealed some errors in the original implementation of this model.

Although these errors had large effects on the numerical results and thus on the overall performance of the code, they were nevertheless not fundamental and could readily be rectified. The poor performance of the original code for Mie scattering indicated some errors in the routines computing the Fourier components of the Mie phase matrix. Since this procedure as a whole was found to be inefficient, it was completely eliminated and replaced by an analytical, more direct and more efficient method. This analytic Fourier decomposition approach yields accurate results for Mie scattering. In contrast to the original package for calculating the Fourier components of the phase matrix, which was restricted to spherical particles only, the new method is also valid for scattering by a wide range of nonspherical particles. Thus, the upgraded version of VDISORT has been generalized and extended to a much broader range of applications. After all corrections and improvements, the results obtained with the new version of VDISORT compare very well with published benchmark values, for both Rayleigh and Mie scattering. The performance of the code for the special test case of a polarized beam source was equally satisfactory.
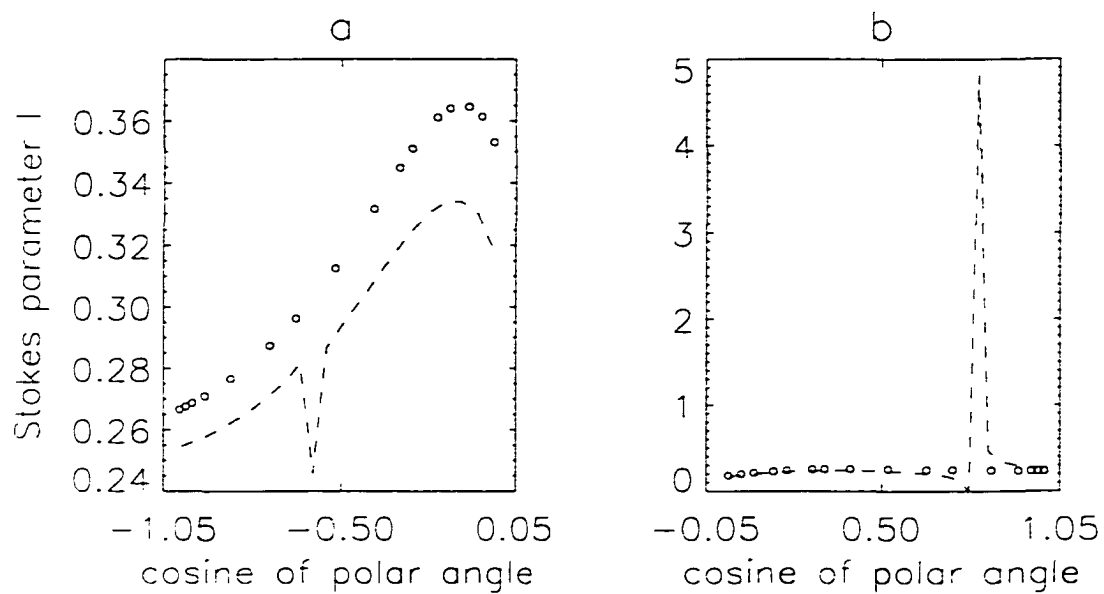
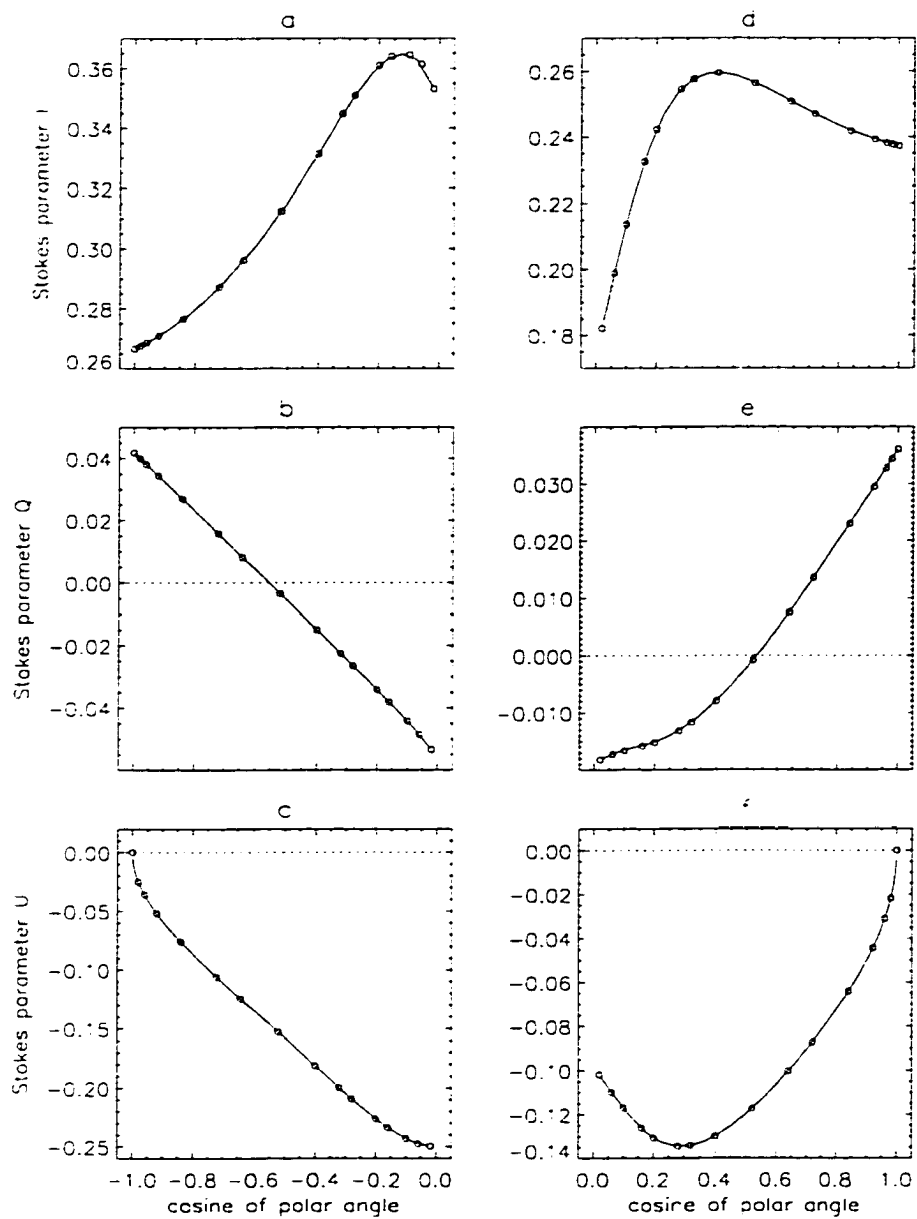Figure 4.1. Rayleigh scattering test. original version of VDISORT

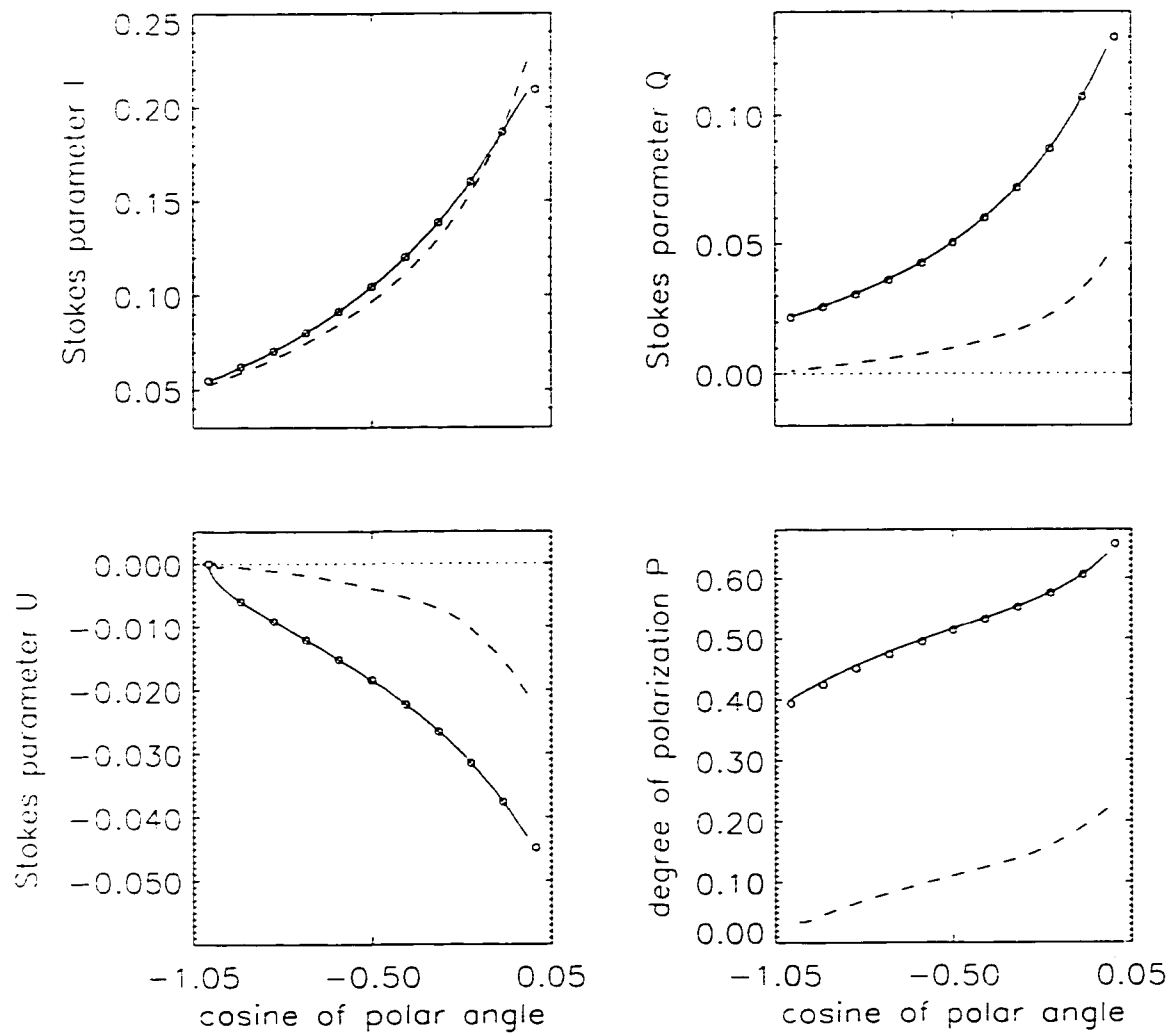Figure 4.2. Rayleigh scattering test, new version of VDISORT

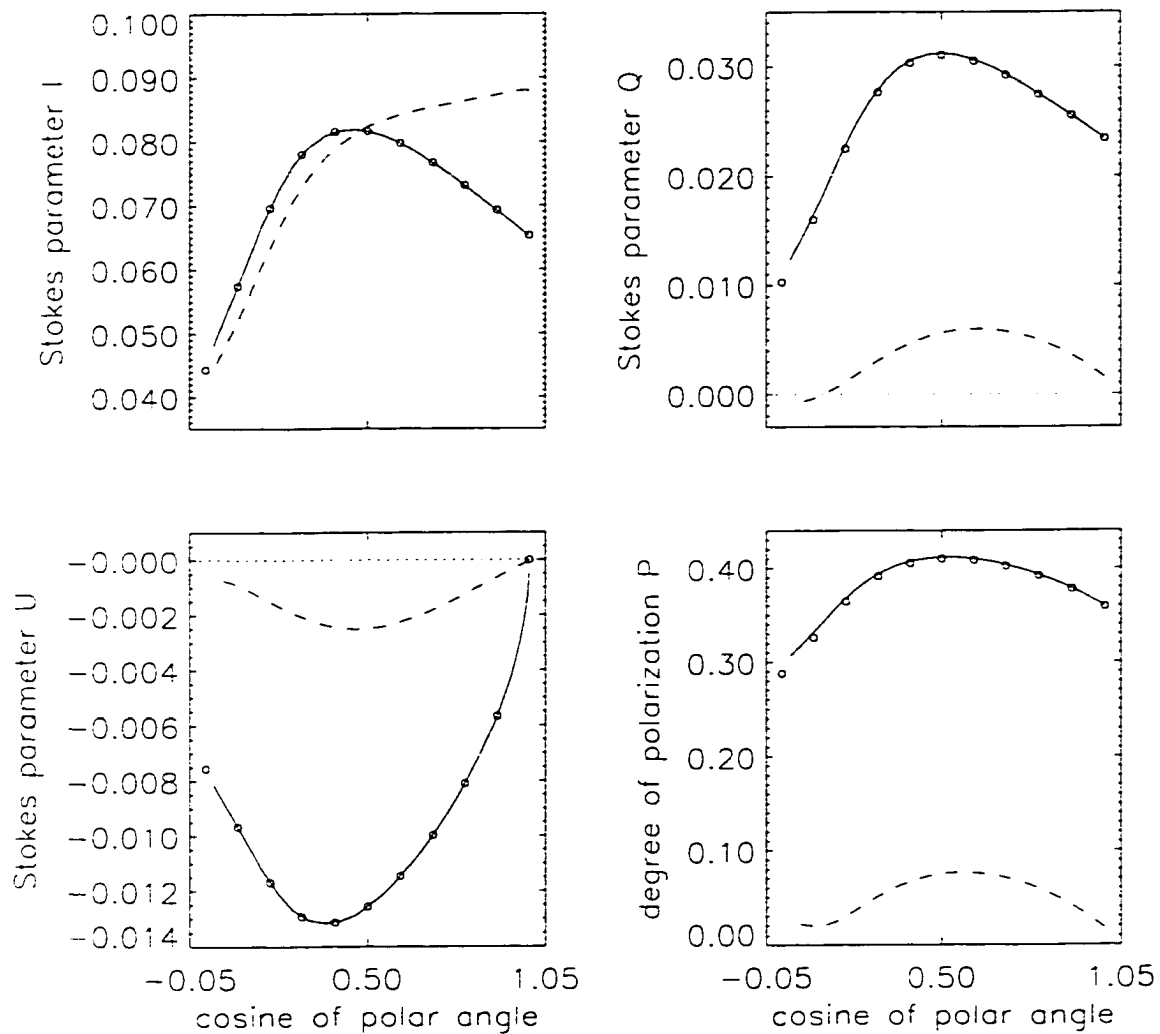Figure 4.3. Mie scattering test, top of medium
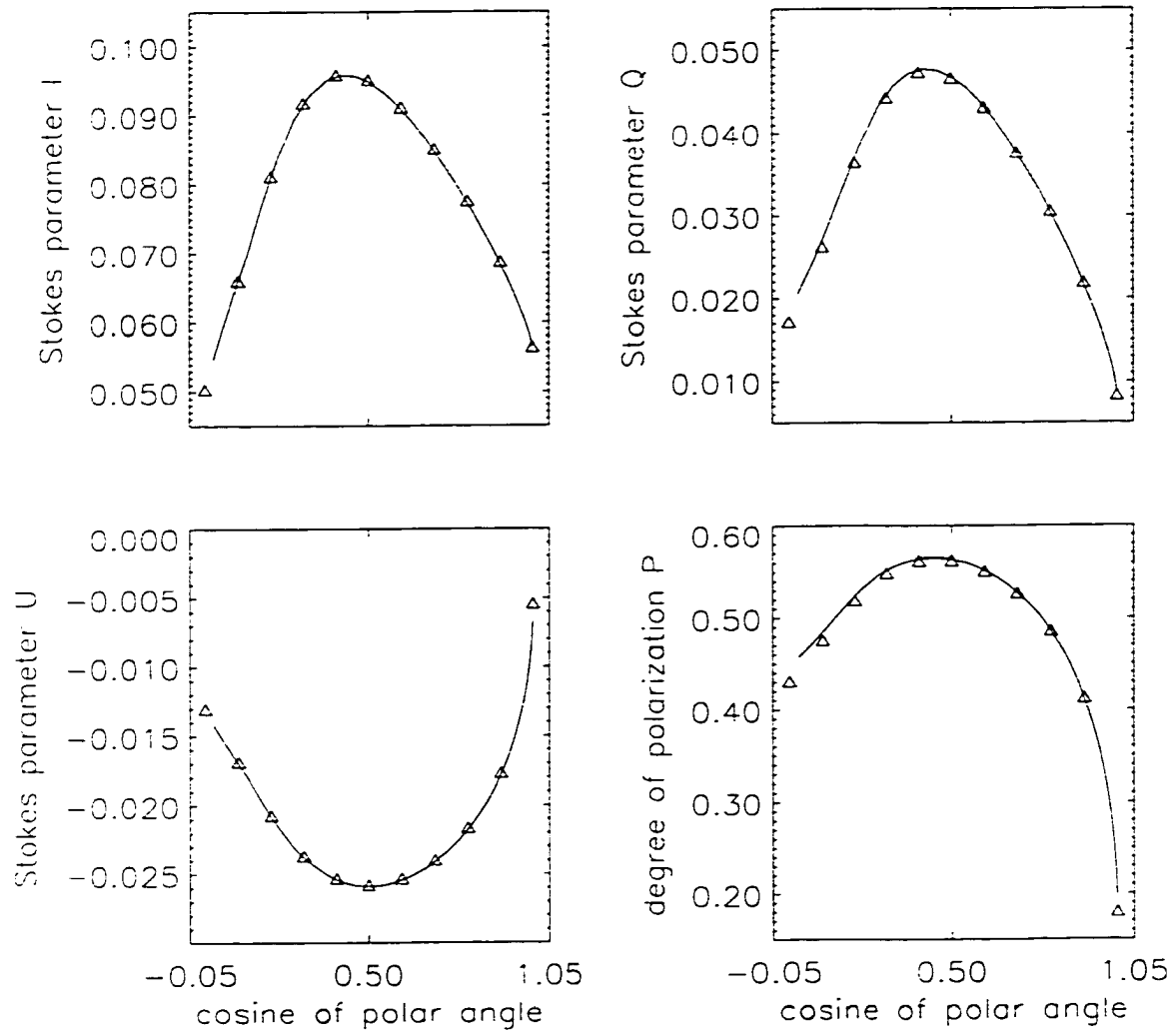
Figure 4.4. Mie scattering test. bottom of medium

Figure 4.5. Polarized beam source test

Chapter 5

Angular distribution of the Stokes vector in VDISORT

The output of VDISORT is the Stokes vector at arbitrary user-specified azimuth angles. and at the discrete quadrature polar angles. A method is needed to calculate the radiation field at arbitrary polar angles other than the discrete ordinates (quadrature angles). In this chapter. a method to calculate analytically the Stokes vector at arbitrary polar angles and optical depths from a given vector discrete ordinate solution is developed [81]. The derived expressions are analytic solutions to the radiative transfer equation for the full 4-vector (polarized) radiative transfer problem. These analytic solutions satisfy the boundary conditions and across-layer continuity conditions in a vertically inhomogeneous slab consisting of multiple plane-parallel layers. The new scheme is tested for Rayleigh scattering. scattering by spherical particles. and scattering by nonspherical particles. In all three test cases. the new scheme proves to be superior to a spline interpolation that has previously been used in connection with the vector discrete ordinate method. in terms of both accuracy and computational speed. In particular. the analytic method presented here has. in contrast to the spline. no difficulties with extrapolations. For the spherical particle case. a numerical imprecision in the discrete ordinate solution is simulated. and the analytic expressions developed here are found to actually improve

the discrete ordinate result.

5.1 Introduction

The discrete ordinate method provides a solution to the radiative transfer equation that is "exact" in the sense that it yields the radiation field at a number of discrete polar quadrature angles (ordinates) that can be increased to approach the exact solution as closely as desired. In practice. however. the computer time required for the discrete ordinate method increases cubically with the number of discrete ordinates. It is therefore cost-effective to obtain the discrete ordinate solution at a rather limited number of quadrature angles and then generate the radiation field at additional angles by using a much less computer-time intensive interpolation scheme. The disadvantage of this approach is that standard interpolation methods. such as the spline procedure. are known to produce poor results when the function to be interpolated has discontinuities or changes rapidly. To overcome this problem in the scalar radiative transfer problem. an analytic method has been developed previously that uses the discrete ordinate solution at the quadrature points to calculate the angular distribution of the intensity at arbitrary angles. This scheme has been referred to as the iteration of the source function method. The analytic expressions for the intensity at arbitrary angles and optical depths obtained by this method satisfy not only the scalar radiative transfer equation. but also the boundary and layer-interface continuity conditions at arbitrary angles (i.e. not just at the quadrature angles) [82]. This method is implemented in the scalar discrete ordinate radiative transfer code DISORT [70] and has been proven to be superior to standard interpolation schemes. For the scalar problem. the existence of this analytic method for calculating the angular dependence of the intensity from the solution at the quadrature points is one of the advantages of the discrete ordinate method over other methods for solving the radiative transfer equation.

The original version of VDISORT [71] uses a conventional spline interpolation for interpolating from the quadrature to arbitrary angles. However. Weng [74] pointed out

130

that it would be desirable to develop a scheme for calculating the angular distribution of each Stokes component in the full 4-vector problem similar to the one used successfully in the scalar case. The purpose of this chapter is (i) to develop such a scheme. (ii) to test its performance against benchmark results. and (iii) to compare it to the performance of a standard spline procedure. It is also found that the iteration of the source function method is capable of actually improving the accuracy of the discrete ordinate solution.

5.2 Formulation of the iteration of the source function method for VDISORT

In a plane parallel horizontally homogeneous slab. the Stokes vector of the radiation field

$$
\mathbf{I} = \begin{pmatrix} I_l \\ I_r \\ U^. \\ V^. \end{pmatrix}
\tag{5.1}
$$

is a function of the vertical optical depth τ. the polar angle θ. and the azimuth angle o. By making a Fourier expansion of $\mathbf{I}$. one may isolate the azimuthal dependency in terms of cosine and sine functions. "Isolation" simply means that each Fourier component $(\alpha. m)$ (where $\alpha = c. s$ denotes cosine and sine modes. respectively. and where m denotes the Fourier order) independently obeys the radiative transfer equation

$$
u \frac{d\mathbf{I}_m^\alpha(\tau. u)}{d\tau} = \mathbf{I}_m^\alpha(\tau. u) - \mathbf{J}_m^\alpha(\tau. u)
\tag{5.2}
$$

where $u = \cos\theta$. and $\mathbf{J}_m^\alpha$ is the source function. Equation (5.2) can be formally integrated to yield analytic expressions for the down- and upwelling radiation field:

$$
\mathbf{I}_m^{\alpha-}(\tau.\mu) = \mathbf{I}_m^{\alpha-}(0.\mu)\,e^{-\tau/\mu} + \int_0^\tau \frac{dt}{\mu}\mathbf{J}_m^\alpha(t.-\mu)\,e^{-(\tau-t)/\mu}
\tag{5.3}
$$

$$
\mathbf{I}_m^{\alpha+}(\tau.\mu) = \mathbf{I}_m^{\alpha+}(\tau^*.\mu)\,e^{-(\tau^*-\tau)/\mu} + \int_\tau^{\tau^*} \frac{dt}{\mu}\mathbf{J}_m^\alpha(t.+\mu)\,e^{-(t-\tau)/\mu}
\tag{5.4}
$$

where $\mathbf{I}_m^{\alpha-}$ and $\mathbf{I}_m^{\alpha+}$ denote the Stokes vector Fourier components of the down- and upwelling radiation. respectively. τ^* is the optical thickness of the slab. and $\mu = |u|$. A vertically inhomogeneous plane-parallel medium can be described by L adjacent. horizontal. homogeneous layers. where the optical properties of the medium are allowed to vary from layer to layer. The cumulative optical depths at the layer-interfaces are

$$\tau_0 = 0. \ \tau_1. \ \tau_2. \ \ldots \ \tau_L = \tau^*. \tag{5.5}$$

If a given optical depth τ falls into the nth layer. i.e. $\tau_{n-1} \leq \tau \leq \tau_n$. then. following Chapter 4. the source function can be expressed with Gaußian quadrature angles u_j and corresponding weights w_j. $j = \pm 1. \ldots. \pm N$. as

$$
\begin{aligned}
\mathbf{J}_{mn}^{\alpha}(\tau. u) \ = \ & \frac{a(\tau_n)}{4} \sum_{\substack{j=-N \\ j \neq 0}}^{N} w_j \left\{ (1 + \delta_{0m}) \, \mathbf{M}_m^c(\tau_n. u, u_j) \, \mathbf{I}_m^{\alpha}(\tau. u_j) \right. \\
& \left. \mp (1 - \delta_{m0}) \, \mathbf{M}_m^s(\tau_n. u. u_j) \, \mathbf{I}_m^{\overline{\alpha}}(\tau. u_j) \right\} \\
& + \mathbf{S}_{mn}^{\alpha}(\tau) \, e^{-\tau/\mu_0} + \delta_{0m} \, \delta_{\alpha.c} \, [1 - a(\tau_n)] \, \mathbf{S}_t(\tau) \tag{5.6}
\end{aligned}
$$

where the upper and lower sign pertains to $\alpha = c$ and $\alpha = s$. respectiveiv. For notational convenience. the symbols

$$
\overline{\alpha} := \begin{cases} c & : \ \alpha = s \\ s & : \ \alpha = c \end{cases} \quad : \quad \delta_{\alpha.c} := \begin{cases} 1 & : \ \alpha = c \\ 0 & : \ \alpha = s \end{cases} .
$$

have been introduced. N denotes the number of streams (quadrature angles) per hemisphere. For the Gaußian quadrature angles. $u_{-j} = -u_j$. $\mathbf{M}_m^{\alpha}(\tau_n. u. u_j)$ denote. as usual. the Fourier components of the phase matrix in the nth layer. and the single scattering source term is

$$\mathbf{S}_{mn}^{\alpha}(\tau) \ = \ \frac{a(\tau_n)}{4\pi} \mathbf{M}_m^{\alpha}(\tau_n. u. -\mu_0) \cdot \mathbf{S}_b. \tag{5.7}$$

$\mathbf{S}_b$ denotes the Stokes vector of the beam source. $-\mu_0$ is the cosine of the solar zenith angle. and $a(\tau_n)$ stands for the single scattering albedo of the nth layer. The thermal source is unpolarized. i.e. in the chosen representation. Eq. (5.1). of the Stokes vector. $\mathbf{S}_t$

is given by $[B(T(\tau))/2, B(T(\tau))/2, 0, 0]^T$, where B is the Planck function. The Fourier components $\mathbf{M}_m^\alpha$ of the phase matrix have, as in Chapter 4, the following form:

$$\mathbf{M}_m^c = \begin{pmatrix} M_{11m}^c & M_{12m}^c & 0 & 0 \\ M_{21m}^c & M_{22m}^c & 0 & 0 \\ 0 & 0 & M_{33m}^c & M_{34m}^c \\ 0 & 0 & M_{43m}^c & M_{44m}^c \end{pmatrix} =: \begin{pmatrix} \mathbf{M}_{1m}^c & \mathbf{0} \\ \mathbf{0} & \mathbf{M}_{2m}^c \end{pmatrix} \tag{5.8}$$

$$\mathbf{M}_m^s = \begin{pmatrix} 0 & 0 & M_{13m}^s & M_{14m}^s \\ 0 & 0 & M_{23m}^s & M_{24m}^s \\ M_{31m}^s & M_{32m}^s & 0 & 0 \\ M_{41m}^s & M_{42m}^s & 0 & 0 \end{pmatrix} =: \begin{pmatrix} \mathbf{0} & \mathbf{M}_{1m}^s \\ \mathbf{M}_{2m}^s & \mathbf{0} \end{pmatrix}. \tag{5.9}$$

Due to the special symmetries of Eqs. (5.8) and (5.9), the source term (5.6) can be simplified in the following way. First one defines new vectors

$$\mathbf{i}_m^c := \begin{pmatrix} I_l^c \\ I_r^c \\ U^s \\ V^s \end{pmatrix} \quad ; \quad \mathbf{i}_m^s := \begin{pmatrix} I_l^s \\ I_r^s \\ U^c \\ V^c \end{pmatrix} \tag{5.10}$$

and similar expressions for the source function $\mathbf{j}_{mn}^\alpha$ and the single scattering source term $\mathbf{s}_{mn}^\alpha$, i.e. one mixes sine and cosine modes of different Stokes vector components in newly defined vectors, analogous to the procedure in Chapter 4. For the unpolarized thermal source term, $\mathbf{s}_t = \mathbf{S}_t$. Likewise, $\mathbf{s}_b = \mathbf{S}_b$ if one is dealing with an unpolarized solar beam term.

Next it is noted that the sine modes start at $m = 1$. Thus, $\mathbf{M}_m^s = \mathbf{0}$ and $\mathbf{I}_m^s = \mathbf{0}$ for $m = 0$. Consequently, the second δ_{0m} factor for $\alpha = c$, and the first two δ_{0m} factors for $\alpha = s$ can be omitted in (5.6). New (4×4) matrices are introduced:

$$\mathbf{a}_m^c(\tau_n, u, u_j) := w_j \frac{a(\tau_n)}{4} \begin{pmatrix} (1 + \delta_{0m}) \mathbf{M}_{1m}^c & \mathbf{M}_{1m}^s \\ -\mathbf{M}_{2m}^s & \mathbf{M}_{2m}^c \end{pmatrix} \bigg|_{(\tau_n, u, u_j)} \tag{5.11}$$

$$\mathbf{a}_m^s(\tau_n. u. u_j) \;:=\; w_j \frac{a(\tau_n)}{4} \left(\begin{array}{cc} \mathbf{M}_{1m}^c & -\mathbf{M}_{1m}^s \\[2mm] \mathbf{M}_{2m}^s & (1+\delta_{0m})\,\mathbf{M}_{2m}^c \end{array} \right) \Bigg|_{(\tau_n.u.u_j)} \tag{5.12}$$

$$\mathbf{a}_m^c(\tau_n. u. u_{j=0}) \;:=\; \frac{a(\tau_n)}{4\pi} \left(\begin{array}{cc} \mathbf{M}_{1m}^c & \mathbf{0} \\[2mm] \mathbf{M}_{2m}^s & \mathbf{0} \end{array} \right) \Bigg|_{(\tau_n.u.-\mu_0)} \tag{5.13}$$

$$\mathbf{a}_m^s(\tau_n. u. u_{j=0}) \;:=\; \frac{a(\tau_n)}{4\pi} \left(\begin{array}{cc} \mathbf{0} & \mathbf{M}_{1m}^s \\[2mm] \mathbf{0} & \mathbf{M}_{2m}^c \end{array} \right) \Bigg|_{(\tau_n.u.-\mu_0)} . \tag{5.14}$$

For notational convenience. the definition $u_j = \mu_0$ for $j = 0$ has been introduced. where $-\mu_0 = \cos\theta_0$. and θ_0 is the polar angle of the solar beam source. One should. however. keep in mind that μ_0 is not one of the quadrature angles. With the definitions (5.10)–(5.14). Eqs. (5.2). (5.6). and (5.7) become

$$u\,\frac{d\mathbf{i}_m^\alpha(\tau. u)}{d\tau} \;=\; \mathbf{i}_m^\alpha(\tau. u) \;-\; \mathbf{j}_{mn}^\alpha(\tau. u) \tag{5.15}$$

$$\mathbf{j}_{mn}^\alpha(\tau. u) \;=\; \sum_{\substack{j=-N \\ j\neq 0}}^{N} \mathbf{a}_m^\alpha(\tau_n. u. u_j)\cdot \mathbf{i}_m^\alpha(\tau. u_j)$$
$$+\,\mathbf{s}_{mn}^\alpha(u)\,e^{-\tau/\mu_0} \;+\; \delta_{0m}\,\delta_{\alpha.c}\,[1 - a(\tau_n)]\,\mathbf{s}_t(\tau) \tag{5.16}$$

$$\mathbf{s}_{mn}^\alpha(u) \;=\; \mathbf{a}_m^\alpha(\tau_n. u. u_{j=0})\cdot \mathbf{s}_b. \tag{5.17}$$

and n is again the layer index so that the condition $\tau_{n-1} \le \tau \le \tau_n$ is satisfied in Eqs. (5.15)–(5.17).

The discrete ordinate method yields a solution to (5.15) that is valid at the quadrature angles u_j and that can be written as

$$\mathbf{i}_m^\alpha(\tau. u_j) \;=\; \sum_{i=0}^{8N} C_{imn}^{\prime\alpha}\,\mathbf{g}_{imn}^\alpha(u_j)\,e^{-\lambda_{imn}^2\,\tau}$$
$$+\,\delta_{0m}\,\delta_{\alpha.c}\,[\mathbf{x}_{0n}(u_j) + \mathbf{x}_{1n}(u_j)\,\tau]. \tag{5.18}$$

where the notation of Chapter 4 is adopted. Note that Eq. (4.40) refers to the components of the $8N$-vectors defined in the previous chapter. whereas Eq. (5.18) is the same equation recast into 4-vector form. which will turn out to be more advantageous for the purpose of this chapter. For $i \neq 0$. λ_{imn}^α and $\mathbf{g}_{imn}^\alpha$ $(i = 1.\dots.8N)$ denote the

$8.N$ eigenvalues and eigenvectors of the discrete ordinate solution determined from the homogeneous radiative transfer equation. and the coefficients C^α_{imn} are the constants of integration determined from the boundary and layer-interface continuity conditions. For $i = 0$. $C^\alpha_{0mn} := 1$. $\lambda^\alpha_{0mn} := 1/\mu_0$. $\mathbf{g}^\alpha_{0mn}(u_j) := \mathbf{z}^\alpha_{mn}(u_j)$ is the particular solution due to the beam source term. and $\mathbf{x}_{0n}(u_j) + \mathbf{x}_{1n}(u_j)\,\tau$ is the particular solution due to the thermal source term. expanded to first order in τ. Substitution of (5.18) into (5.16) yields

$$\mathbf{j}^\alpha_{mn}(\tau. u) = \sum_{i=0}^{8.N} \mathbf{l}^\alpha_{imn}(u)\, e^{-\lambda^\alpha_{imn}\tau}$$
$$+ \mathbf{q}^\alpha_{mn.0}(u) + \mathbf{q}^\alpha_{mn.1}(u)\cdot\tau \tag{5.19}$$

where

$$\mathbf{l}^\alpha_{imn}(u) := \sum_{\substack{j=-N\\ j\neq 0}}^{N} C^\alpha_{imn}\, \mathbf{a}^\alpha_m(\tau_n. u. u_j)\cdot \mathbf{g}^\alpha_{imn}(u_j)$$
$$+ \delta_{i0}\, \mathbf{s}^\alpha_{mn}(u) \tag{5.20}$$

$$\mathbf{q}^\alpha_{mn.0}(u) := \delta_{0m}\,\delta_{\alpha.c}\left\{ \sum_{\substack{j=-N\\ j\neq 0}}^{N} \mathbf{a}^\alpha_m(\tau_n. u. u_j)\cdot \mathbf{x}_{0n}(u_j) + [1 - a(\tau_n)]\,\mathbf{b}_0 \right\} \tag{5.21}$$

$$\mathbf{q}^\alpha_{mn.1}(u) := \delta_{0m}\,\delta_{\alpha.c}\left\{ \sum_{\substack{j=-N\\ j\neq 0}}^{N} \mathbf{a}^\alpha_m(\tau_n. u. u_j)\cdot \mathbf{x}_{1n}(u_j) + [1 - a(\tau_n)]\,\mathbf{b}_1 \right\}. \tag{5.22}$$

As in VDISORT. an approximation of the Planck function linear in τ is assumed: $B(T(\tau)) = B_0 + B_1\cdot\tau$. and thus in (5.21) and (5.22). $\mathbf{b}_0 = [B_0. B_0.0.0]^T$. $\mathbf{b}_1 = [B_1. B_1.0.0]^T$.

For the L-layer model and with the lower-case 4-vectors defined in (5.10). Eqs. (5.3) and (5.4) become

$$\mathbf{i}^{\alpha-}_m(\tau.\mu) = \mathbf{i}^{\alpha-}_m(0.\mu)\,e^{-\tau/\mu} + \sum_{p=1}^{n-1} \int_{\tau_{p-1}}^{\tau_p} \frac{dt}{\mu}\,\mathbf{j}^\alpha_{mp}(t.-\mu)\,e^{-(\tau-t)/\mu}$$
$$+ \int_{\tau_{n-1}}^{\tau} \frac{dt}{\mu}\,\mathbf{j}^\alpha_{mn}(t.-\mu)\,e^{-(\tau-t)/\mu} \tag{5.23}$$

$$i_m^{\alpha+}(\tau,\mu) = i_m^{\alpha+}(\tau^*,\mu)\,e^{-(\tau^*-\tau)/\mu} + \int_\tau^{\tau_n} \frac{dt}{\mu}\,j_{mn}^\alpha(t,+\mu)\,e^{-(t-\tau)/\mu}$$

$$+ \sum_{p=n+1}^{L} \int_{\tau_{p-1}}^{\tau_p} \frac{dt}{\mu}\,j_{mp}^\alpha(t,+\mu)\,e^{-(t-\tau)/\mu} \tag{5.24}$$

The condition $\tau_{n-1} \leq \tau \leq \tau_n$ is actually not unambiguous and should be rewritten more precisely as $\tau_{n-1} < \tau \leq \tau_n$, if $\cos\theta = u < 0$, and $\tau_{n-1} \leq \tau < \tau_n$, if $u > 0$. If one substitutes (5.19) into (5.23) and (5.24), the integration can be carried out analytically. The result is

$$i_m^{\alpha-}(\tau,\mu) = i_m^{\alpha-}(0,\mu)\,e^{-\tau/\mu}$$

$$+ \sum_{i=0}^{8N} \left\{ \sum_{p=1}^{n-1} l_{imp}^\alpha(-\mu)\,f_-(\tau,\tau_{p-1},\tau_p;\lambda_{imp}^\alpha,\mu) \right.$$

$$\left. + l_{imn}^\alpha(-\mu)\,f_-(\tau,\tau_{n-1},\tau;\lambda_{imn}^\alpha,\mu) \right\}$$

$$+ \sum_{p=1}^{n-1} q_{mp,0}^\alpha(-\mu)\,f_-(\tau,\tau_{p-1},\tau_p;0,\mu)$$

$$+ q_{mn,0}^\alpha(-\mu)\,f_-(\tau,\tau_{n-1},\tau;0,\mu)$$

$$+ \sum_{p=1}^{n-1} q_{mp,1}^\alpha(-\mu)\,h_-(\tau,\tau_{p-1},\tau_p;\mu)$$

$$+ q_{mn,1}^\alpha(-\mu)\,h_-(\tau,\tau_{n-1},\tau;\mu) \tag{5.25}$$

$$i_m^{\alpha+}(\tau,\mu) = i_m^{\alpha+}(\tau^*,\mu)\,e^{-(\tau^*-\tau)/\mu}$$

$$+ \sum_{i=0}^{8N} \left\{ l_{imn}^\alpha(\mu)\,f_+(\tau,\tau,\tau_n;\lambda_{imn}^\alpha,\mu) \right.$$

$$\left. + \sum_{p=n+1}^{L} l_{imp}^\alpha(\mu)\,f_+(\tau,\tau_{p-1},\tau_p;\lambda_{imp}^\alpha,\mu) \right\}$$

$$+ q_{mn,0}^\alpha(\mu)\,f_+(\tau,\tau,\tau_n;0,\mu)$$

$$+ \sum_{p=n+1}^{L} q_{mp,0}^\alpha(\mu)\,f_+(\tau,\tau_{p-1},\tau_p;0,\mu)$$

$$+ q_{mn,1}^\alpha(\mu)\,h_+(\tau,\tau,\tau_n;\mu)$$

$$+ \sum_{p=n+1}^{L} q_{mp,1}^\alpha(\mu)\,f_+(\tau,\tau_{p-1},\tau_p;\mu) \tag{5.26}$$

where

$$f_\pm(\tau, \tau_1, \tau_2; \beta, \mu) := \pm \frac{1}{1 \pm \mu\beta}[e^{-\beta\tau_1} e^{\pm(\tau-\tau_1)/\mu} - e^{-\beta\tau_2} e^{\pm(\tau-\tau_2)/\mu}] \quad (5.27)$$

$$h_\pm(\tau, \tau_1, \tau_2; \mu) := \pm[e^{\pm(\tau-\tau_1)/\mu}(\tau_1 \pm \mu) - e^{\pm(\tau-\tau_2)/\mu}(\tau_2 \pm \mu)]. \quad (5.28)$$

The terms $i_m^{\alpha-}(0, \mu)$ and $i_m^{\alpha+}(\tau^*, \mu)$ are determined from the boundary conditions, see Chapter 4.

It can be easily verified that the expressions (5.25) and (5.26) satisfy the radiative transfer equation by substituting them into (5.15) and taking into account (5.19). The functions (5.27) and (5.28) are continuous functions of τ, and thus the expressions obtained for the Stokes vectors in the upper and lower hemisphere are also continuous. particularly across the interfaces of the computational layers. Furthermore, for $\tau \to 0$, n in Eq. (5.25) is 1, and thus there is no sum over the summation index p in (5.25). Only the first term in this expression survives, since $f_-(\tau, 0, \tau; \lambda_{imn}^\alpha, \mu)$ and $h_-(\tau, 0, \tau; \mu)$ go to zero for $\tau \to 0$. Thus. $i_m^{\alpha-}(\tau, \mu) \to i_m^{\alpha-}(0, \mu)$ for $\tau \to 0$. Similarly. $i_m^{\alpha+}(\tau, \mu) \to i_m^{\alpha+}(\tau^*, \mu)$ for $\tau \to \tau^*$. So the resulting expressions (5.25) and (5.26) are solutions to the radiative transfer equation that satisfy the boundary conditions at the top and bottom of the atmosphere as well as the continuity conditions across layer-interfaces. In contrast to the solution (5.18) at the quadrature points. these solutions satisfy the boundary and continuity conditions not only at the discrete set of quadrature angles, but at arbitrary angles u. The expressions (5.25) and (5.26) do not. however. constitute an alternative solution to the radiative transfer problem that replaces the discrete ordinate method. since they rely on the knowledge of the quantities λ_{imp}^α and, via Eqs. (5.20)–(5.22). C_{imn}^α. g_{imn}^α. z_{mn}^α. x_{0n}. and x_{1n}. and thus on the discrete ordinate solution. One may therefore be tempted to regard this scheme as a sophisticated interpolation formula. It will later become clear that this notion is not quite correct. Therefore. the expressions (5.25) and (5.26) shall be referred to as the iteration of the source function expressions. or. for the sake of brevity. as the ISF expressions. The existence of such a scheme that allows one to analytically calculate the radiation field at arbitrary angles and optical depths from the discrete ordinate solution. both in the scalar radiative transfer problem (Ref. [82])

and, as shown in this Chapter, in the full 4-vector problem including polarization, is one of the unique advantages of the discrete ordinate method.

5.3 Numerical Tests

As can be seen from the ISF equations, the only information that is necessary in addition to the discrete ordinate solution in order to apply this scheme is the knowledge of the matrices $\mathbf{a}_m^\alpha(\tau_n, u, u_j)$, and consequently, according to the Eqs. (5.11)–(5.14) defining these matrices, the knowledge of the phase matrix Fourier components $\mathbf{M}_m^\alpha$ at polar angle cosines (u, u_j). These Fourier components can, however, be calculated very efficiently for arbitrary angles from the expansion coefficients of the scattering matrix by the method proposed by Siewert [80, 35], as explained in Chapter 4. Thus, the new interpolation scheme can easily be applied in connection with VDISORT.

As a first test case to compare the performance of the ISF scheme to benchmark results and to the performance of a spline interpolation, a simple Rayleigh scattering atmosphere is considered with an optical depth 1, overlying a black surface (albedo= 0), the sun incident at $\mu_0 = 0.8$, and with the azimuth between the sun and the direction of observation $o - o_0 = 90°$. The radiative transfer problem is solved with VDISORT for the Stokes components at the quadrature angles. Subsequently, the Stokes components are computed at user-specified angles with either the ISF expressions or a spline interpolation. The user-angles are set to values at which one can find benchmark results in the literature [75] for the Stokes vector components in this test case. In order to optimize the performance of the spline interpolation, the radiation field has been interpolated separately in each hemisphere ($u > 0$ and $u < 0$). This way one avoids the notorious problems associated with spline interpolations at discontinuities, such as that occurring in the Stokes components at $\mu = 0$ at the bottom or top of the medium. The down-welling radiation ($u < 0$ in the convention used here) is considered at the bottom of the slab. The Stokes components I, Q, and U obtained with either method (ISF or spline) as a function of user specified angles can be compared to the benchmark values, and an

average error can be computed for each scheme. In general. this error will depend on the number of quadrature points $2N$. often referred to as the number of streams. that is chosen in the discrete ordinate method to solve the radiative transfer problem at the quadrature points. The number of streams have been varied between six and 28. i.e. between $N = 3$ and $N = 14$ streams per hemisphere. Figure 5.1 shows the absolute error in the computation of I. Q. and U as a function of the number of hemispherical streams N. obtained with the ISF expressions and the spline (represented by the crosses and the circles. respectively). and the CPU time needed for either method. As expected. the spline performs particularly poorly if the number of streams between which the interpolation is carried out is low. whereas the analytic ISF expressions yield much more accurate results for low N. The Stokes components Q and even more so U clearly show that the ISF method yields superior results to the spline even for higher N. The CPU time increases cubically with N for both test cases and lies about 35 % higher for the ISF method than for the spline. The ISF scheme considerably improves the computational efficiency for the Stokes components Q and U. For a twelve-stream model. for instance. the Q component is computed with an accuracy of $5 \cdot 10^{-5}$ by the ISF scheme. The required CPU time on an Alpha workstation is about 0.70 s. In order to obtain the same accuracy with the spline. one needs to employ a 24-stream model. which required 1.76 s of computer time. an increase by 250 %. The situation is even more dramatic for the U component. where the computational accuracy of the ISF scheme is unmatched by the spline in the considered interval of streams. In case of the intensity component. there is little gain in computational accuracy with increasing N for higher values of N. But even here. when considering. for instance. a 20-stream model. the ISF scheme computes the I component with $1.5 \cdot 10^{-4}$ accuracy, using 1.62 s CPU time. To achieve the same accuracy. the spline needs a 24-stream model. which requires 9 % more computer time. Although computer time is of no serious concern in this simple Rayleigh model. the above considerations illustrate the progress in accuracy and efficiency achieved by the ISF method generalized here to the 4-vector radiative transfer problem.
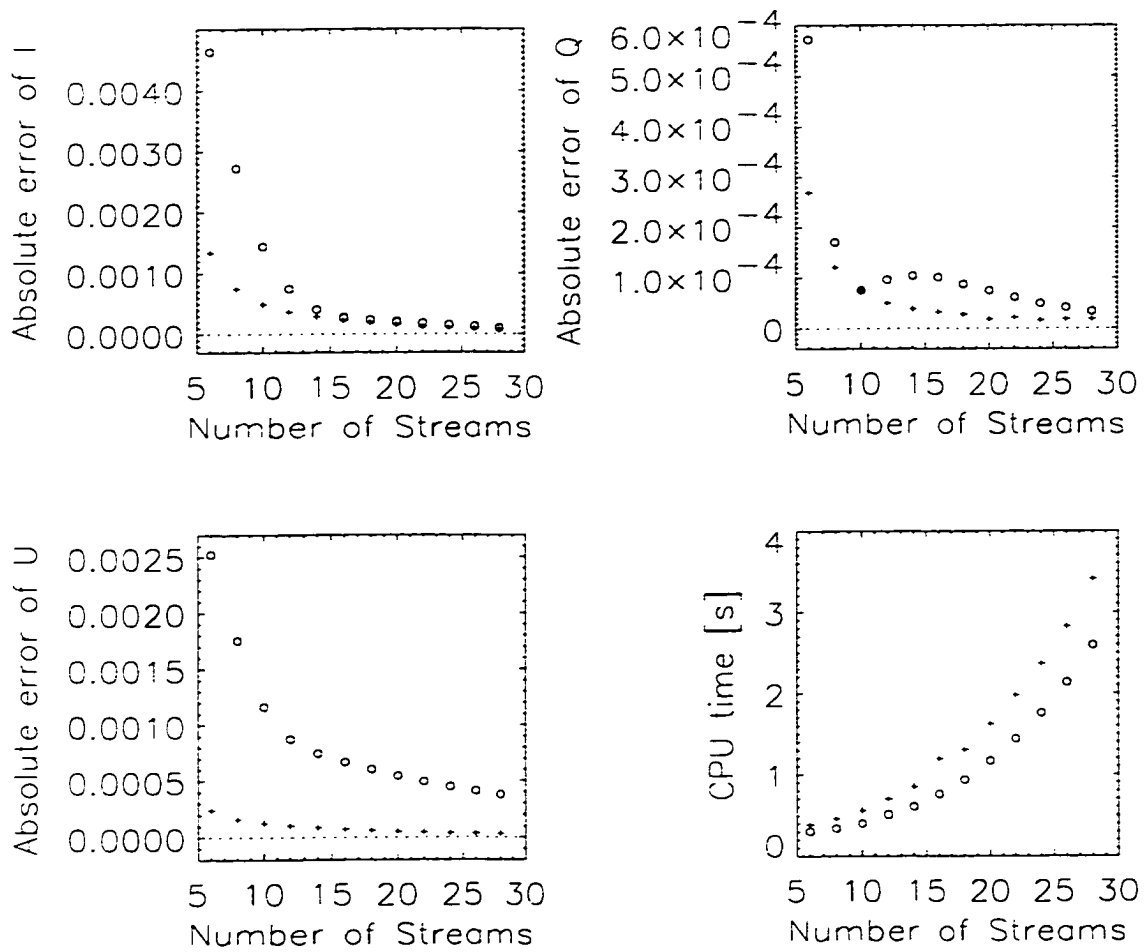
Figure 5.1. Test for Rayleigh scattering

In order to gain some more insight in the particular advantages of the ISF method. a second test case is considered which involves scattering by a size-shape distribution of randomly oriented prolate spheroidal particles with index of refraction $1.19 + 0.055i$. The power law size-distribution has an effective area-equivalent-sphere size parameter of 3 and an effective variance of 0.02. The aspect ratio of the spheroids varies between 5 and 11. and all aspect ratios inside that interval occur with equal probability in the shape distribution. The optical properties of this ensemble of nonspherical particles have been computed with the new method described in Chapter 2. The optical depth of the slab is 1. the underlying Lambertian surface has an albedo of 0.1. and the unpolarized beam source is incident at $\cos\theta_0 = 0.2$. The results for the optical properties and for the radiation field in this and similar test cases are presented in Chapters 6 and 7. Here. the radiation field is considered at an azimuth $\Delta\phi = 180°$ away from the beam source and at the bottom of the scattering medium. At this azimuth. the U and V components of the Stokes vector are zero. First. the nonzero I and Q components are computed with VDISORT for a 36-stream model at the corresponding quadrature angles. Next. the computation of the radiation field is repeated for a twelve-stream model. i.e. for a much smaller number of discrete ordinates. The solution is obtained for the new set of twelve quadrature angles (six per hemisphere). Then. the original 36 quadrature angles are specified as user-angles. the radiation field at these angles is computed both with the spline and with the ISF scheme from the twelve-stream solution. and the results are compared to the original 36-stream discrete ordinate solution. It should be recalled that the use of the two schemes compared here is to reduce the number of streams in the discrete ordinate computation (in this example from 36 to twelve). and then to compute the radiation field with less computational effort at any other points (in this case at the original 36 discrete ordinates) with either the spline or the ISF scheme. The comparison carried out here is therefore a good indication for the usefulness of the spline and the ISF scheme. respectively. It is required that the spline or ISF scheme results compare well

with the original 36-stream solution. Figure 5.2 shows the relative error of the intensity

$$\delta I \;=\; 1 - \frac{I_{12}}{I_{36}} \tag{5.29}$$

(top). and the relative error of the degree of linear polarization

$$\delta P_l \;=\; 1 - \frac{|Q_{12}|/I_{12}}{|Q_{36}|/I_{36}} \tag{5.30}$$

(bottom) as a function of the cosine of the polar angle. The subscripts 12 and 36 denote the Stokes components obtained from the twelve-stream model in connection with the spline or ISF scheme. and those obtained with the 36-stream model. respectively. The dotted and dashed lines represent these relative errors for the ISF and spline scheme. respectively. The plots clearly demonstrate again the superiority of the new ISF method. The maximum error observed for the spline interpolation is 19 % for the intensity and 36 % for the degree of linear polarization. In contrast. the error of the ISF results never exceeds 1 % for both quantities. Figure 5.2 also provides a clearer picture of the weaknesses of the spline and the strengths of the new method. The spline's performance is particularly poor near the edges of the interval. The reason is the following: In the 36-stream model. the quadrature points at the edges of the interval [0,1] are 0.043 and 0.998. whereas in the twelve-stream model. the edge points are 0.125 and 0.982. Thus. when calculating the radiation field at 0.043 and 0.998 from the discrete ordinate solution in the twelve-stream model. the spline interpolation is actually not interpolating but extrapolating to these points. which considerably degrades its performance. The poor results for the spline near $\cos\theta = \pm 1$ must be considered a particularly serious drawback of this method and an important advantage of the ISF method. since accurate modeling results in the zenith and nadir direction are required for many applications.

The L=13 case described in Chapter 4 is used for another test of the new scheme. which will reveal an additional interesting advantage of the ISF method. Figure 5.3 shows the I and Q component as a function of the cosine of the polar angle at the bottom of the medium and at an azimuth $\Delta o = 90°$ from the beam source. The crosses represent the correct VDISORT solution at the seven hemispherical quadrature points
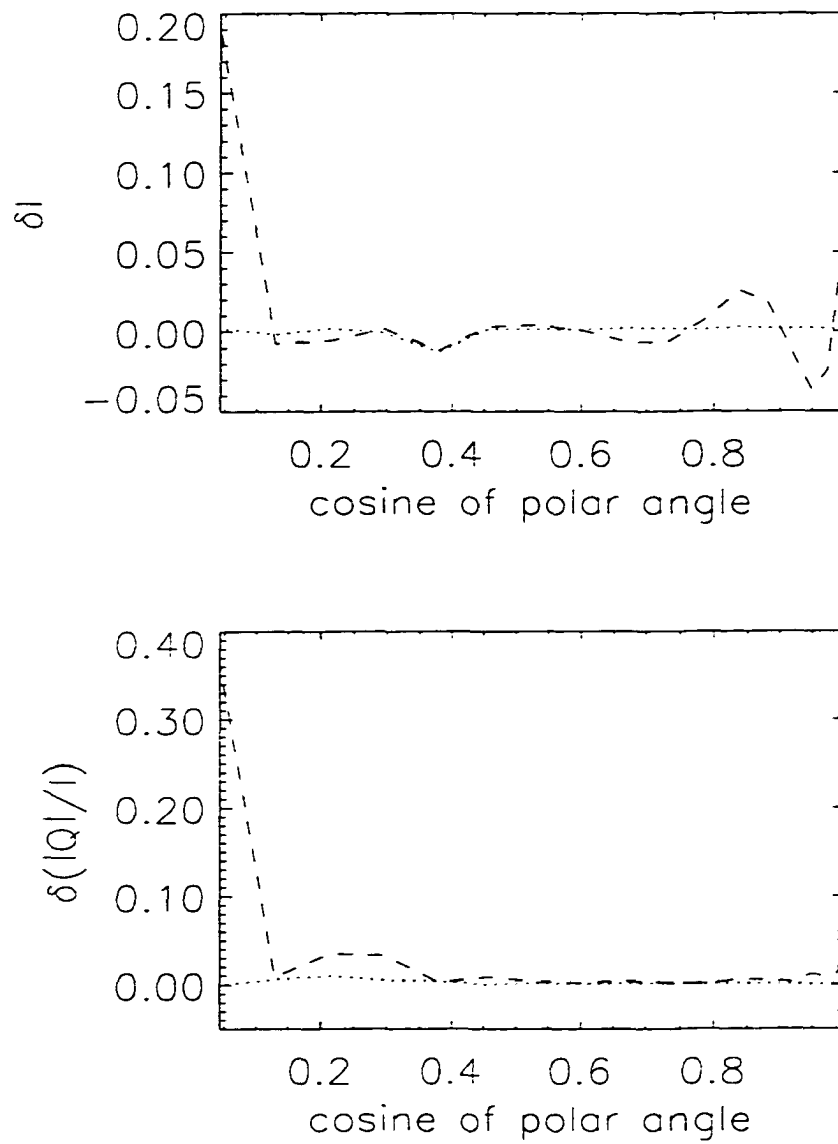
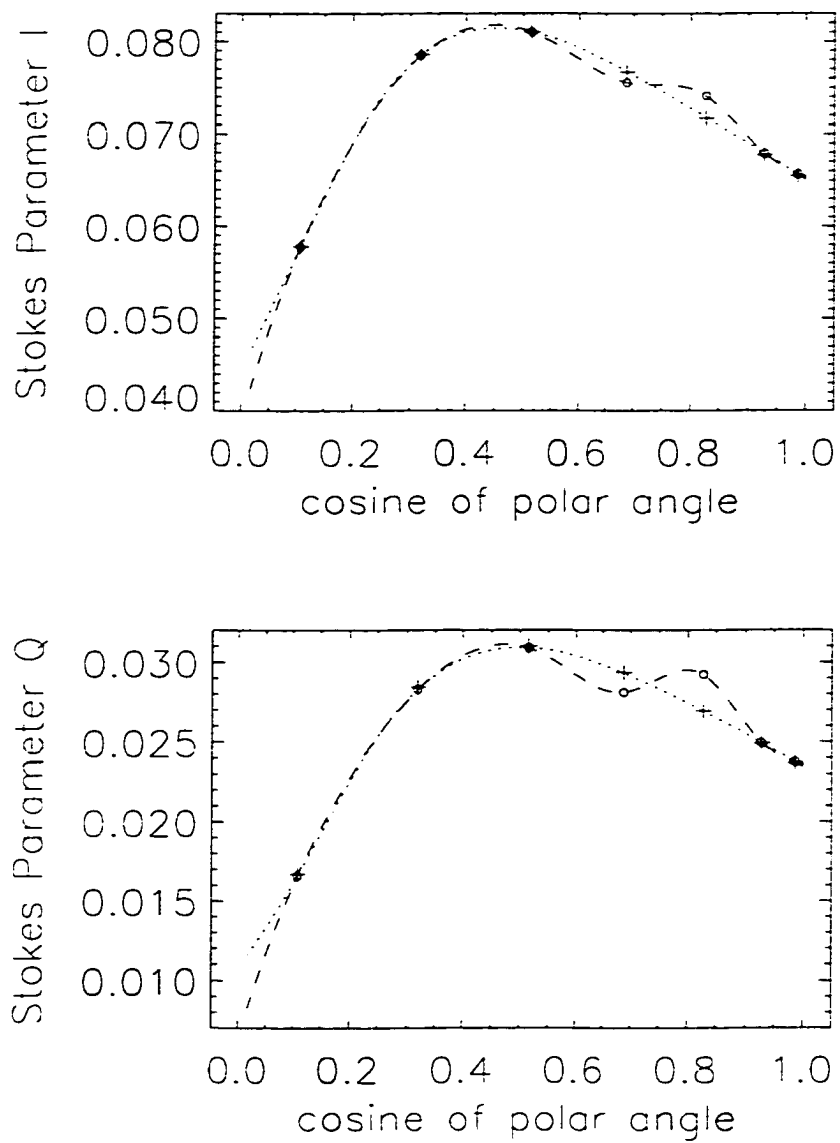Figure 5.2. Test for scattering by nonspherical particles

Figure 5.3. Test for scattering by spherical particles, simulated imprecision

in the 14-stream model used here. The correct solution at $\cos\theta = 0.65$ and 0.85 is now deliberately manipulated in order to simulate a numerical imprecision of the solution at these quadrature points. To this end. the l-component of the particular beam source solution $z_{mn}^c(u_j)$ is deliberately increased by 20% at $u = 0.85$ and decreased by 10% at $u = 0.65$ for all Fourier modes. The manipulated values of I and Q at the quadrature points are represented by circles in the figure. As can be seen. the spline (dashed line) takes the incorrect values as a given and places a smooth least-square fit polynomial through them. In contrast. the ISF scheme improves the "incorrect" quadrature solution and produces a curve that fits the correct solution at the quadrature points. The reason for this kind of behavior is the fact that the ISF method is not primarily bound by the provided quadrature solution. but rather by the radiative transfer equation and the boundary and continuity conditions. If the values at the quadrature points are not quite in agreement with the radiative transfer equation under the given boundary and continuity conditions. then the ISF scheme will tend to bring the solution closer to the correct solution. If the error is only slight. as in this example. then the one iteration step provided by the ISF method is enough to yield an accurate solution. It is also noted that the spline and ISF curves diverge again near $\cos\theta = 0$ on account of the poor performance of the spline in the extrapolation region.

5.4 Summary

A new scheme for analytically calculating the angular distribution for the full 4-vector radiative transfer problem including polarization has been developed. The theoretical development of this scheme is conceptually similar to the iteration of the source function (ISF) method for the intensity in the scalar discrete ordinate method. The resulting formula is an analytic expression for the Stokes vector Fourier components as a function of μ and τ. which satisfies both the radiative transfer equation and the boundary conditions and the layer-interface continuity conditions. This analytic solution depends on the knowledge of the discrete ordinate solution at the quadrature angles and can therefore

only be used in connection with the discrete ordinate method.

A first test of the new interpolation scheme for a Rayleigh scattering medium showed that it yields more accurate results than a standard spline interpolation for a given number of quadrature angles. To achieve a given computational accuracy. the spline interpolation clearly proved to be less efficient in terms of computer time than the ISF scheme.

A second test for a medium containing a size-shape distribution of randomly oriented nonspherical particles revealed that the spline's deficiencies become particularly apparent in the extrapolation region near the angular edge points of the interval. The error in the calculation of the interpolated intensity and degree of linear polarization was as high as 19% and 36%. respectively. for the spline interpolation. The ISF scheme. on the other hand. showed no such deficiencies. the error in the fit of the benchmark values was less than 1% at all angles for both the intensity and the degree of linear polarization.

In the third test case of a Mie scattering medium. a numerical imprecision has been simulated by deliberately manipulating the discrete ordinate solution at some of the quadrature points. The spline produced. as expected. a least square fit to the "incorrect" quadrature points. The new ISF method improved and actually restored the correct solution. in spite of the fact that this scheme relies on the discrete ordinate solution. This remarkable property of the ISF method is due to the fact that it inherently satisfies the radiative transfer equation and the boundary and continuity across layer-interface conditions.

Chapter 6

Shape-Sensitivity Study of Optical Properties

One is now in a position to model from first principles single and multiple scattering in size-shape distributions of randomly oriented spheroidal particles. The model described in Chapter 2 starts with the Helmholtz equation and computes the single scattering optical properties of size-shape distributions of randomly oriented spheroidal particles. These optical properties, i.e. the expansion coefficients of the Stokes scattering matrix and the single scattering albedo, can be directly used as input to VDISORT in order to solve the radiative transfer equation and perform multiple scattering calculations.

In this chapter, the single scattering model is applied to conduct a sensitivity study to assess the effect of particle shape on the optical properties of size-shape distributions of randomly oriented prolate spheroidal particles [58]. The emphasis is on covering a large range of the spheroids' aspect ratio in order to include the effects of highly aspherical particles. The investigation reveals that the elements F_{11}, F_{22}/F_{11}, and F_{34}/F_{11} of the Stokes scattering matrix are very sensitive to the effective aspect ratio of a shape distribution in the test cases under consideration, which will impact the radiance, the degree of linear polarization and the degree of circular polarization of light singly scattered by such an ensemble of particles. The same elements are only mildly sensitive to a

146

variation in the effective variance of the shape-distribution. The remaining elements of the scattering matrix are only mildly sensitive to a variation of the effective aspect ratio. and rather insensitive to a variation of the effective variance of the shape-distribution. The single scattering albedo and the asymmetry parameter are found to be near-linear functions of the effective aspect ratio of the shape-distribution and rather insensitive to the effective variance. Comparison of averages over a shape-distribution with a varying number of averaging points shows that only a few averaging points are necessary to obtain converging results for the optical properties.

6.1   Introduction

A recent investigation by Mishchenko that relied on the use of spheroidal particles has provided strong indications that when considering a size-shape distribution of randomly oriented particles. the additional averaging over shape. i.e. over the spheroids' aspect ratio in this case. yields a smooth featureless phase function qualitatively resembling the phase functions that one typically observes in natural aerosol layers [27]. This result suggests that the crucial difference between a spherical and nonspherical particle model is not just the additional averaging over particle orientations. but also the additional averaging over different particle shapes. This result also justifies the use of a simple particle shape. such as the spheroid. since the conspicuous features related to particle shape disappear in the averaging process. The spheroidal shape is in fact. as pointed out earlier. particularly appealing for modeling purposes. If a spherical particle model is found to be inadequate for a particular application. then a spheroidal particle model introduces just one additional parameter. the spheroid's aspect ratio. which can be varied to obtain a wide range of particle shapes including flat oblate disks. spheres. and elongated prolate needles.

The recent study by Mishchenko [27] on the phase-function of size-shape distributions of spheroids raises a number of interesting questions. Firstly. the sensitivity of the optical single-scattering properties to the parameters characterizing the shape-distribution needs

to be investigated. It is well-known that the optical properties of size-distributions of spherical particles are very sensitive to variations in the effective radius. They do not. however. depend very strongly on the effective variance of the size-distribution. One can similarly define an effective aspect ratio and an effective variance for a shape-distribution of polydisperse randomly oriented spheroids and investigate the sensitivity of the optical properties to variation in these quantities. In particular. Mishchenko's study showed that a relatively narrow shape distribution was enough to average out any shape-related features in the phase function. which may lead to the hypothesis that the phase function is rather insensitive to increasing the width of a shape distribution. Secondly. whereas the phase function only concerns the intensity (radiance) of the scattered radiation. one has to investigate the effect of particle shape on polarization. For this purpose. the full Stokes scattering matrix has to be considered. The interpretation of polarization measurements by instruments on the ground. on balloons. on aircraft. or in space can add valuable information to the measured intensity [60. 61. 62. 63. 64. 65. 66. 67]. The correct interpretation of polarimetric data stemming from ice clouds and aerosol layers therefore requires a suitable nonspherical particle model and a more thorough understanding of the sensitivity of polarization to particle shape.

Mishchenko's investigation [27] relied on the use of the extended boundary condition method (EBCM) [13. 14. 15. 16. 17], which calculates the particle's T-matrix. The study of shape-sensitivity of the optical properties with the EBCM is.however. limited to mildly aspherical spheroids due to the inherent ill-conditioning of the EBCM when dealing with highly aspherical particles. Thus. the dependency of the phase function on the variance of the shape distribution has so far only been investigated for a narrow range of mildly aspherical particles. The dependence of the optical properties on the effective aspect ratio. i.e. the center of the shape-distribution. still remains to be explored. It is the subject of this chapter to begin filling these gaps in our understanding of the impact of particle shape. particularly moderate and extreme departures from sphericity. on intensity and polarization.

6.2 Methods

The new method developed in Chapter 2 allows one to calculate the $\mathcal{T}$-matrix in spheroidal coordinates (denoted by caligraphic font), and it thereby entirely avoids the ill-conditioning encountered in the EBCM. The spheroidal $\mathcal{T}$-matrix can easily be transformed into the spherical coordinate system, on which the EBCM relies. Then, one can apply the well-established procedure of analytical averaging over orientational angles [32] in order to compute the optical properties of ensembles of randomly oriented particles. In this way, one is not limited to mildly aspherical shapes. The modified SVM approach will be applied in connection with the analytical averaging procedure to conduct the sensitivity study.

A spheroid can be characterized by its major and minor axes a and b. Alternatively, the aspect ratio $\epsilon = a/b$ determines the shape of the spheroid, whereas its size can be characterized by the radius of an area-equivalent sphere, or by the radius of a volume-equivalent sphere.

For the form of the size distribution, a power-law distribution is assumed:

$$n_{size}(r) = \begin{cases} C & : \ r \leq r_1 \\ C\,(r_1/r)^3 & : \ r_1 \leq r \leq r_2 \\ 0 & : \ r > r_2 \end{cases} \tag{6.1}$$

where r is the area-equivalent sphere radius. The constant C is chosen such that

$$\int_0^\infty dr\, n_{size}(r) \ = \ 1. \tag{6.2}$$

A size distribution can be characterized [69] by its effective radius

$$r_{eff} \ = \ \frac{1}{G} \int_0^\infty dr\, r\pi r^2 n_{size}(r) \tag{6.3}$$

and its effective variance

$$\nu_{eff} \ = \ \frac{1}{r_{eff}^2 G} \int_0^\infty dr\, (r - r_{eff})^2\, \pi r^2 n_{size}(r) \tag{6.4}$$

where the averaged cross sectional area is

$$G = \int_0^\infty dr\, \pi r^2 n_{size}(r).$$

(6.5)

The parameters r_1 and r_2 in (6.1) can be expressed in terms of r_{eff} and ν_{eff}.

For the size-distribution of spheroids that is to be considered. an effective size parameter of the size distribution $x_{eff} = 2\pi r_{eff}/\lambda = 3$ is chosen. where λ is the wavelength of light. The effective variance is taken to be $\nu_{eff} = 0.2$. and the index of refraction is $n = 1.19 + 0.055\,i$.

Very little quantitative information is available about the distribution of shapes in natural cirrus clouds or aerosol layers. The description of natural shape-distributions is complicated by the irregularity of the shapes of natural particles. An exact description of such shape-distributions which would account for every individual shape. is impractical and from a modeling standpoint undesirable. since it would introduce a large number of parameters. The shape-distribution of spheroidal particles that will be considered is described by only one parameter. namely the aspect ratio $\epsilon = a/b$. Such a shape distribution is therefore ideal for modeling purposes and a natural generalization of the in many cases over-simplified spherical particle model. For the form of the shape distribution. this study shall follow Mishchenko's work [27] and assume an equiprobable distribution of the aspect ratio

$$n_{shape}(\epsilon) = \begin{cases} C & : \ \epsilon_1 \le \epsilon \le \epsilon_2 \\ 0 & : \ \text{otherwise} \end{cases}$$

(6.6)

where $C = 1/(\epsilon_2 - \epsilon_1)$. The effective aspect ratio ϵ_{eff} and effective variance μ_{eff} of the equiprobable shape distribution are defined as

$$\epsilon_{eff} = \frac{\epsilon_1 + \epsilon_2}{2}$$

(6.7)

$$\mu_{eff} = \frac{\epsilon_1 - \epsilon_2}{2}.$$

(6.8)

In this investigation. the size-distribution is kept constant. whereas the parameters characterizing the shape-distribution are varied. and the effect on the optical single-scattering properties will be observed.

One of the optical properties of interest is the Stokes scattering matrix $\mathbf{F}$. which for spheroidal particles is of the special form (4.62). F_{11} connects the scattered and incident intensity and is therefore identical with the phase function. The other elements of the Stokes scattering matrix describe the change in polarization in a single scattering event as a function of the scattering angle Θ.

6.3 Results

Figure 6.1 shows the six independent elements of the Stokes scattering matrix for the size distribution defined above and for three fixed aspect ratios $\epsilon = 1.1$ (dotted line). 8 (dashed line). and 15 (solid line). The particles are randomly oriented. Note that the phase function F_{11} is plotted on a logarithmic scale. whereas the other elements of the scattering matrix are shown in relation to the phase function. One can see that the elements F_{11}. F_{22}. and F_{34} vary considerably with shape. The other three elements clearly vary when going from $\epsilon = 1.1$ to $\epsilon = 8$. but not much more when going from $\epsilon = 8$ to $\epsilon = 15$. It is also noted that the deviation of F_{22}/F_{11} from 1 appears to be a good measure for asphericity. as previously suggested by Yang and Liou [10].

The first question that needs to be addressed is how sensitive the elements of the Scattering matrix are to variations of the effective aspect ratio ϵ_{eff} in a size-shape distribution of randomly oriented prolate spheroids. Figure 6.2 shows the elements of the scattering matrix for an ensemble of randomly oriented particles of the same size distribution as in Fig. 6.1. but instead of having fixed aspect ratios. one now considers equiprobable shape distributions. The effective variance of all five shape distributions is $\mu_{eff} = 3$. and the effective aspect ratio is $\epsilon_{eff} = 4$ (solid line). 6 (dotted line). 8 (dashed line). 10 (dashed-dotted line). and 12 (triple-dot-dashed line). In all cases. the shape distribution has been averaged over seven equidistant points. Thus. the solid curve. for instance. has been obtained by averaging over $\epsilon = 1, 2, \ldots, 7$. One observes a strong dependency of F_{11}. F_{22}/F_{11}. and F_{34}/F_{11} on ϵ_{eff}. as one might have guessed from Fig. 6.1. The other three elements F_{33}/F_{11}. F_{44}/F_{11}. and $-F_{12}/F_{11}$ do not change by more
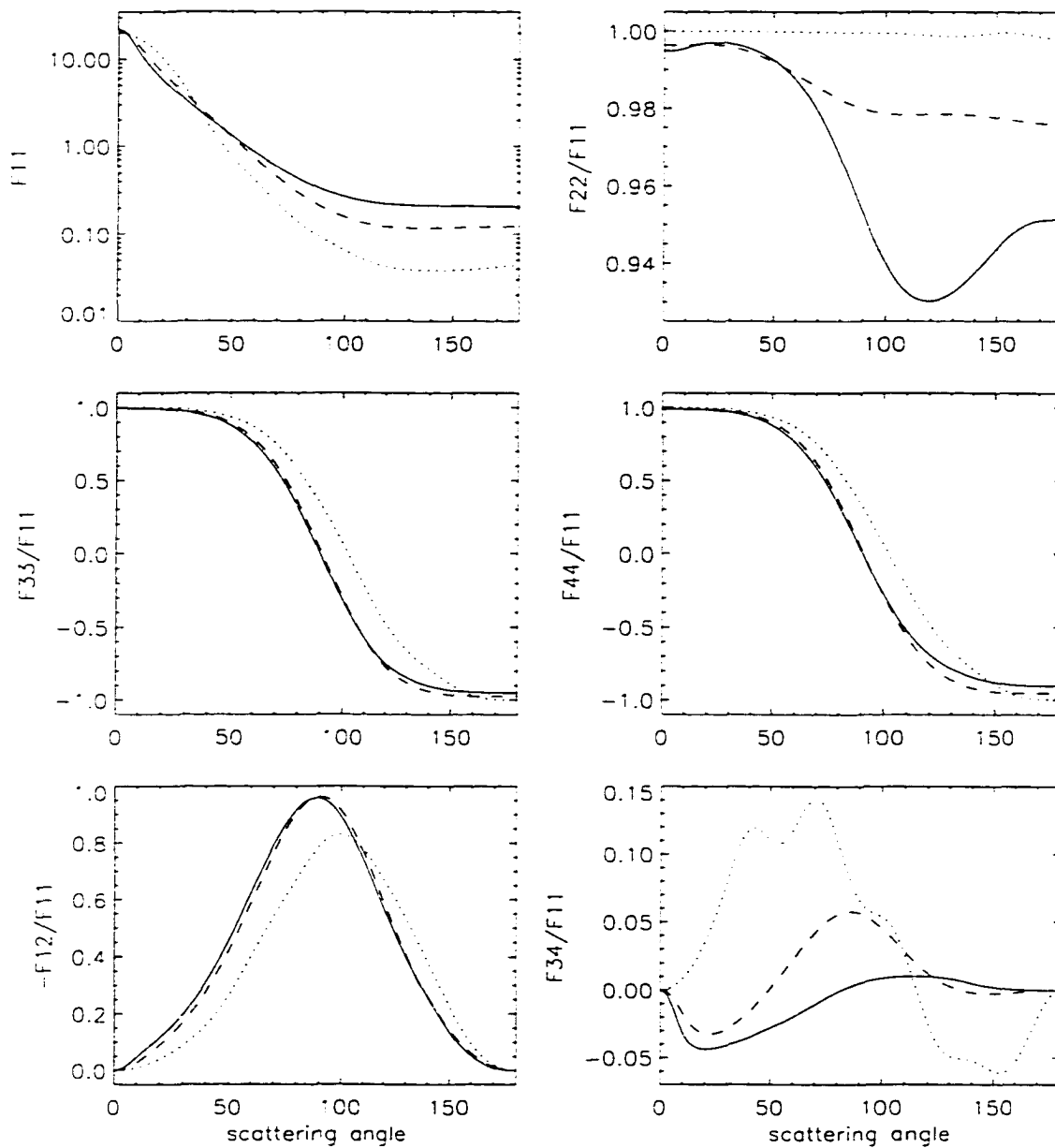
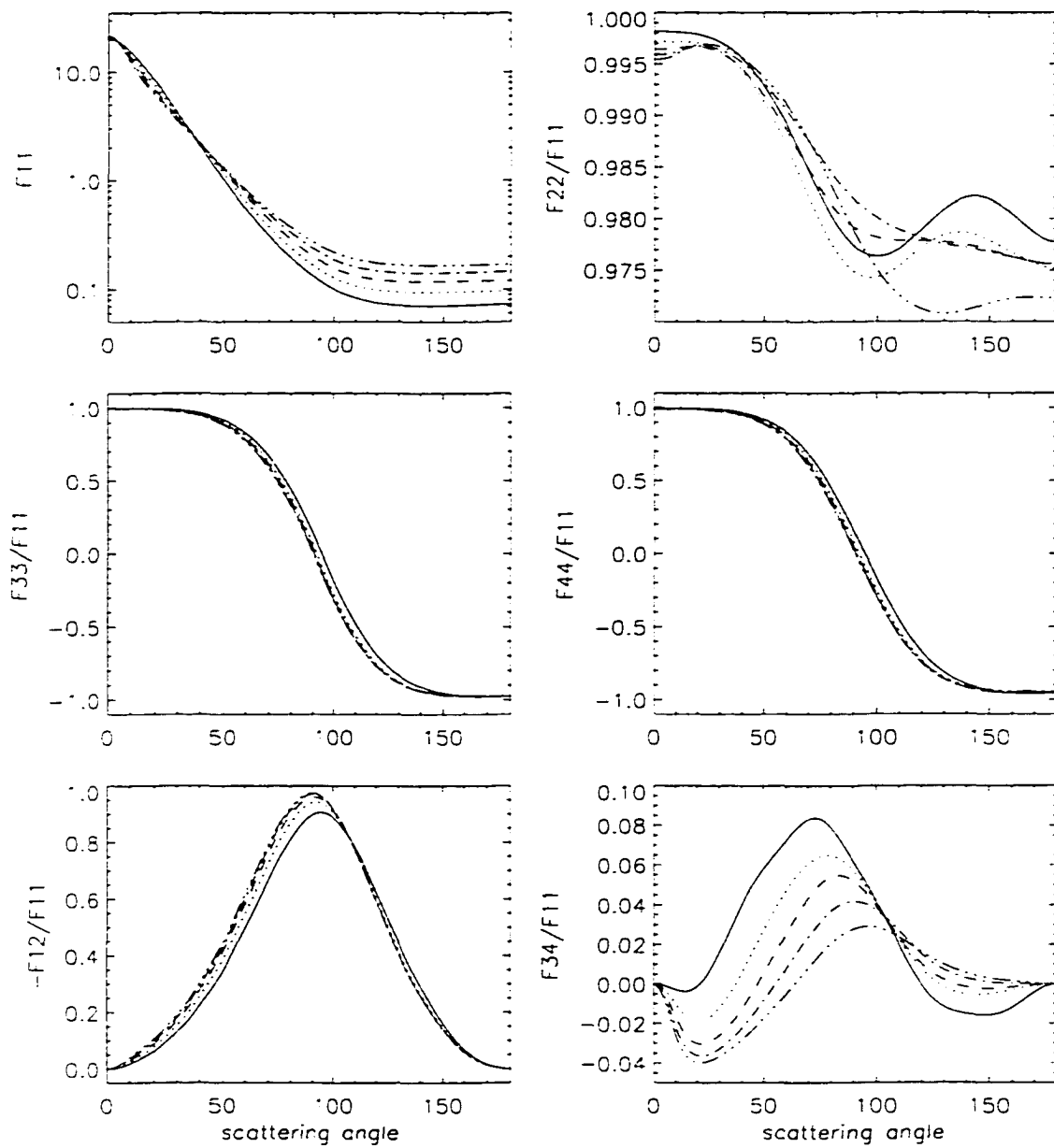Figure 6.1. Stokes scattering matrix for size distribution of spheroids

Figure 6.2. Stokes scattering matrix, variation in effective aspect ratio

than 5–10% with ϵ_{eff}. The phase function F_{11} relates the scattered field intensity to the incident field intensity. The element F_{22} relates the corresponding Stokes vector Q-components to one another, and the element F_{34} constitutes the linear relation between the U- and V- components of the incident and scattered field. Thus, both the intensity and the degree of linear polarization and the degree of circular polarization of radiation singly scattered in a size-shape distribution of randomly oriented spheroids will be sensitive to the effective aspect ratio ϵ_{eff} of the shape distribution.

It is also noted that particularly the element F_{34}/F_{11} as a function of the scattering angle in Fig. 6.1 shows strongly shape-characteristic qualitative features. For an aspect ratio of 1.1, it has two local maxima at ca. 40° and 70°, one local minimum at 155°, and two saddle points at 100° and 140°. For $\epsilon = 8$, it has only one local maximum at 80° and two local minima at 25° and 140°, whereas for $\epsilon = 15$, only one local maximum and one local minimum at 110° and at 20°, respectively, are left. Thus, when the ensemble-average is carried out only over size and orientation, and when the aspect ratio of the spheroids is assumed to be the same for all particles in the ensemble, the function F_{34}/F_{11} changes not only quantitatively but also qualitatively with ϵ. In Fig. 6.2, on the other hand, where the ensemble-average includes an additional averaging over shape, one obtains smoothly varying functions that basically have the same qualitative features, a local minimum in the forward-scattering region, a local maximum in the side scattering direction, and another local minimum at higher scattering angles, which slowly disappears with increasing effective aspect ratio. The minimum in the forward scattering region shifts to higher angles and deepens. The maximum also shifts to higher angles and becomes more flat with increasing ϵ_{eff}.

In Fig. 6.3, the dependency of the scattering matrix components on the effective variance of the shape-distribution is investigated. The effective aspect ratio ϵ_{eff} is 8 for all three curves, and the effective variance μ_{eff} is 7 (solid line), 4 (dotted line), and 1 (dashed line). In all three cases, the averaging over shape involved 15 equidistantly-spaced aspect ratios. Thus, for instance, the solid curve has been obtained by averaging
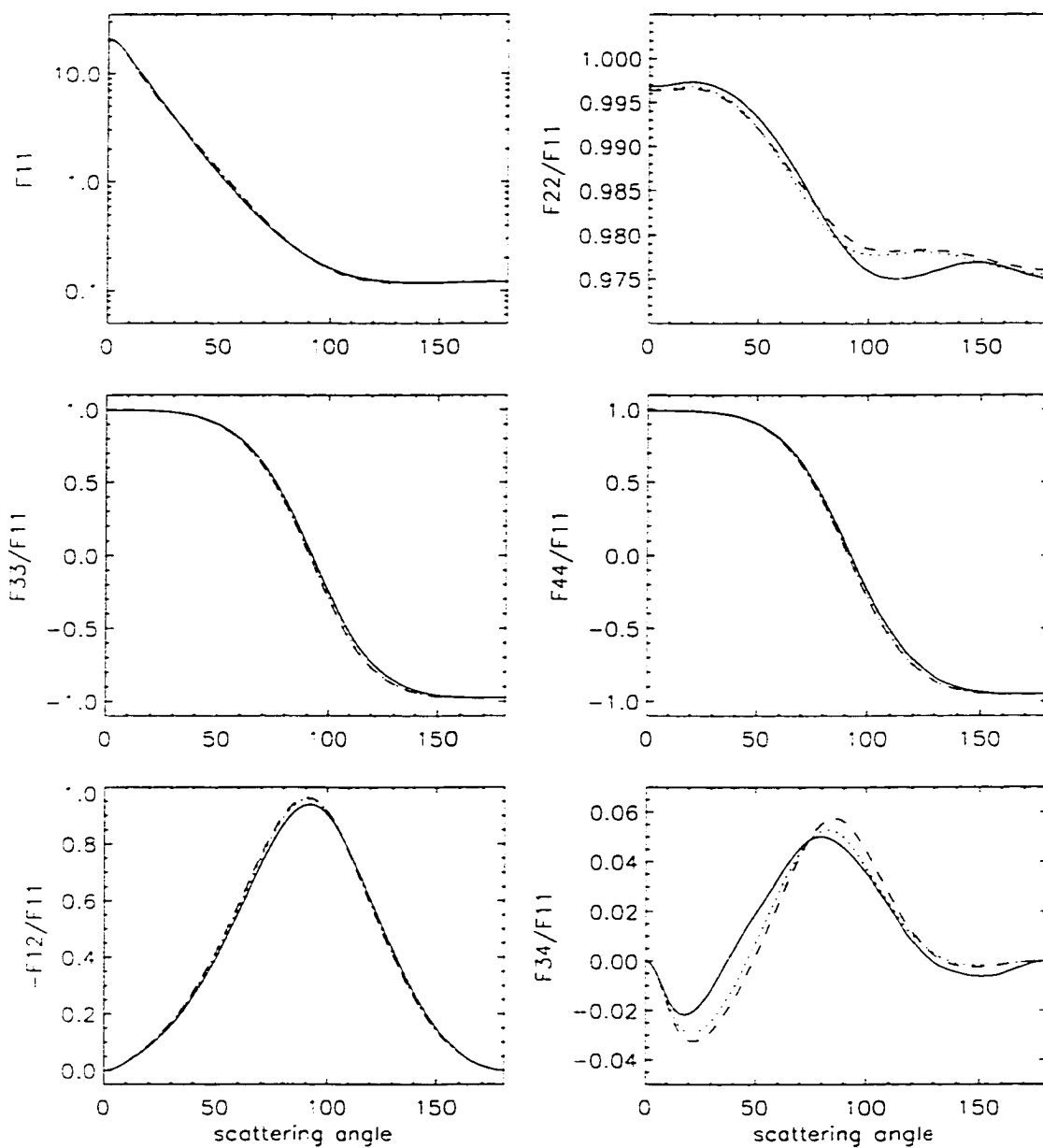
Figure 6.3. Stokes scattering matrix, variation in effective variance

over $\epsilon = 1, 2, \ldots, 15$. The elements F_{11}, $-F_{12}/F_{11}$, F_{33}/F_{11}, and F_{44}/F_{11} are insensitive to a variation in μ_{eff}. The element F_{22}/F_{11} shows some slight sensitivity in the region between 90–140°, but only when going to a high variance of $\mu_{eff} = 7$, where the deep minimum of highly aspherical spheroids, which is observed in Fig. 6.1, brings the curve somewhat down in this angular region. The element F_{34}/F_{11} also seems to be somewhat sensitive to the effective variance. However, by comparing Fig. 6.3 to Fig. 6.2, one can conclude that the sensitivity of the scattering matrix to a variation in the effective variance μ_{eff} is rather small for the two elements F_{22}/F_{11} and F_{34}/F_{11}. The effect of a variation of ϵ_{eff} is clearly much more pronounced.

It is noted that in Fig. 6.2, curves have been compared that were obtained by averaging over an equal number of equidistant points in the shape distribution. The same is true in Fig. 6.3. If this were not the case, then one could not be sure that the observed effects may not be statistical artifacts due to a varying number of averaging points. For practical calculations, it is interesting to get a feeling for how many points one actually has to use for averaging over shape in the size-shape-distribution in order to obtain converging results. Figure 6.4 shows the elements of the Stokes scattering matrix for a size-shape distribution of randomly oriented particles with the usual size distribution and an equiprobable shape-distribution of $\epsilon_{eff} = 8$ and $\mu_{eff} = 4$, which is identical to the dotted curve in Fig. 6.3. The three different curves in Fig. 6.4 are obtained by carrying out the averaging over shape over a varying number N of equidistant aspect ratios, namely $N = 15$ (solid line), 8 (dotted line), and 3 (dashed line). Thus, for instance, the dashed curve has been obtained by averaging over $\epsilon = 4, 8, 12$. One observes remarkably little change by going from $N = 3$ to $N = 8$, and virtually no change by going from $N = 8$ to $N = 15$. Consequently, a relatively small number of points appears to be enough for obtaining converging results when averaging over shape, at least in an equiprobable shape-distribution.

The sensitivity of the single scattering albedo and the asymmetry parameter to shape will now be investigated. First, an identical-shape size-distribution of randomly oriented
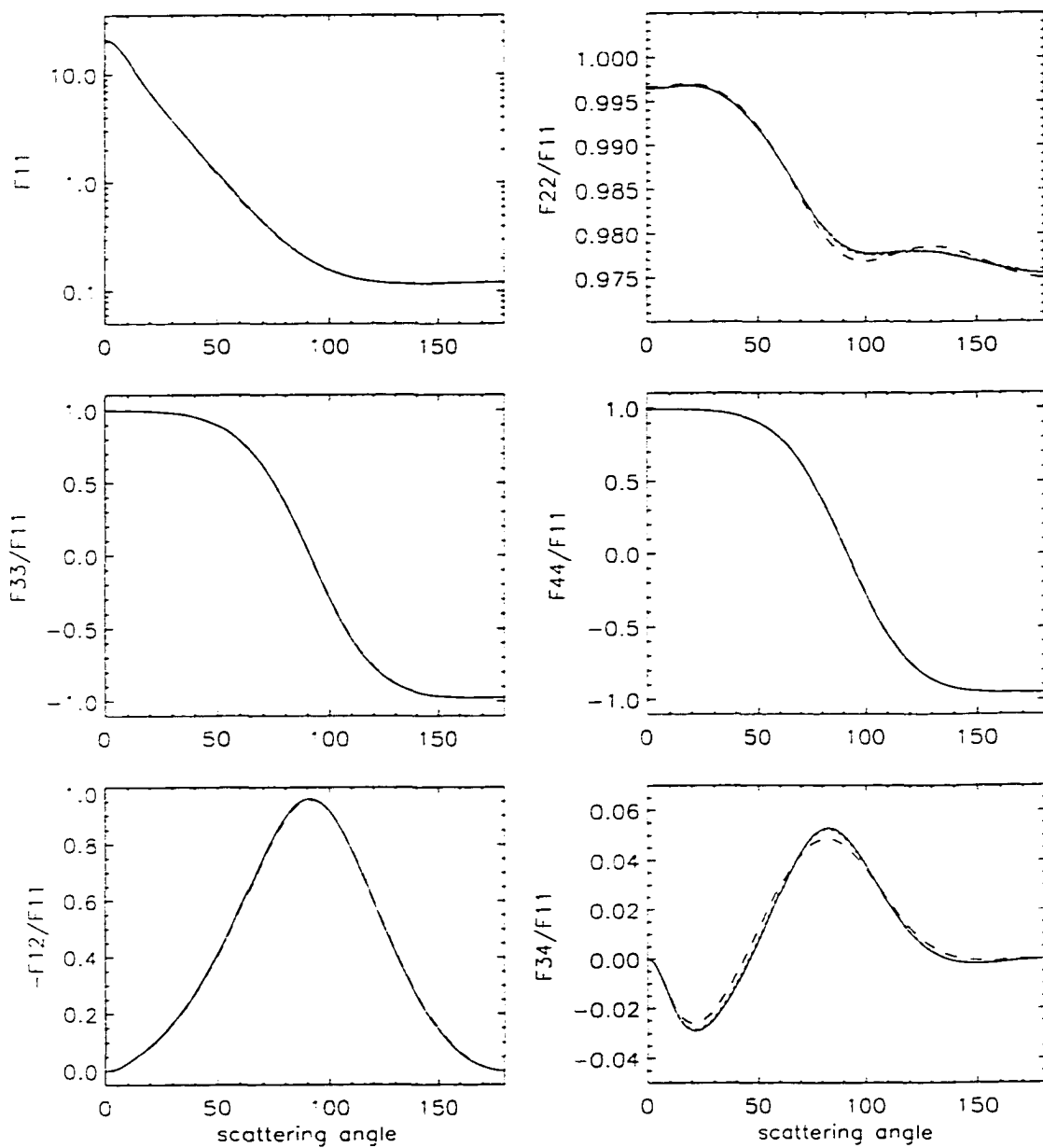
Figure 6.4. Stokes scattering matrix. variation in the number of averaging points

prolate spheroids is considered in which all particles have the same aspect ratio. By calculating the optical properties for different ensembles with different aspect ratios ϵ. one obtains the single scattering albedo and the asymmetry parameter in a single-shape size-distribution of randomly oriented particles as a function of ϵ. The result is shown in Fig. 6.5. Both parameters are near-linear functions of the aspect ratio. Figure 6.6 shows the same parameters for size-shape distributions as a function of the effective aspect ratio. The effective variance and the number of averaging points is as in Fig. 6.2. One observes hardly any difference between Fig. 6.5 and Fig. 6.6. which is to be expected due to the near-linear behavior of the two parameters (note the difference in the range of the abscissae in Figs. 6.5 and 6.6). Due to this near-linear dependency. the single scattering albedo and the asymmetry parameter in these size-shape distributions are insensitive to changes in the effective variance or to changes in the number of averaging points. Both the scattering cross section and the extinction cross section decrease with increasing effective aspect ratio. The monotonous decrease of the single scattering albedo is due to the fact that the scattering cross section decreases stronger with an increase of the effective aspect ratio than the extinction cross section.

6.4 Summary

The sensitivity of the elements of the Stokes scattering matrix. the single scattering albedo. and the asymmetry parameter to changes in the parameters characterizing the particle shape has been investigated. As a model system. a size-shape distribution of randomly oriented prolate spheroids has been considered. The shape-parameters in this study covered the whole range from mildly aspherical to extremely elongated prolate spheroidal particles. It was found that the elements F_{11}. F_{22}/F_{11}. and F_{34}/F_{11} of the scattering matrix are strongly dependent on the effective aspect ratio. whereas F_{33}/F_{11}. F_{44}/F_{11}. and $-F_{12}/F_{11}$ are only mildly sensitive to changes in ϵ_{eff}. As a result. the intensity (radiance). the degree of linear polarization and the degree of circular polarization of the radiation will be sensitive in a single-scattering event to a variation of
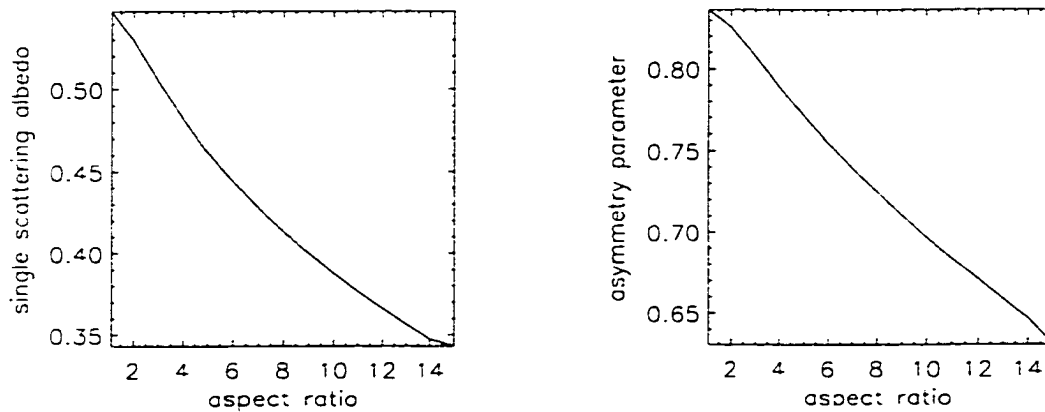
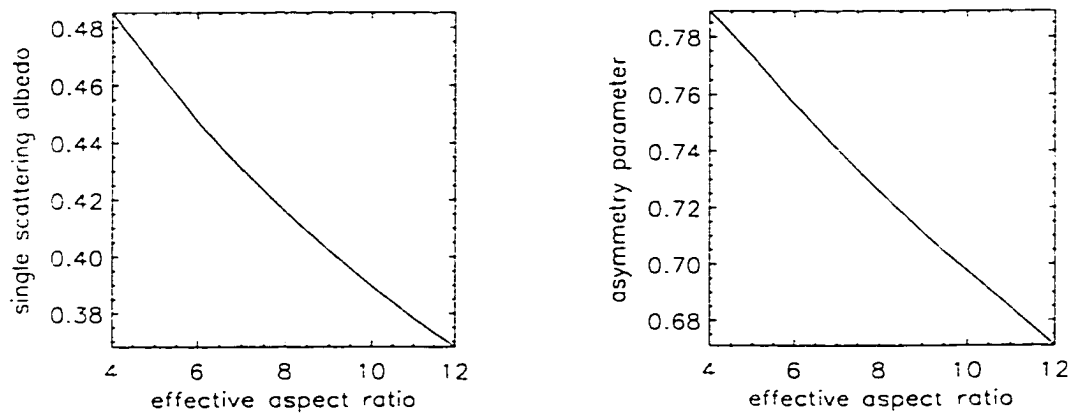Figure 6.5. Single scattering albedo and asymmetry parameter vs. aspect ratio

Figure 6.6. Single scattering albedo and asymmetry parameter vs. eff. aspect ratio

the effective aspect ratio ϵ_{eff}. In contrast. a variation of the effective variance of the shape-distribution had only little effect on the elements F_{22}/F_{11}. and F_{34}/F_{11}. and virtually no effect on the other four elements of the scattering matrix including the phase function. It was further found that averaging over only 3-8 points (aspect ratios) in the shape-distribution was enough to obtain converging results.

The single-scattering albedo and the asymmetry parameter were found to be near-linear monotonously decreasing functions of the aspect ratio. As a consequence. the additional averaging over shape in the size-shape distributions yielded almost exactly the same near-linear functions with the aspect ratio ϵ replaced by the effective aspect ratio ϵ_{eff}. Also. due to the near-linear dependency of the single-scattering albedo and the asymmetry parameter on ϵ. both parameters are fairly insensitive to a variation of the effective variance in a shape-distribution.

Chapter 7

Shape-Sensitivity Study of the Radiance and Polarization

The results from the last chapter strongly suggest that the intensity and polarization of radiation undergoing single scattering by an ensemble of nonspherical particles is strongly sensitive to the effective aspect ratio of the shape-distribution. The next question is whether this shape-sensitivity is also observed in macroscopic media. or whether multiple scattering tends to smear out the shape-sensitivity observed in the single scattering optical properties. In this chapter. the vector discrete ordinate radiative transfer (VDISORT) model described in Chapters 4 and 5 is applied to investigate the shape-sensitivity of the radiance (intensity). the degree of linear polarization. and the degree of circular polarization [59]. The investigation confirms that all three quantities are strongly sensitive to a variation of the effective aspect ratio in the considered case. This shape-sensitivity is observed consistently from size-shape distributions containing mainly moderately aspherical particles to those containing predominantly extremely aspherical particles. Within a range of the effective aspect ratio from 4 to 12. the degree of linear polarization changes by as much as 0.15. At certain angles from the sun. the radiance changes by as much as 60% within the same range of the effective aspect ratio.

161

7.1 Introduction

Most retrieval algorithms employing radiance and polarimetric remote sensing data rely on the use of spherical particle models in order to model the scattering and absorption of radiation. However. when observing ice clouds. aerosol layers. or air bubbles in sea ice. just to name a few examples. the assumption of spherical shape is not justified. The newly developed model presented in the previous chapters allows one to systematically study the effect of particle shape on atmospheric radiation over a wide range of size parameters. refractive indices. and. most importantly. shapes.

As a demonstration of the capabilities of the model. a particular case is investigated. in which the same nonspherical particle model as in the previous chapter is considered. The results of Chapter 6 for the single scattering optical properties are used as input to VDISORT. The question addressed here is how the changes of the single scattering properties with shape affect the radiative transfer. which includes multiple scattering of radiation. in a medium.

7.2 Results

The size-distribution in the model system considered here is as in Chapter 6. The shape-distribution is again assumed to be equiprobable. One result of Chapter 6 was that the crucial parameter characterizing the shape of the size-shape distribution of randomly oriented spheroids is the effective aspect ratio. because the single scattering optical properties are considerably more sensitive to ϵ_{eff} than to μ_{eff}. Therefore. the effective variance of the shape-distribution is kept constant at $\mu_{eff} = 3$. and the sensitivity of the radiative transfer in the medium to the shape-parameter ϵ_{eff} is quantitatively investigated.

The medium containing the ensemble of prolate spheroidal particles is assumed to be plane-parallel and homogeneous with an optical depth $\tau = 1$. the sun incident at $\mu_0 = |\cos\theta_0| = 0.2$. $\phi_0 = 0$. and with an underlying Lambertian surface of albedo= 0.1.

The single scattering optical properties of the size-shape distribution of randomly oriented spheroids. i.e. the single scattering albedo and the Stokes scattering matrix. have been computed in Chapter 6 by means of the modified separation of variables method (Chapter 2). The optical properties are used as input to VDISORT (Chapters 4 and 5), which performs the radiative transfer (multiple scattering) calculations. The number of streams (polar quadrature angles) was set to 36. The output is the Stokes vector of the diffuse radiation with components $I. Q. U. V$ as a function of the polar and azimuthal angle and as a function of the optical depth.

Figure 7.1 shows the upwelling radiance I (top row) and the degree of linear polarization $P_l = \sqrt{Q^2 + U^2}/I$ (bottom row) at the top of the medium ($\tau = 0$) for three different azimuth angles $\phi = 0$ (left column). 90° (middle column). and 180° (right column) as a function of the cosine of the polar angle $u = \cos\theta$. The five curves are for a size-shape distribution of randomly oriented spheroids with an effective aspect ratio of $\epsilon_{eff} = 4$ (solid line). 6 (dotted line). 8 (dashed line). 10 (dotted-dashed line). and 12 (triple-dotted dashed). For all three azimuths. the shape-sensitivity of the radiance (intensity) is seen to be larger in the horizontal looking direction near $u = 0$. At $\phi = 0$. the radiance decreases with ϵ_{eff}. whereas at $\phi = 90°$ and $\phi = 180°$. the order is reversed. The degree of linear polarization P_l is strongly shape-sensitive and increases with ϵ_{eff} at $\phi = 0$ and $\phi = 90°$. At $\phi = 180°$. one observes in fact also a strong shape-sensitivity of the linear polarization between $u = -1$ and $u = -0.6$. as can be seen from comparing the different ordinate scales in the bottom row plots. The increase in P_l when going from $\epsilon_{eff} = 4$ to $\epsilon_{eff} = 12$ is as high as 0.15 when looking in the nadir direction.

Figure 7.2 is analogous to Figure 7.1. except that now the downwelling radiation at the bottom of the medium ($\tau = 1$) is shown. The intensity is seen to be strongly shape-sensitive for all polar directions at $\phi = 0$ and $\phi = 90°$ and decreasing with ϵ_{eff} at these azimuths. At $\phi = 180°$. the change of intensity with shape is mostly observed at intermediate polar angles. At $u = 0.3$ and $\phi = 0$. the intensity decreases by as much as 60% when ϵ_{eff} is increased from 4 to 12. The degree of linear polarization
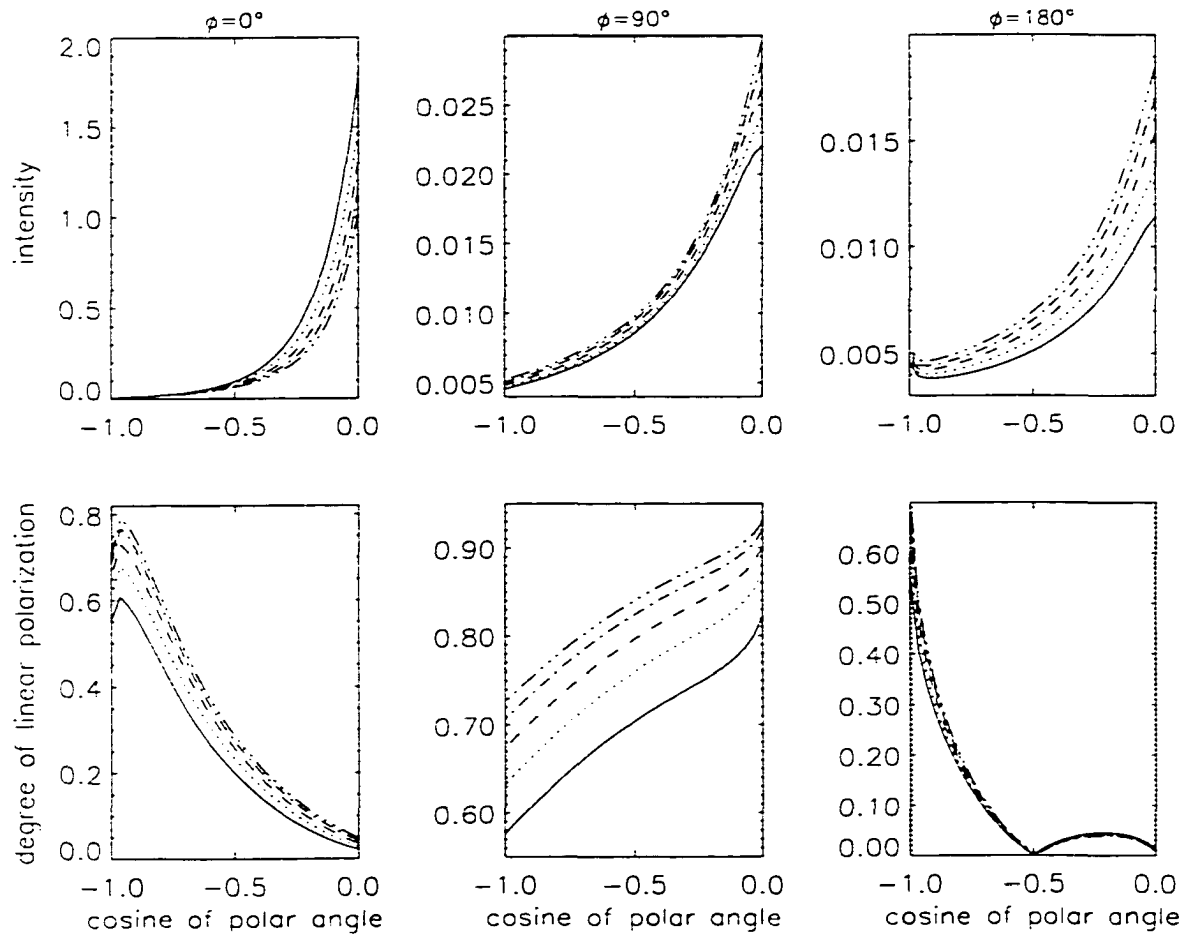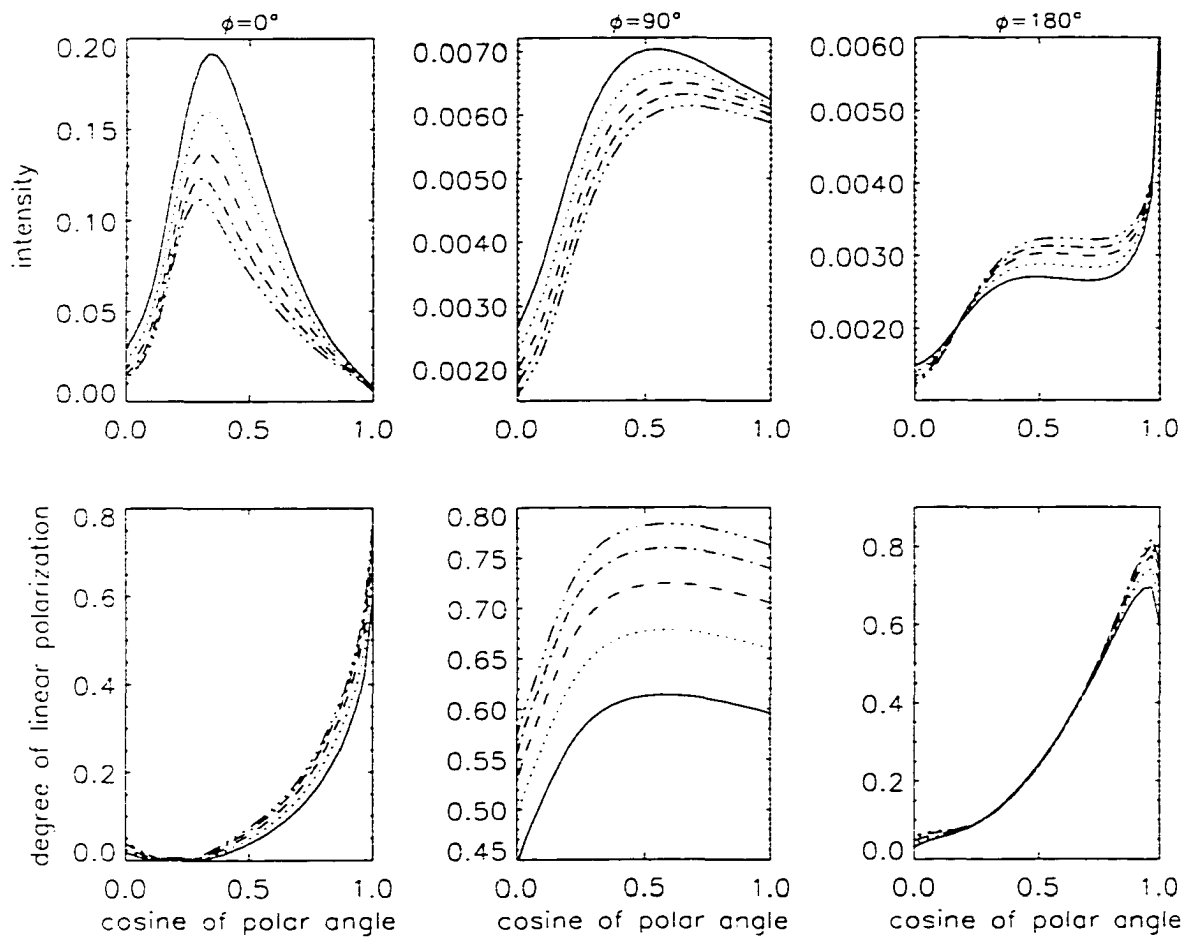
Figure 7.1. Radiance and linear polarization, top of medium

Figure 7.2. Radiance and linear polarization, bottom of medium

is strongly shape-sensitive and increasing with ϵ_{eff} at $o = 90°$ and at all polar angles. At $o = 0$. the situation is similar except when looking at the diffuse radiation in the direction of the sun at $u = 0.2$. At an azimuth of $o = 180°$. P_l is fairly insensitive to changes in ϵ_{eff} at intermediate polar angles. slightly shape-sensitive when looking in near-horizontal directions (around $u = 0$). and strongly shape-sensitive for small polar angles (near $u = 1$). When observing in the zenith direction. the degree of linear polarization increases by 0.16 from 0.60 at $\epsilon_{eff} = 4$ to 0.76 at $\epsilon_{eff} = 12$.

Figure 7.3 depicts the degree of circular polarization $P_c = V/I$ as a function of u at the top (left) and bottom (right) of the medium and at $o = 90°$. It is noted that V is zero at $o = 0$ and $o = 180°$. The curves shown are for the same size-shape distributions of randomly oriented spheroids as in the preceding figures. The degree of circular polarization in the atmosphere is generally very small. However. one observes that the relative change of P_c with ϵ_{eff} is very strong. The graphs of P_c as a function of u do not merely shift or become more or less "flat". as in Figs. 7.1 and 7.2. but actually change their qualitative appearance very sensitively when varying the effective aspect ratio.

In the three figures. one observes that the radiance and the degree of linear and circular polarization depend sensitively on shape even for extremely elongated particles. i.e. they change. for instance. even when going from $\epsilon_{eff} = 9$ to $\epsilon_{eff} = 12$. One also observes that at an azimuth of $o = 90°$. the radiance. the degree of linear polarization and the degree of circular polarization show a consistently strong sensitivity to particle shape for all polar angles. both at the top and at the bottom of the medium.

7.3 Summary

The radiance and the degree of linear and circular polarization of radiation that undergoes multiple scattering in a medium containing a size-shape distribution of randomly oriented nonspherical particles has been modeled by employing a spheroidal particle model. This model introduces. compared to a spherical particle model. only one param-

eter in addition to the size parameter. namely the aspect ratio of the spheroids. or. in a shape-distribution. the effective aspect ratio. This model is therefore ideally suited to asses in a controlled manner the effect of particle shape on the radiative transfer properties of a medium. The results show a generally strong dependence of both the radiance and the linear and the circular polarization on shape in the size-shape distribution. One also observes that this shape-sensitivity does not disappear for extremely elongated particles departing significantly from spherical shape. Retrieval algorithms for remote sensing data involving scattering by nonspherical particles. such as ice crystals. aerosols. or air bubbles in sea ice. will have to employ a suitable nonspherical particle model for interpreting the measurements. In particular. correct interpretation of the measured degree of polarization, which can be obtained with very high accuracy. will depend on a thorough understanding of the effect of particle shape on polarization. One result obtained for the model systems studied here ranging from $\epsilon_{eff} = 4$ to $\epsilon_{eff} = 12$ is that the impact of particle shape on polarization alone. while keeping all other physical properties of the particles constant. can be on the order of 0.15. which is substantial. The relative change in radiance can be as much as 60%.

At azimuths of $o = 90°$. a consistently strong shape-sensitivity of all three quantities. the radiance. the degree of linear and the degree of circular polarization. is observed over the entire range of polar angles. Measurements at and around this azimuth over a range of polar angles therefore appears to be ideal for obtaining information on the shape of the scattering particles.
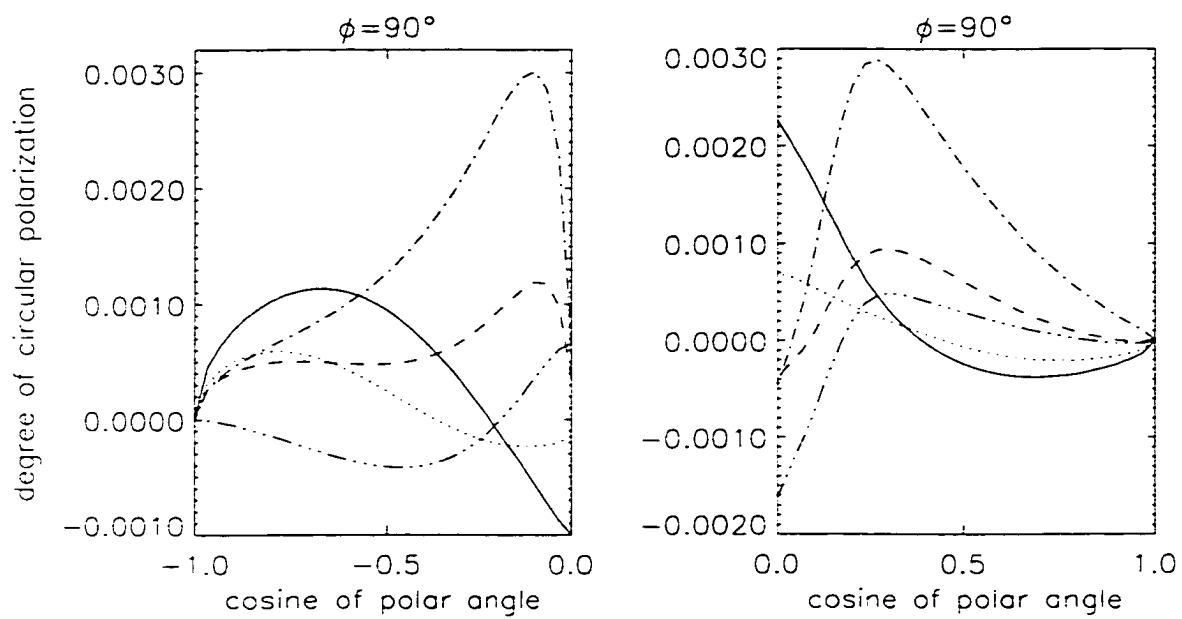
Figure 7.3. Circular polarization, top and bottom of medium

Chapter 8

Summary

A comprehensive model for scattering of electromagnetic radiation by nonspherical particles has been developed and tested. The model starts from first principles by rigorously solving the vector Helmholtz equation in spheroidal coordinates for a single spheroidal particle. It proceeds by analytically calculating the ensemble-averaged single scattering optical properties for a size-shape distribution of randomly oriented nonspherical particles. and concludes by solving the radiative transfer equation for the full 4-vector problem (including polarization). using the results from the single-scattering computations.

The new Separation of Variables Method (SVM) developed here for solving the vector Helmholtz equation is capable of covering a large range of aspect ratios. The output in form of the T-matrix allows one to perform the ensemble-average over orientational angles in an ensemble of randomly oriented particles *analytically*. This new approach to the single scattering problem therefore circumvents the disadvantages of the SVM and the Extended Boundary Condition Method (EBCM). respectively. while it retains the advantages of both methods. Thus. this new SVM approach allows for efficient computation of the optical properties of size-shape distributions of randomly oriented small nonspherical particles over a range of shapes unprecedented by previous methods. One can therefore. for the first time. systematically study the effect of particle shape on the single scattering optical properties over an extensive range of particle shape.

169

The formalism of point group theory has been applied to the electromagnetic scattering problem in order to systematically study the relation between geometrical symmetries of scattering particles and symmetry relations for the electromagnetic scattering solution. The results obtained result in a substantial reduction of the computer time needed for the single scattering solution.

The optical properties in the model output are in the correct format to be directly used in a vector discrete ordinate radiative transfer model (VDISORT). which has been corrected. improved. and generalized to apply for nonspherical particles. The iteration of the source function (ISF) method has been generalized to the full 4-vector radiative transfer problem to allow for accurate computation of the angular distribution of the Stokes vector (at arbitrary angles) from the VDISORT solution at the discrete angles. The new scheme has been implemented in VDISORT and tested. In particular. the ISF method has been found to be superior. both in terms of accuracy and in terms of computer time. to a spline interpolation.

A sensitivity study of the optical properties in a particular test case revealed that the elements F_{11}. F_{22}. and F_{34} of the Stokes scattering matrix as well as the single scattering albedo and asymmetry parameter are strongly sensitive to a variation in the effective aspect ratio of a shape distribution. but only mildly sensitive to a variation in the effective variance. The remaining elements of the scattering matrix were only mildly sensitive to a variation in the effective aspect ratio. and rather insensitive to a variation in the effective variance. Also. it was found that a small number of averaging points in the shape distribution was sufficient to obtain converging results for the shape-averaged optical properties. The extinction cross section decreases with increasing effective aspect ratio of the shape distribution. As a consequence. highly aspherical particles will show less IR emission in remote sensing measurements than mildly aspherical particles of comparable size. In particular. a spherical particle model applied to IR emission measurements on ice clouds will overestimate the IR emission. and thus the cloud temperature. which results in an underestimate of the cloud height. The scattering cross section decreases

even faster than the extinction cross section with an increase in the effective aspect ratio. As a result. their ratio. the single scattering albedo. is monotonously decreasing with the effective aspect ratio. This decrease was found to be near-linear. Similarly. the asymmetry parameter was found to be near-linearly monotonously decreasing with the effective aspect ratio.

A sensitivity study of the intensity. the degree of linear polarization. and the degree of circular polarization. using the results for the optical properties as input to VDISORT. showed a strong dependency on the effective aspect ratio of all three quantities at most angles. In particular. the shape-sensitivity was consistently strong for all three quantities and for all polar angles at an azimuth of 90° from the beam source. which suggests that remote sensing observations at and around this azimuth are expected to be ideal for retrieving shape-information of ice cloud and aerosol layers. Even for ensembles of highly aspherical particles. no convergence of the intensity or polarization of the radiation field with increasing departure from spherical shape was found. which underscores the importance of a model that is not confined to only a limited range of shapes. The intensity was found to change by as much as 60% when varying the effective aspect ratio from 4 to 12. which shows the dramatic impact that particle shape can have on remotely sensed radiance and possibly on heating/cooling rates in climate models. and the inadequacy of modeling scattering by ensembles of nonspherical particles by spheres. The linear polarization changed by as much as 0.15 over the same range of the effective aspect ratio. It is therefore essential to accurately account for shape effects in the interpretation of remotely sensed polarization of aerosol layers and ice clouds. The circular polarization as a function of the polar angle was found to be strongly sensitive to a variation of the effective aspect ratio. which makes this quantity a potential candidate for future remote sensing measurements targeted at the retrieval of particle shape information.

The model developed in this work fills a gap because existing models either are limited to only mildly aspherical shapes or are numerically too inefficient to be applied to realistic size-shape distributions of randomly oriented particles. The new model can

be used. as already demonstrated in the applications presented here. to investigate the extent of shape-sensitivity for different size-distributions and refractive indices. and to devise new remote sensing experiments that may be used to retrieve shape information in future applications. It can also be used for the development of shape-parameterizations for climate models. as well as for the development of new retrieval algorithms for remotely sensed radiative measurements of ice clouds or aerosol layers.

Bibliography

[1] K. N. Liou and Y. Takano. Light scattering by nonspherical particles: Remote sensing and climatic implications. *Atmos. Res.*, 31:271–298, 1994.

[2] S. Asano and M. Sato. Light scattering by randomly oriented spheroidal particles. *Appl. Opt.*, 19:962–974, 1980.

[3] M. I. Mishchenko. Light scattering by size-shape distributions of randomly oriented axially symmetric particles of a size comparable to a wavelength. *Appl. Opt.*, 32:4652–4665, 1993.

[4] M. I. Mishchenko and L. D. Travis. Satellite retrieval of aerosol properties over the ocean using polarization as well as intensity of reflected sunlight. *J. Geophys. Res.*, 102:16.989–17.013, 1997.

[5] A. A. Lacis, J. Chowdhary, M. I. Mishchenko, and B. Cairns. Modeling errors in diffuse-sky radiation: Vector *vs.* scalar treatment. *Geophys. Res. Lett.*, 25:135–138, 1998.

[6] D. L. Mitchell, A. Macke, and Y. Liu. Modeling cirrus clouds. Part II: Treatment of radiative properties. *J. Atmos. Sci.*, 53:2967–2988, 1996.

[7] P. Yang and K. N. Liou. Light scattering by ice crystals of complex shapes. In *Ninth Conference on Atmospheric Radiation, Long Beach, California, February 2-7, 1997*, pages 373–377, Boston, Mass., 1997. Am. Meteorol. Soc.

[8] P. Yang and K. N. Liou. Light scattering by hexagonal ice crystals: Solutions by a ray-by-ray integration algorithm. *J. Opt. Soc. Am. A.* 14:2278–2289. 1997.

[9] P. Yang. K. N. Liou. and W. P. Arnott. Extinction efficiency and single-scattering albedo for laboratory and natural cirrus clouds. *J. Geophys. Res.*. 102:21.825–21.835. 1997.

[10] P. Yang and K. N. Liou. Finite-difference time domain method for light scattering by small ice crystals in three-dimensional space. *J. Opt. Soc. Am. A.* 13:2072–2085. 1996.

[11] P. Yang and K. N. Liou. Geometric-optics-integral-equation method for light scattering by nonspherical ice crystals. *Appl. Opt.*. 35:6568–6584. 1996.

[12] P. Yang and K. N. Liou. Light scattering by hexagonal ice crystals: Comparison of finite-difference time domain and geometric optics models. *J. Opt. Soc. Am. A.* 12:162–176. 1995.

[13] P. C. Waterman. Matrix formulation of electromagnetic scattering. *Proc. IEEE.* 53:805–812. 1965.

[14] P. C. Waterman. Symmetry. unitarity. and geometry in electromagnetic scattering. *Phys. Rev. D.* 3:825–839. 1970.

[15] P. Barber. *Differential scattering of electromagnetic waves by homogeneous isotropic dielectric bodies.* PhD thesis. University of California. Los Angeles. 1973.

[16] P. Barber and C. Yeh. Scattering of electromagnetic waves by arbitrarily shaped dielectric bodies. *Appl. Opt.*. 14:2864–2872. 1975.

[17] P. C. Waterman. Matrix methods in potential theory and electromagnetic scattering. *J. Appl. Phys.*. 50:4550–4566. 1979.

[18] D. J. Wielaard. M. I. Mishchenko. A. Macke. and B. E. Carlson. Improved T-matrix computations for large. nonabsorbing and weakly absorbing nonspherical particles

and comparison with geometrical-optics approximation. *Appl. Opt.*. 36:4305–4313. 1997.

[19] S. Asano and G. Yamamoto. Light scattering by a spheroidal particle. *Appl. Opt.*. 14:29–49. 1975.

[20] V. G. Farafonov. Scattering of electromagnetic waves by a perfectly conducting spheroid. *Radio Engineering and Electronic Physics*. 29:39–45. 1984.

[21] N. V. Voshchinnikov and V. G. Farafonov. Optical properties of spheroidal particles. *Astrophys. Space Sci.*. 204:19–86. 1993.

[22] N. V. Voshchinnikov. Electromagnetic scattering by homogeneous and coated spheroids: Calculations using the separation of variable method. *J. Quant. Spectrosc. Radiat. Transfer*, 55:627–636. 1996.

[23] J. Stamnes. Exact two-dimensional scattering of an arbitrary wave by perfectly reflecting elliptical cylinders, strips. and slits. *Pure Appl. Opt.*. 4:841–855. 1995.

[24] J. Stamnes and H. A. Eide. Exact and approximate solutions for focusing of two-dimensional waves. I. Theory. *J. Opt. Soc. Am. A*. 1998. (in press).

[25] H. A. Eide and J. Stamnes. Exact and approximate solutions for focusing of two-dimensional waves. II. Numerical comparisons amongst exact. Debye. and Kirchhoff theories. *J. Opt. Soc. Am. A*. 1998. (in press).

[26] H. A. Eide and J. Stamnes. Exact and approximate solutions for focusing of two-dimensional waves. III. Numerical comparisons between exact and Rayleigh-Sommerfeld theories. *J. Opt. Soc. Am. A*. 1998. (in press).

[27] M. I. Mishchenko. L. D. Travis. R. A. Kahn. and R. A. West. Modeling phase functions for dustlike tropospheric aerosols using a shape mixture of randomly oriented polydisperse spheroids. *J. Geophys. Res.*. 102:16,831–16,847. 1997.

[28] F. M. Schulz, K. Stamnes, and J. J. Stamnes. Scattering of electromagnetic waves by spheroidal particles: A novel approach exploiting the T-matrix computed in spheroidal coordinates. *Appl. Opt.*, 1998. (in press).

[29] P. N. Francis. Some aircraft observations of the scattering properties of ice crystals. *J. Atmos. Sci.*, 52:1142–1154, 1995.

[30] B. A. Wielicki, J. T. Suttles, A. J. Heymsfield, R. M. Welch, J. D. Spinhirne, M.-L. C. Wu, D. O'C. Starr, L. Parker, and R. F. Arduini. The 27-28 October 1986 FIRE IFO cirrus case study: Comparison of radiative transfer theory with observations by satellite and aircraft. *Mon. Wea. Rev.*, 118:2356–2376, 1990.

[31] M. I. Mishchenko, W. B. Rossow, A. Macke, and A. A. Lacis. Sensitivity of cirrus cloud albedo, bidirectional reflectance and optical thickness retrieval accuracy to ice particle shape. *J. Geophys. Res.*, 101:16.973–16.985, 1996.

[32] M. I. Mishchenko. Light scattering by randomly oriented axially symmetric particles. *J. Opt. Soc. Am. A.*, 8:871–882, 1991.

[33] R. A. West, M. G. Tomasko, and L. R. Doose. Optical properties of small mineral dust particles at visible-near IR wavelengths: Numerical calculations and laboratory measurements. In *Eighth Conference on Atmospheric Radiation, Nashville, Tennessee, January 23-28, 1994.* pages 341–343, Boston, Mass., 1994. Am. Meteorol. Soc.

[34] R. D. M. Garcia and C. E. Siewert. A generalized spherical harmonics solution for radiative transfer models that include polarization effects. *J. Quant. Spectrosc. Radiat. Transfer*, 36:401–423, 1986.

[35] J. F. de Haan, P. B. Bosma, and J. W. Hovenier. The adding method for multiple scattering calculations of polarized light. *Astron. Astrophys.*, 183:371–391, 1987.

[36] F. M. Schulz. K. Stamnes, and F. Weng. VDISORT: An improved and generalized discrete ordinate radiative transfer model for polarized (vector) radiative transfer computations. *J. Quant. Spectrosc. Radiat. Transfer.* 1998. (in press).

[37] C. Flammer. *Spheroidal Wave Functions.* Stanford University Press. 1957.

[38] C. J. Bouwkamp. On spheroidal wave functions of order zero. *J. Math. Phys..* 26:79–93. 1947.

[39] M. I. Mishchenko and L. D. Travis. Light scattering by polydispersions of randomly oriented spheroids with sizes comparable to wavelengths of observation. *Appl. Opt..* 33:7206–7225. 1994.

[40] M. I. Mishchenko. L. D. Travis. and A. Macke. Scattering of light by polydisperse. randomly oriented. finite circular cylinders. *Appl. Opt..* 35:4927–4940. 1996.

[41] M. I. Mishchenko. L. D. Travis. and D. W. Mackowski. T-matrix computations of light scattering by nonspherical particles: A review. *J. Quant. Spectrosc. Radiat. Transfer.* 55:535–575. 1996.

[42] M. F. Iskander. A. Lakhtakia. and C. H. Durney. A new procedure for improving the solution stability and extending the frequency range of the EBCM. *IEEE Trans. Antennas Propag..* 31:317–324. 1983.

[43] M. F. Iskander and A. Lakhtakia. Extension of the iterative EBCM to calculate scattering by low-loss or lossless elongated dielectric objects. *Appl. Opt..* 23:948–952. 1984.

[44] P. M. Morse and H. Feshbach. *Methods of Theoretical Physics.* McGraw-Hill Book Company Inc.. 1953.

[45] C.-T. Tai. *Dyadic Green Functions in Electromagnetic Theory.* IEEE Press. 1993.

[46] A. J. Giarola. Dyadic Green's functions in the prolate spheroidal coordinate system. In *IEEE Antennas and Propagation Society International Symposium. 1995 Digest V.2.* pages 826–829. New York. NY. 1995. IEEE.

[47] R. H. Hackman. The transition matrix for acoustic and elastic wave scattering in prolate spheroidal coordinates. *J. Acoust. Soc. Am..* 75:35–45. 1984.

[48] R. H. Hackman. Development and application of the spheroidal coordinate based T matrix solution to elastic wave scattering. *Radio Science.* 29:1035–1049. 1994.

[49] L. Tsang. J. A. Kong. and R. T. Shin. Radiative transfer theory for active remote sensing of a layer of nonspherical particles. *Radio Sci..* 19:629–642. 1984.

[50] V. V. Varadan and V. K. Varadan. Multiple scattering of electromagnetic waves by randomly distributed and oriented dielectric scatterers. *Phys. Rev. D.* 21:388–394. 1980.

[51] N. G. Khlebtsov. Orientational averaging of light-scattering observables in the T-matrix approach. *Appl. Opt..* 31:5359–5365. 1992.

[52] S. Hanish. R. V. Baier. A. L. van Buren. and B. J. King. *Tables of Radial Spheroidal Wave Functions.* volume 1-6. Naval Research Laboratory. 1970.

[53] J. W. Hovenier. Multiple scattering of polarized light in planetary atmospheres. *Astron. Astrophys..* 13:7–29. 1971.

[54] J. J. Stamnes and B. Spjelkavik. New method for computing eigenfunctions (Mathieu functions) for scattering by elliptical cylinders. *Pure Appl. Opt..* 4:251–262. 1995.

[55] F. M. Schulz. K. Stamnes. and J. J. Stamnes. Point group symmetries in electromagnetic scattering. *J. Opt. Soc. Am. A.* 1998. (submitted).

[56] D. A. Varshalovich. A. N. Moskalev. and V. K. Khersonskii. *Quantum Theory of Angular Momentum.* World Scientific, 1988.

[57] L. Tsang. J. A. Kong. and R. T. Shin. *Theory of Microwave Remote Sensing*. John Wiley & Sons. 1995.

[58] F. M. Schulz. K. Stamnes. and J. J. Stamnes. Shape-dependence of the optical properties in size-shape distributions of randomly oriented prolate spheroids. including highly elongated shapes. *J. Geophys. Res..* 1998. (submitted).

[59] F. M. Schulz. K. Stamnes. and J. J. Stamnes. Modeling of the radiative transfer properties of media containing particles of moderately and extremely elongated shape. *Geophys. Res. Lett..* 1998. (submitted).

[60] J. Chowdhary. L. D. Travis. and A. A. Lacis. Incorporation of a rough ocean surface and a semi-infinite water body in multiple scattering computations of polarized light in an atmosphere-ocean system. In R. Santer. editor. *Atmospheric Sensing and Modeling*. SPIE Proceedings 2311. 1994.

[61] M. Herman. J. Y. Balois. L. Gonzalez. P. Lecomte. J. Lenoble. R. Santer. and C. Verwaerde. Stratospheric aerosol observations from a balloon-borne polarimetric experiment. *Appl. Opt..* 25:3573–3584. 1986.

[62] J. L. Deuzé. F. M. Bréon. P. Y. Deschamps. C. Devaux. M. Herman. A. Podaire. and J. L. Roujean. Analysis of the POLDER (POLarization and Directionality of Earth's Reflectance) airborne instrument observations over land surfaces. *Remote Sens. Environ..* 45:137–154. 1993.

[63] P. Y. Deschamps. F. M. Bréon. M. Leroy. A. Podaire. A. Bricaud. J.-C. Buriez. and G. Sèze. The POLDER mission: Instrument characteristics and scientific objectives. *IEEE Transactions on Geoscience and Remote Sensing.* 32:598–615. 1994.

[64] F. M. Bréon and P. Y. Deschamps. Optical and physical parameter retrieval from POLDER measurements over the ocean using an analytical model. *Remote Sens. Environ..* 43:193–207. 1993.

[65] J. L. Deuzé. C. Devaux. M. Herman, R. Santer. J. Y. Balois. L. Gonzalez, P. Lecomte. and C. Verwaerde. Photopolarimetric observations of aerosols and clouds from balloon. *Remote Sens. Environ..* 29:93–109. 1989.

[66] J. C. Roger. R. Santer. M. Herman. and J. L. Deuzé. Polarization of the solar light scattered by the Earth-atmosphere system as observed from the U.S. shuttle. *Remote Sens. Environ..* 48:275–290. 1994.

[67] A. Dollfus. M. Deschamps, and L. V. Ksanfomaliti. The surface texture of the Martian soil from the Soviet spacecraft Mars-5 photopolarimeters. *Astron. Astrophys..* 123:225–237. 1983.

[68] J. Hansen. W. Rossow. B. Carlson. A. Lacis. L. Travis. A. Del Genio. I. Fung. B. Cairns. M. Mishchenko. and M. Sato. Low-cost long-term monitoring of global climate forcings and feedbacks. *Clim. Change.* 31:247–241. 1995.

[69] J. E. Hansen and L. D. Travis. Light scattering in planetary atmospheres. *Space Sci. Rev..* 16:527–610. 1974.

[70] K. Stamnes. S.-C. Tsay. W. Wiscombe. and K. Jayaweera. Numerically stable algorithm for discrete-ordinate-method radiative transfer in multiple scattering and emitting layered media. *Appl. Opt..* 27:2502–2509. 1988.

[71] F. Weng. A multi-layer discrete-ordinate method for vector radiative transfer in a vertically-inhomogeneous. emitting and scattering atmosphere—I. Theory. *J. Quant. Spectrosc. Radiat. Transfer.* 47:19–33. 1992.

[72] K. Stamnes and P. Conklin. A new multi-layer discrete ordinate approach to radiative transfer in vertically inhomogeneous atmospheres. *J. Quant. Spectrosc. Radiat. Transfer.* 31:273–282. 1984.

[73] J. W. Hovenier and C. V. M. van der Mee. Fundamental relationships relevant to the transfer of polarized light in a scattering atmosphere. *Astron. Astrophys..* 128:1–16. 1983.

[74] F. Weng. A multi-layer discrete-ordinate method for vector radiative transfer in a vertically-inhomogeneous. emitting and scattering atmosphere—II. Application. *J. Quant. Spectrosc. Radiat. Transfer.* 47:35–42. 1992.

[75] K. L. Coulson. J. V. Dave. and Z. Sekera. *Tables Related to Radiation Emerging from a Planetary Atmosphere with Rayleigh Scattering.* University of California Press. 1960.

[76] H. C. van de Hulst. *Light Scattering by Small Particles.* John Wiley & Sons. Inc.. 1957.

[77] P. Vestrucci and C. E. Siewert. A numerical evaluation of an analytical representation of the components in a Fourier decomposition of the phase matrix for the scattering of polarized light. *J. Quant. Spectrosc. Radiat. Transfer.* 31:177–183. 1984.

[78] R. D. M. Garcia and C. E. Siewert. The F_N method for radiative transfer models that include polarization effects. *J. Quant. Spectrosc. Radiat. Transfer.* 41:117–145. 1989.

[79] C. E. Siewert. On the equation of transfer relevant to the scattering of polarized light. *Astrophys. J..* 245:1080–1086. 1981.

[80] C. E. Siewert. On the phase matrix basic to the scattering of polarized light. *Astron. Astrophys..* 109:195–200. 1982.

[81] F. M. Schulz and K. Stamnes. Angular distribution of the Stokes vector in a plane parallel. vertically inhomogeneous medium in the vector discrete ordinate radiative transfer (VDISORT) model. *J. Quant. Spectrosc. Radiat. Transfer.* 1998. (submitted).

[82] K. Stamnes. On the computation of angular distributions of radiation in planetary atmospheres. *J. Quant. Spectrosc. Radiat. Transfer.* 28:47–51. 1982.